![University of Glasgow logo]

Alhathlaul, Nada (2023) *Room temperature electro-carboxylation of styrene and stilbene derivatives: a comparative study.* PhD thesis.

Room Temperature Electro-carboxylation of Styrene and Stilbene Derivatives: A Comparative Study

VIA VERITAS VITA

Nada Alhathlaul

Submitted in fulfillment of the requirements for the

Degree of Doctor of Philosophy

School of Chemistry

College of Science and Engineering

University of Glasgow

September 2023

Abstract

Electrochemistry is a rapidly growing discipline within the physical sciences that encompasses a wide range of processes across various domains. Although electrochemistry has already found its place in applications, there exists significant potential for further advancement in other fields. In response to the growing demand for environmentally sustainable practices to supplant conventional, ecologically harmful methods, the electro-reduction of carbon dioxide emerges as a promising solution in numerous sectors.

In Chapter 1, there will be an introductory discussion regarding carbon dioxide and the importance of reducing carbon dioxide, then an analysis of some previous studies of electrochemical carbon dioxide reduction under different reaction conditions. Chapter 2 of the thesis will delve into a comprehensive discussion of the various techniques utilized, including electrochemical techniques such as cyclic voltammetry and chronopotentiometry, and analytical techniques such as nuclear magnetic resonance (NMR) and mass spectrometry (MS).

Chapter 3 presents results obtained relating to the reduction of various phenyl alkenes in the presence of carbon dioxide using a nickel mesh working electrode. Data on the cyclic voltammetry and reduction potentials of these alkenes will be shown, and the Faradic efficiency, product distributions and yields for each substrate will be discussed. The chapter also includes an analysis of products using NMR (both ^{1}H-NMR and ^{13}C-NMR). Further product analysis using mass spectrometry (MS) and Fourier Transform Infrared (FT-IR) techniques will be given.

Chapter 4 will examine the results of the reduction of phenyl alkene substrates in the presence of carbon dioxide using benzonitrile as a homogeneous catalyst. Subsequently, a comparative analysis will be conducted to evaluate the yield and Faradic efficiency achieved, comparing the results obtained using the nickel mesh and, in the presence, / absence of benzonitrile (BN) while maintaining identical reaction conditions. The objective is to identify any trends in reaction outcomes associated with nickel mesh electrodes. Last, Chapter 5 will summarize and discuss what is been done and suggest some ideas for future work.

Table of Contents

List of Conferences and Courses

- **Bristol Electrosynthesis Meeting 2022,** Poster Presentation "Production of Dicarboxylic Acids by Electrochemical CO_2 Reduction Using Alkenes as Substrates"

- **Electrochemistry Conference 2022 Edinburgh**, Oral presentation **"**Di-carboxylation of Phenyl-substituted Alkenes by Electrochemical Reduction in the Presence of CO_2

- **Basics of Nuclear Magnetic Resonance 2021,** 5-week online course, University of Lille, France.

- **Electrochemistry Conference 2023 Bristol**, Oral presentation "Room Temperature Electro-carboxylation of Styrene and Stilbene Derivatives: A Comparative Study"

List of Publications

1. *Room Temperature Electro-carboxylation of Styrene and Stilbene Derivatives: A Comparative Study*, Nada Alhathlaul, Zeliha Ertekin, Stephen Sproules and Mark D. Symes**,** Manuscript accepted 25 October 2023.

Acknowledgments

Author's declaration

I declare that, except where explicit reference is made to the contribution of others, this thesis is the result of my own work and has not been submitted for any other degree at the University of Glasgow or any other institution.

I declare that this thesis has been produced in accordance with the University of Glasgow's Code of Good Practice in Research.

I acknowledge that if any issues are raised regarding good research practice based on the review of the thesis, the examination may be postponed pending the outcome of any investigation of the issues.

Printed name: **Nada Alhathlaul**

Signature:

List of Abbreviations

δ	Chemical Shift
bipy	2,2′bipyridine
CV	Cyclic Voltammetry
DMF	N,N-dimethylformamide
$CDCL_3$	Deuterated Chloroform
E	Electrochemical potential
$E_{1/2}$	Half-potential of a redox wave
eq.	Equivalents
F	Faraday Constant
h	Hours
i	Current
LSV	Linear Sweep Voltammetry
m	Number of Moles or Mass
Me	Methyl
MHz	Megahertz
min	Minutes
MS	Mass spectrometry
m/z	Mass-to-charge ratio
n	Number of electrons Transferred per Ion
NMR	Nuclear Magnetic Resonance
IR	Infrared
SEM-EDX	Scanning electron microscope (SEM) and Energy Dispersive X-ray Spectroscopy (EDX).
XRD	X-ray Diffraction
ppm	Part(s) per million
Q	Charge
R	Resistance
r.t	Room Temperature
SCE	Saturated Calomel Electrode

T	Temperature
TEOA	Triethanolamine
nBu_4PF_6	Tetrabutylammonium hexafluorophosphate
BN	Benzonitrile

1. Introduction.

Amongst the C_1 carbon synthons, carbon monoxide (CO), cyanide (CN^-), and formaldehyde (HCHO) are commonly employed. However, these sources are toxic and require the necessity for careful handling. On a contrasting note, carbon dioxide (CO_2) stands as an abundant, cost-effective, and non-toxic C_1 source. However, due to its inherent low reactivity and high stability, effectively incorporating carbon dioxide into organic compounds has traditionally demanded severe reaction conditions such as elevated pressure, high temperature, and/or strong alkaline environments [1].

Most important, the science behind CO_2 fixation is fascinating and has garnered considerable attention lately due to its crucial role in producing carboxylic acid derivatives and combating the escalating levels of carbon dioxide, a pressing environmental concern. The surge in industrial expansion has significantly contributed to the rise in CO_2 emissions, disrupting the natural carbon cycle. On the part of the carbon dioxide cycle, it plays a critical role in environmental processes, impacting a variety of natural systems and organisms. This cycle includes many aspects such as the carbon sources that enter the atmosphere through natural phenomena like organism respiration, volcanic eruptions, and organic matter decomposition. Human activities such as fossil fuel combustion and deforestation also contribute significantly to CO_2 emissions. Another carbon dioxide source is organisms, including plants, animals, and microbes, which release CO_2 during respiration.

Plants, algae, and certain bacteria use CO_2 in photosynthesis to generate organic compounds and oxygen. This process is pivotal in removing CO_2 from the atmosphere and

converting it into biomass. On the other hand, oceans act as substantial carbon sinks, absorbing atmospheric CO_2 through various physical and biological mechanisms. However, rising CO_2 levels can trigger ocean acidification, impacting marine ecosystems and biodiversity. With all this huge industrial development, the natural cycle would not be able to cope with human-induced activity and climate change issues. Consequently, the overall equilibrium of the carbon cycle should be controlled [2,3]

Coincidingly, carbon dioxide harbors the potential to function as a crucial cornerstone for producing synthetic chemicals with augmented value. In this context, electrochemical methodologies aimed at curtailing carbon dioxide emissions or incorporating it into substrate materials emerge as a captivating resolution. Notably, the inherent scalability of electrochemical technologies presents an added advantage, allowing for direct alignment with renewable energy sources [1, 4].

In the pursuit of attaining gentle and environmentally friendly reaction conditions that go beyond the extensively explored thermochemical and photo redox catalysis methods, the concept of electro-carboxylation (electrocatalysis) has emerged within the field of organic synthetic chemistry. Electrocatalysis indeed offers various advantages for synthesis, including:

1- Eliminating the need for a sacrificial electron donor in reduction reactions, by utilizing electrons as the reducing agent.

2- Electrochemistry displays scalability and modularity, functioning effectively at both small and large scales. This means that it can be seamlessly extended to larger setups by stacking more cells.

3- Promoting mild reaction conditions.

An electrocatalytic process involves cathodic reduction and anodic oxidation, ultimately allowing (at least in theory) control over what the reduced and oxidized final products are.

When compared to thermochemical and photochemical carboxylation methods, several distinctions arise. Firstly, thermo/photochemical processes often require precious-metal catalysts or additives, whereas electrocatalytic transformations can take place in some cases without relying on such catalysts. Secondly, the majority of electrocatalytic processes operate without requiring external oxidizing or reducing agents. Thirdly, electrocatalytic processes align well with global sustainability, as (at least in theory) they can make use of renewable energy sources for driving reactions. In contrast, achieving a specific transformation through a thermochemical route often necessitates high reaction temperatures, pressures and/or sacrificial reagents. As a result, it is clear that electrocatalysis can play a crucial role in sustainable carboxylation reactions [4].

The process of electrochemical carbon dioxide fixation entails integrating carbon dioxide into organic compounds through an electrochemical reaction. This method has gained renewed attention as an environmentally friendly and sustainable approach to organic synthesis. Carbon dioxide fixation encompasses a few distinct main reaction types. The first involves direct reduction of carbon dioxide in the absence of any other chemical

substrates. This type will give simple small molecules, for example, oxalic acid and formic acid [5]. The second type of carbon dioxide fixation reaction involves forming a carbon-carbon bond between carbon dioxide and an organic substrate, resulting in the production of carboxylic acids by functionalization of the substrate [6, 7]. A third type involves creating a carbon-heteroatom bond between a carbon atom of CO_2 and a heteroatom within an organic substrate. Notably, this latter type of reaction does not lead to the formation of a carbon-carbon bond.

Considering several critical elements influence the selectivity and product formation during CO_2 electro-reduction. These include the characteristics of the cathode surface, the composition of the electrolyte, the voltage applied, the number of electrons, and the type of cell utilized [8]. Here are some examples:

1. Aqueous solvents

$$CO_2 + H_2O + 2\ e^- \rightarrow HCOO^- + OH^- \qquad E^0 = -0.43V \quad \text{(Equation 1)}$$

$$CO_2 + H_2O + 2\ e^- \rightarrow CO + 2\ OH^- \qquad E^0 = -0.52V \quad \text{(Equation 2)}$$

$$CO_2 + 6\ H_2O + 8\ e^- \rightarrow CH_4 + 8\ OH^- \qquad E^0 = -0.25V \quad \text{(Equation 3)}$$

$$2\ CO_2 + 8\ H_2O + 12\ e^- \rightarrow C_2H_4 + 12\ OH^- \qquad E^0 = -0.34V \quad \text{(Equation 4)}$$

$$2\ CO_2 + 9\ H_2O + 12\ e^- \rightarrow C_2H_5OH + 12\ OH^- \qquad E^0 = -0.33V \quad \text{(Equation 5)}$$

2. Non-aqueous solvents [8]:

$$CO_2 + e^- \rightarrow CO_2^{\cdot-} \qquad E^0 = -1.97\ V \text{ vs SHE in DMF} \quad \text{(Equation 6)}.$$
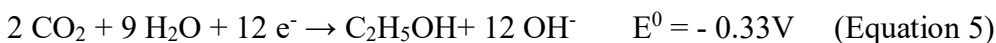
All above mentioned equations are examples among large number of examples on how the applied potential and number of electrons have influence on the resulted product [8].

Further, cathode materials have also influence on the product (s) type, for instance, Zn, Ag, Au, Ga, and Pd typically yield carbon monoxide, whereas Pt, Ni, Fe, and Ti tend to generate hydrogen. Additionally, formic acid production can be facilitated by cathode materials such as In, Hg, Pb, Sn, and Cd, to name but a few. Chaplin and Wragg, 2003 shows that there is strong evidence of CO_2 adsorbs on the nickel surface very strongly. Based on this summary, herein this project there will be a focused investigation on Ni electrode only [9].

This thesis will focus on approaches for catalyzing a carbon-carbon bond-forming reaction between CO_2 and organic substrates to produce carboxylic acids, a process commonly known as electrochemical carboxylation. Chapter 1 discusses various substrates, including vinyl bromides, triflates, difluoro ethylbenzenes, polyfluoroarenes, benzal diacetates, phenyl-substituted alkenes, enamides, and α-amino sulfones. As a result, utilizing electrochemical processes to incorporate carbon dioxide into organic compounds through carbon-carbon bond-forming reactions is effective for generating a number of valuable carboxylic acids. The practical applications of these findings introduce several recent discoveries in the field [1, 10].
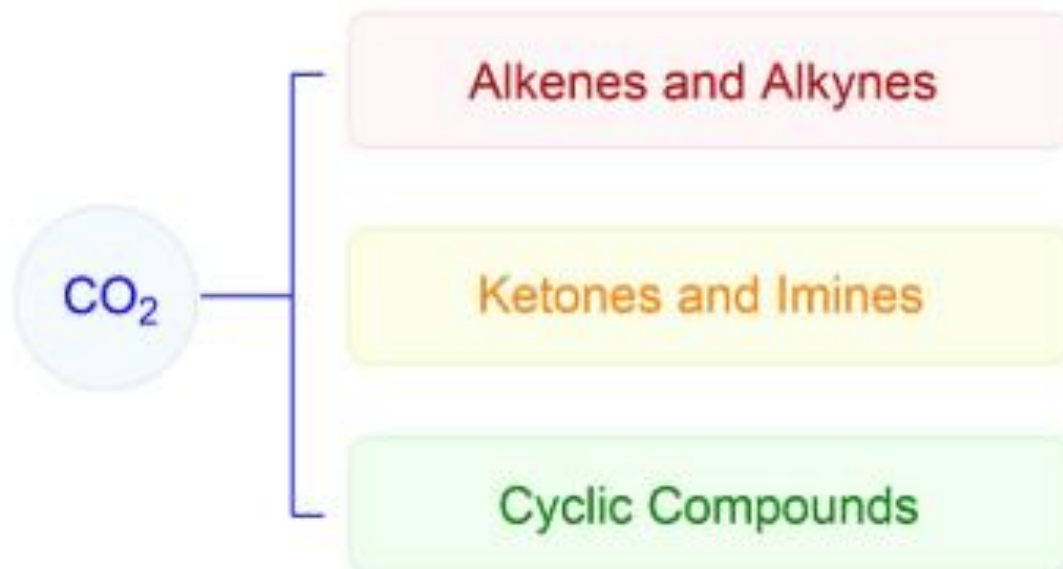
Figure 1: *Shows some possible chemical substrates which can be used in electro-carboxylation reactions* [10].

Carbon dioxide is a molecule that possesses a linear and centrosymmetric structure. The C=O bond within CO_2 has a bond length of 116.3 pm, which is notably shorter than that of a C-O single bond. Despite the polar nature of the C=O bonds in CO_2, the molecule exhibits a dipole moment of zero due to its linear arrangement, which causes the two bond dipoles to cancel each other out. In addition, the carbon center in CO_2 displays electrophilic properties. The bonding electrons are predominantly associated with oxygen rather than carbon, primarily due to the discrepancy in their electron negativities. CO_2 itself represents a highly stable form of carbon, featuring a C=O bond energy of 805 kJ mol^{-1} [11]. Using carbon dioxide as a reagent will therefore require considerable activation energy.

Concerning carboxylic acids, they play a crucial role in numerous biologically active molecules, natural products, and commercially available drugs. Moreover, the carboxyl groups present in these acids can be easily transformed into esters and amides. Alternatively, through reduction, they can be converted into aldehydes, ketones, and alcohols, which can potentially alter the biological activity of a specific molecule. Electro-carboxylation of olefins is indeed a useful approach for producing substituted succinic and propanoic acids, offering significant benefits in polymer chemistry and the pharmaceutical industry, for example, pregabalin and ibuprofen (a carboxylic acid-containing drug). For instance, 2-arylsuccinic acids, which are highly valued compounds, find application as antitumor agents and act as synthetic precursors to produce diverse macromolecules [12, 13].

In 1989, Derien et. al. [14] suggested the electro carboxylation of alkynes in the presence of carbon dioxide. Their study involved varied substituted alkynes and a $[Ni(bipy)]^{2+}$ catalyst at various temperatures. Scheme 1 gives an example of the optimal conditions identified in Derien et.al.'s 1989 work.
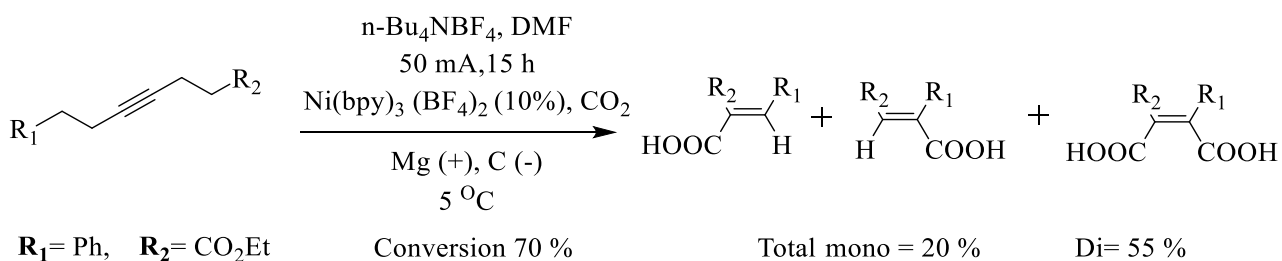
Scheme 1. *The electrochemical reduction of alkynes in the presence of a Nickel (II) bipyridine catalyst* [14].

Carboxylation of olefins with varying hetero-substituents has been documented. Substituents like RS-, R_3Si-, and RO- attached to the double bond confer increased electron density, and in certain instances, these olefins exhibit an extra coordination site for metal interaction. Notably, the electrochemical investigation revealed a robust interaction between Ni and olefins in the case of phenyl vinyl sulfide. When subjected to electro-carboxylation in the presence of Ni-PMDTA (pentamethyldiethylene triamine), this compound predominantly underwent diacid formation due to a dual 1,2-CO_2 incorporation onto the double bond (see Scheme 2).
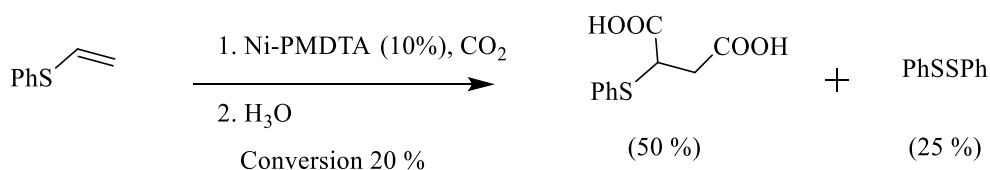
Scheme 2. *Shows the electrochemical reduction of phenyl vinyl sulfide in the presence of a Ni-PMDTA catalyst* [15].

Another class of chemical substrates is 1,4 diphenylbutadienes which have been reported to undergo an electro-carboxylation process (Scheme 3). The product we acquired displayed a Z configuration in its double bond, and this outcome may be attributed to the presence of a nickelacylcyclopentene intermediate.
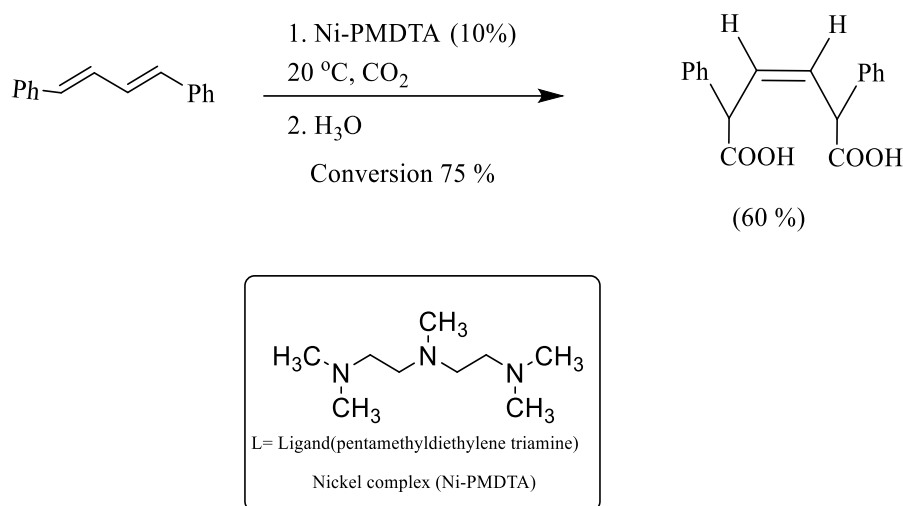
Scheme 3. *Shows the electrochemical reduction of 1,4 diphenylbutadienein the presence of a Ni-PMDTA catalyst* [15].

The reduction of 1,4 diphenylbutadiene with the help of nickel catalyst in the presence of PMDTA as the ligand affords unsaturated diacids in 60 % yield at 1 atm, and 20 ^{O}C.

considering, the utilization of CO_2 through chemical activation involves its coordination with transition metal compounds. Notably, electron-rich nickel (0) complexes have demonstrated effectiveness in facilitating the incorporation of CO_2 into unsaturated substrates like alkenes. The advancement of catalytic systems aimed at synthesizing functionalized compounds utilizing CO_2 holds significant interest. In the study (scheme 3), The addition of nickel catalyst is to help in the reduction process 1,4 diphenylbutadienein and convert as much as amount it can convert and faster the reaction with going back to its original structure by the end of the reaction. Moreover,in Scheme 3, the product obtained with a 60% yield exhibits exclusively the Z configuration in its double bond, which could be attributed to the presence of nickelacyclopentene. This

intermediate is believed to form during the reaction process, ultimately leading to the final product with a 60% yield.

Allylic halides have been used as another chemical substrate. Senboku (2021) electro-reduced allylic halides under the following conditions (Scheme 4) to give β, γ-unsaturated carboxylic acid as the major product [16].
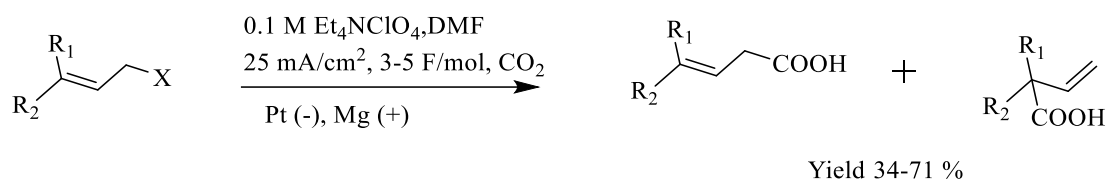
Scheme 4. *Shows the electrochemical reduction of allylic halides in the presence of an aprotic medium.*

Electrochemical direct carboxylation of benzyl alcohols which have an EWG on the phenyl ring produces arylacetic acids (Scheme 5).

Scheme of electrochemical reduction showing:

Reaction conditions: 0.1 M Bu$_4$NBF$_4$, DMF, 20 mA/cm^2, 6 F/mol, CO$_2$, Pt (-), Mg (+), 0 °C

Benzyl alcohol
Conversion 15 %

3-Phenyl propionic acid
< 18 %

4-(hydroxymethyl)benzonitrile
Conversion 98 %

3-(4-cyanophenyl) propanoic acid
78 %
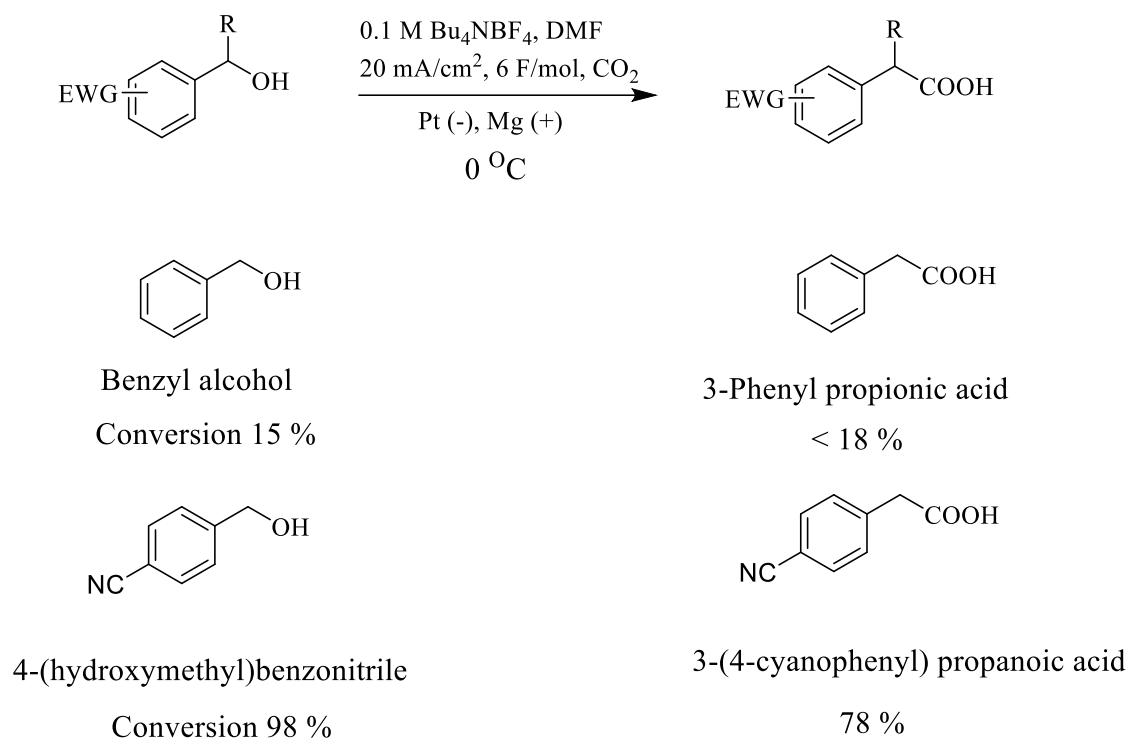
Scheme 5. *Shows the electrochemical reduction of benzyl alcohol in the presence of carbon dioxide* [17].

Electro-carboxylation gives superior results when utilizing compounds with electron-withdrawing groups, delivering higher yields compared to benzyl alcohol, which yields less than 18%.

Regioselective electrochemical defluorinative carboxylation of polyfluoroarenes has been studied having different substituted groups at the para position such as R=H, Me, and F to give a yield of 66, 76, and 65 % respectively.

11
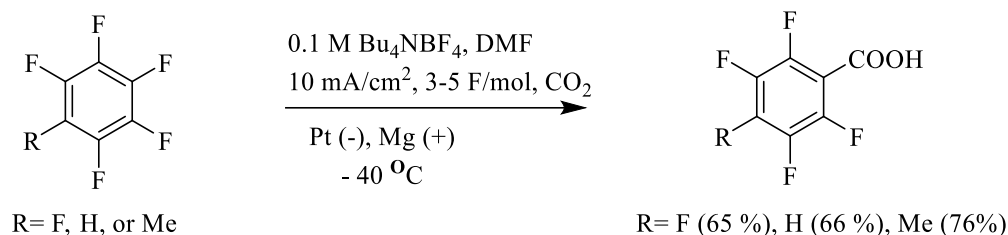
Scheme 6. *Shows the electrochemical reduction of polyfluoroarenes the at – 40 ^{O}C* [1].

By employing a Ni cathode and an Al sacrificial anode, the process of electro-carboxylation was effectively carried out on polycyclic aromatic hydrocarbons such as naphthalene, using carbon dioxide at a pressure of 4 MPa. This reaction took place within an undivided cell containing n-Bu$_4$NBr-DMF as the supporting electrolyte. A constant current was applied at room temperature, resulting in the successful production of corresponding trans-dicarboxylic acids to give a yield of 62% of the carboxylate [18].
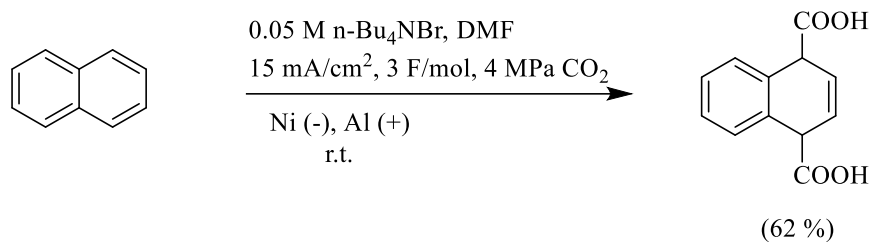
Scheme 7. *Illustrates the electro-carboxylation of naphthalene.*

The mechanism for this process can take two pathways and can be described as follows (Scheme 8):

(1).

(2). $CO_2 + {}^-e \longrightarrow \left[CO_2\right]^{\bullet -}$
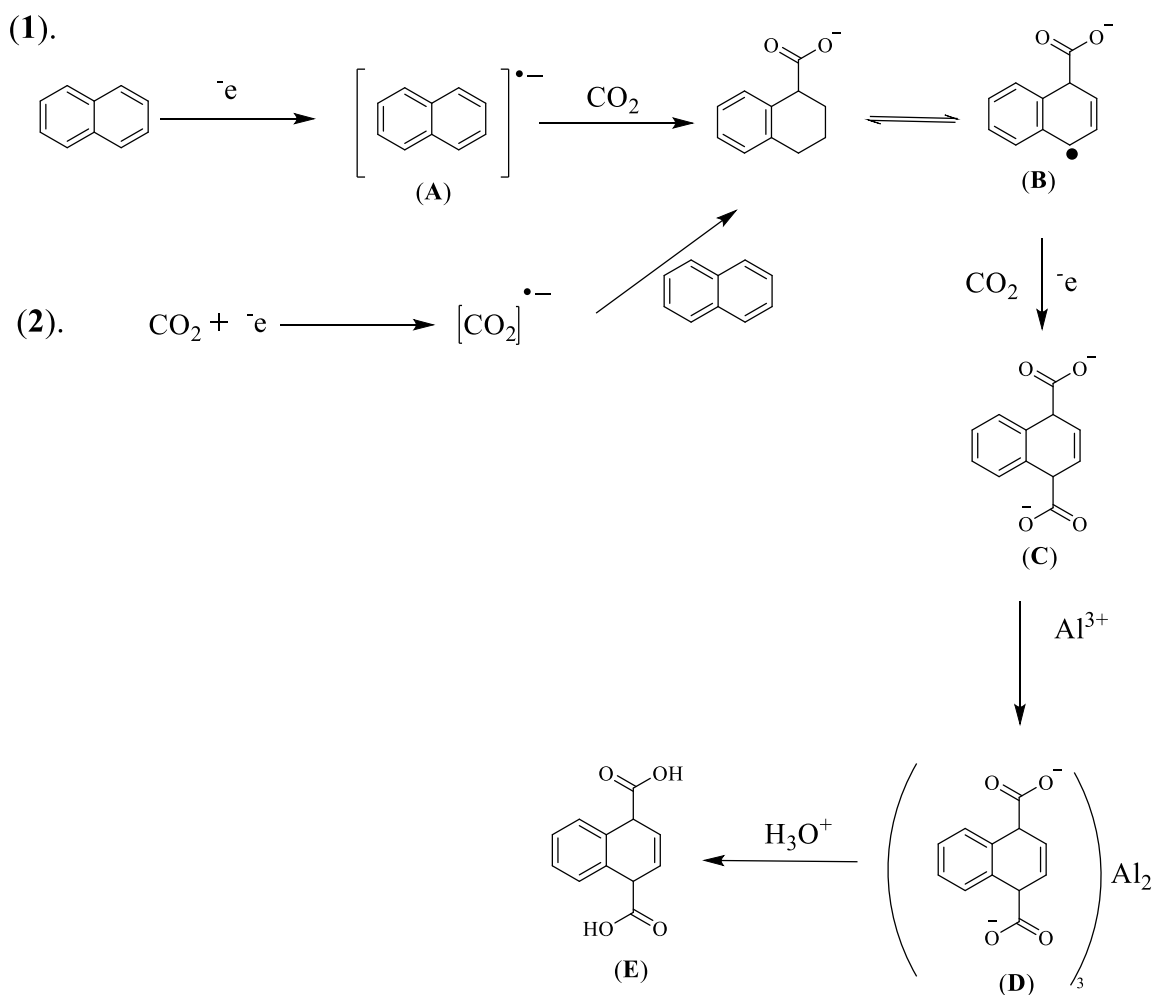
Scheme 8. *Illustrates two pathways mechanism for naphthalene.*

Yuan et al. (2010) outlined the reaction mechanism involving naphthalene and CO_2, as presented in Scheme 8. The process initiates with the reduction of naphthalene into its radical anion (A), which subsequently attacks CO_2, yielding intermediate (B). Alternatively, CO_2 acquires an electron, forming a CO_2 radical anion that reacts with naphthalene, producing (B). Through a further one-electron reduction of (B) and its interaction with CO_2, a dicarboxylate anion (C) is generated. In the electrolyte solution, (C) combines with Al^{3+} ions originating from oxidation of the aluminum anode, leading

to the formation of the aluminum carboxylate complex D. Finally, treatment of the metal

carboxylates with acid results in the production of dicarboxylic acid (E).

α,β-unsaturated esters have been electro-carboxylated by Sheta et. al. (2021) under the

following conditions (Scheme 9). I this study, Triethanolamine is used as a proton source

in the electrocarboxylation process.
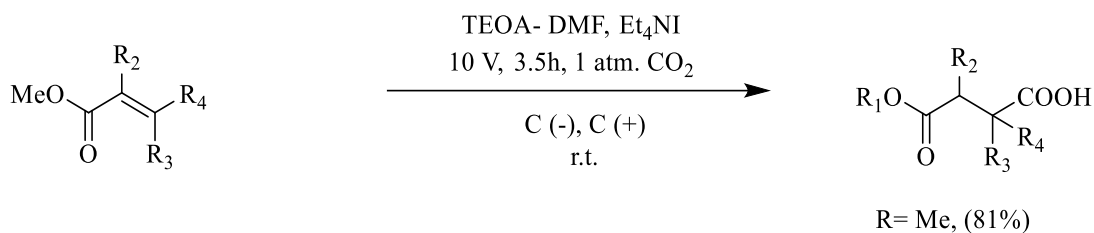
Scheme 9. Illustrates the electro-carboxylation of ester [19].

However, Hisanori et.al., 2006 [20], ekectro-carboxylated saturated ketones in a

consistent current electrolysis process within a solution of Acetonitrile (CH_3CN). This

solution contained a concentration of 0.1 M of Bu_4NBF_4 and was set up with a platinum

cathode and a magnesium anode. This electrolysis was carried out under atmospheric

pressure of CO_2. The outcome of this procedure was the successful incorporation of CO_2

at the α-position of the carbonyl group in the ketones. As a result, the corresponding β-

keto carboxylic acids were obtained.

cyclopentanone   OR

2-oxocyclopentanecarboxylic acid   (28 %)

cycloheptanone   OR

0.1 M Bu$_4$NBF$_4$, CH$_3$CN
15 mA/cm^2, 10 F/mol, CO$_2$

Pt (-), Mg (+)
0 ^{O}C

keto acids   (47 %)

cyclooctanone   OR

keto acids   (53 %)

cyclododecanone

2-oxocyclododecanecarboxylic acid   (92 %)
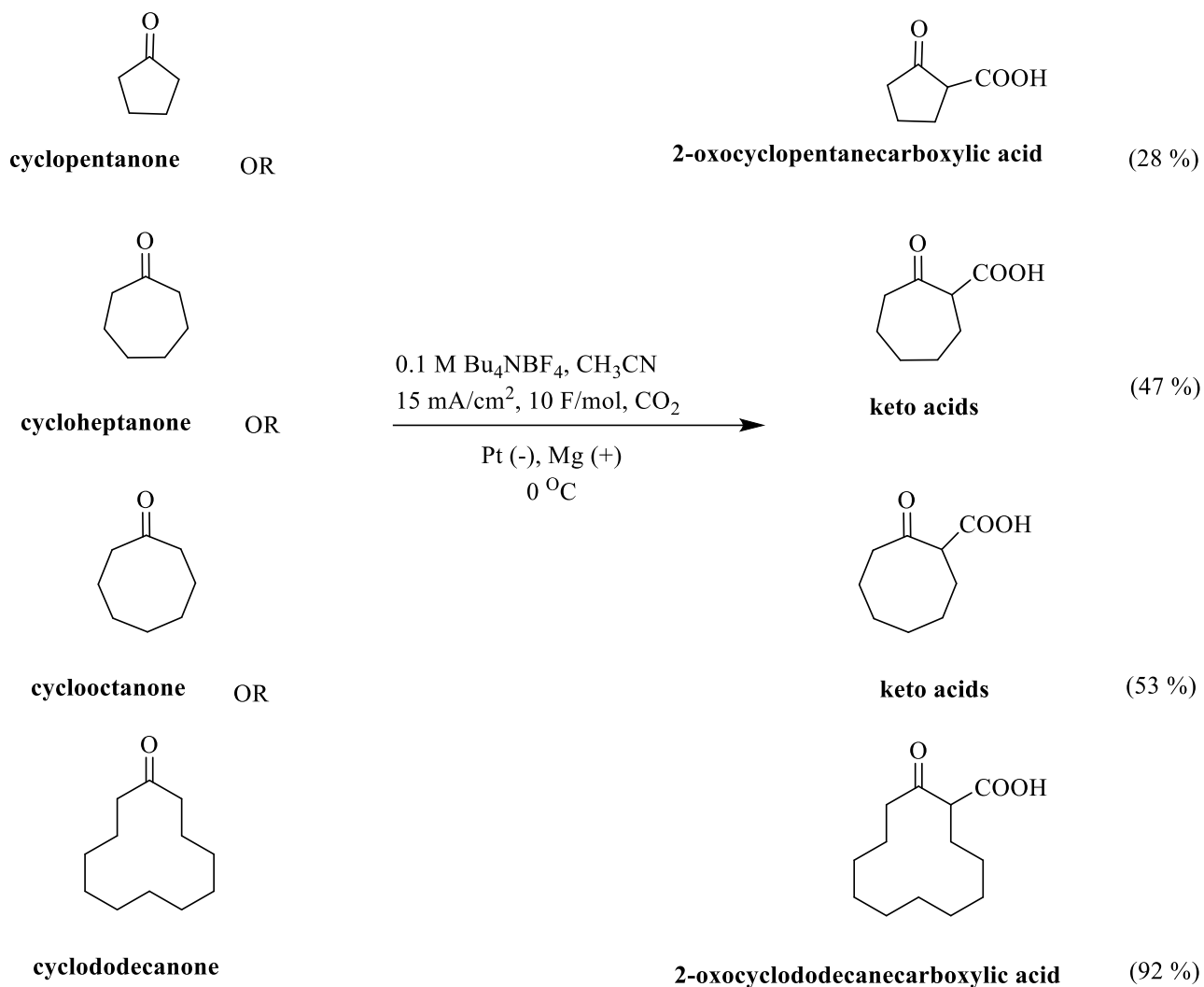
Scheme 10. *Illustrates the electro-carboxylation of varied cyclo-ketones under the same conditions resulting in the formation of the corresponding β-keto carboxylic acids.*

A study by Senboku et al. (2006) also involved aliphatic ketones which were electro-carboxylated as follows (Scheme 11).
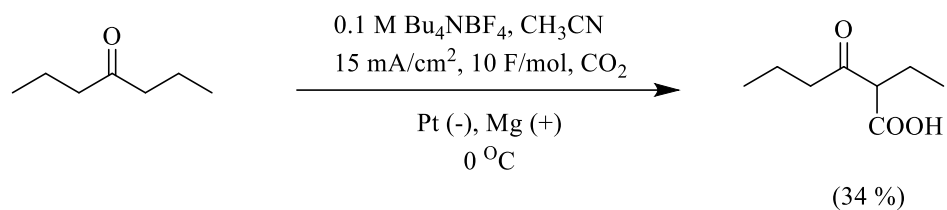
Scheme 11. *Shows the electro-carboxylation of 4-heptanone under the same conditions as in scheme 10 resulting in the corresponding 2-ethyl-3-oxohexanoic acid.*

The electro-carboxylation mechanism of ketones will take only one pathway as is explained in Scheme 12, with two suggested intermediates which go on to form keto acids after protonation.
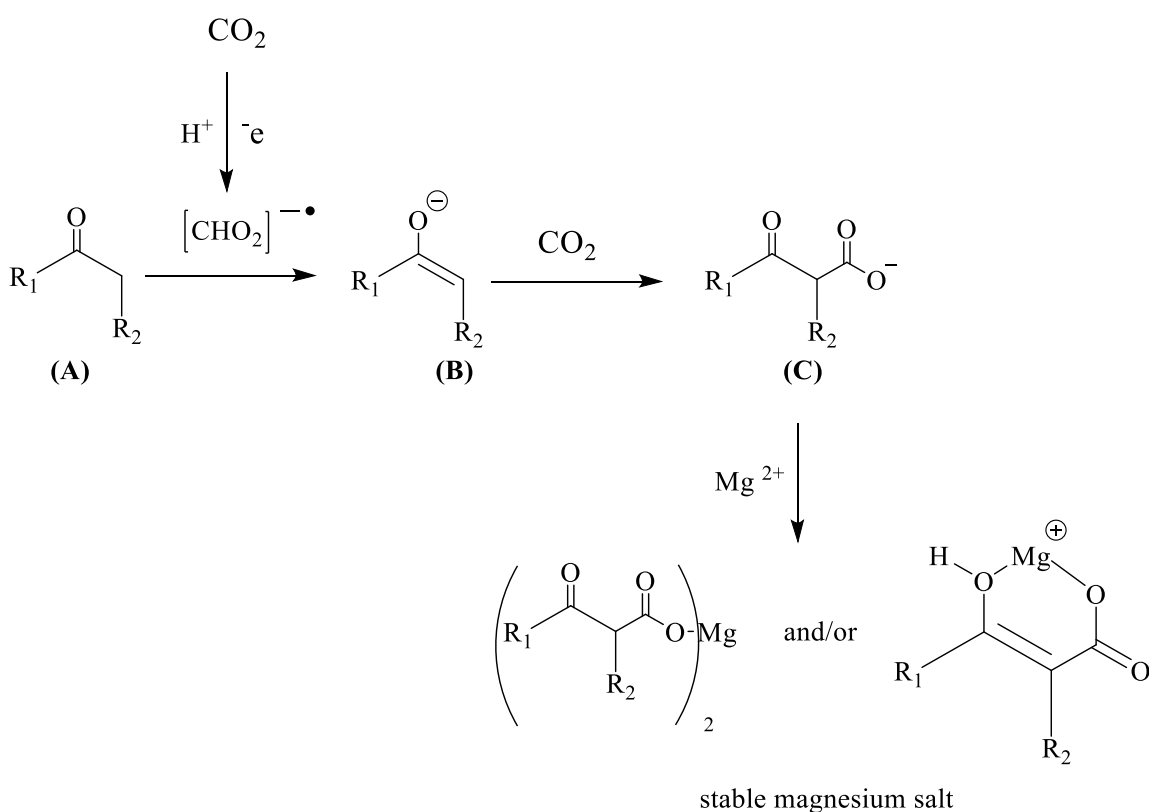
Scheme 12. *Shows the electro-carboxylation mechanism of ketones* [21].

16

This study illustrates that the reduction process will take place at carbon dioxide first and then a formate radical will form (Scheme 12). This radical (CHO_2^-) will then react with ketone (A) to form (B). Addition of another equivalent of carbon dioxide gives C. Then C will react with magnesium cations which were already oxidized at the anode, to form stable magnesium salts.

Aldehydes also have a share of research related to electro-carboxylation. In the year 1986, Silvestri et. al. showed the possibility of aldehydes' electro-carboxylation to the corresponding α-hydroxy acids [21].
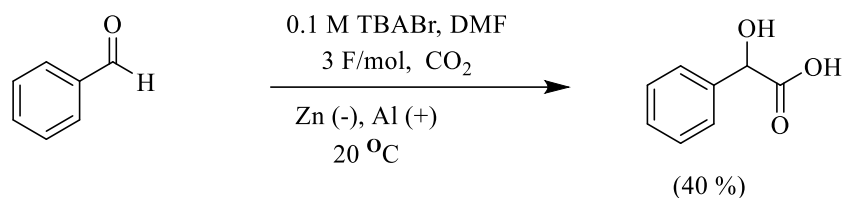
Scheme 13. Shows the electro-carboxylation of varied Aliphatic ketones under the same conditions resulting corresponding α-hydroxy acids.

This study investigated benzaldehyde electro-carboxylation and proved the production of mandelic acid (1) (Equation A in Scheme 14). However, Seidler et.al., 2023 discussed what would be produced if a protic or impure medium (i.e. containing water) was used in the reaction. They proposed that the products in that case would be benzyl alcohol (1) and hydrobenzoin (2) (Equation B).

A.

Propylene carbonate, 0.3 M Bu_4NI
2F/mol, 8 mA/cm^2, CO_2

graphite (-), graphite (+)
r.t,

1

(56 %)

B.

Protic impurities

1   +   **2**
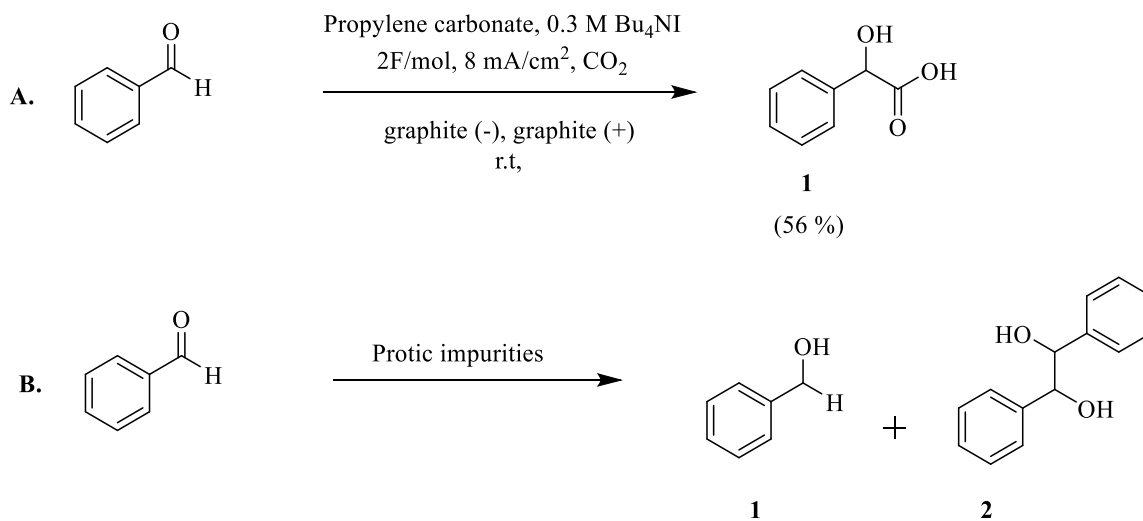
Scheme 14. *Shows the electro-carboxylation of aldehydes with/out water resulting in different carbon dioxide fixation and attachment positions on the same aldehyde substrate* [22].

The following description encapsulates the mechanism (Scheme 15).
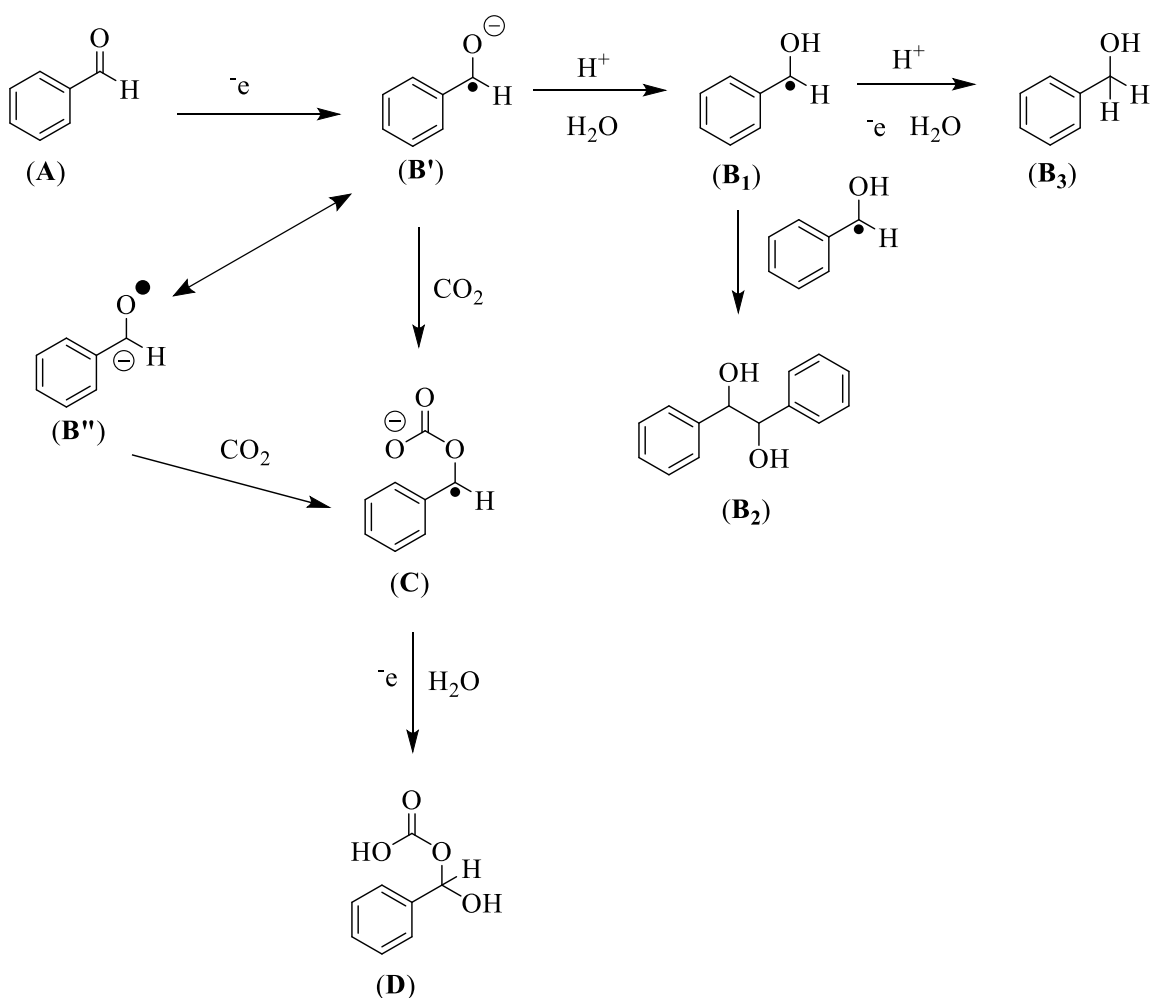
Scheme 15. *Shows the possible products from the electro-carboxylation of benzaldehyde with/without water impurities* [22].

The mechanism of the electro-carboxylation of aldehydes has been reported in this study (Scheme 15). After the reduction of the aldehyde (A) to the ketyl radical (B), the latter undergoes protonation and is either further reduced to the alcohol (B_1, B_3) or combines with another radical to form the pinacol species (B_2). However, in this study, benzyl alcohol was only detected during bulk electrolysis when water was added to the solvents. Otherwise, only hydro benzoin (D) was observed when CO_2 was present and reacted with

ketyl radical (B') to fix carbon dioxide to one of the terminal positions on the aldehyde structure.

In a 2014 study, Li and colleagues explored the single-step creation of N-bromoamino acids through the electrolysis of imines and carbon dioxide (4 MPa pressure). This electrosynthetic process took place within an undivided cell utilizing a nickel cathode and an aluminum sacrificial anode. The supporting electrolyte used was n-Bu₄NBr-DMF, and a consistent current was applied at ambient temperature. The outcome of this approach resulted in a 68% yield of N-bromoamino acids [23].

0.07 M n-Bu$_4$NBr, DMF
10 mA/cm^2, 4 F/mol, CO$_2$

Ni (-), Al (+)
r.t.

Conversion 70 %

Benzylideneaniline

COOH

Br

(68 %)
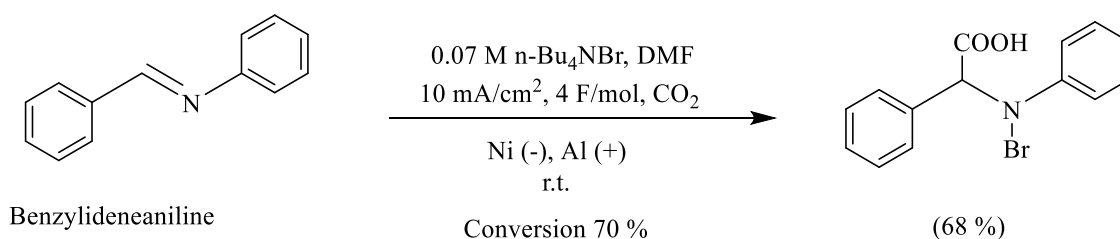
Scheme 16. *Benzylideneaniline electro-carboxylation* [23].

The mechanism of benzylideneaniline electrocarboxylation can be summarized as follows (Scheme 17):

At the Anode:

$$Al \longrightarrow Al^{3+} + 3e$$
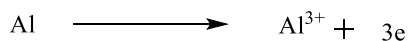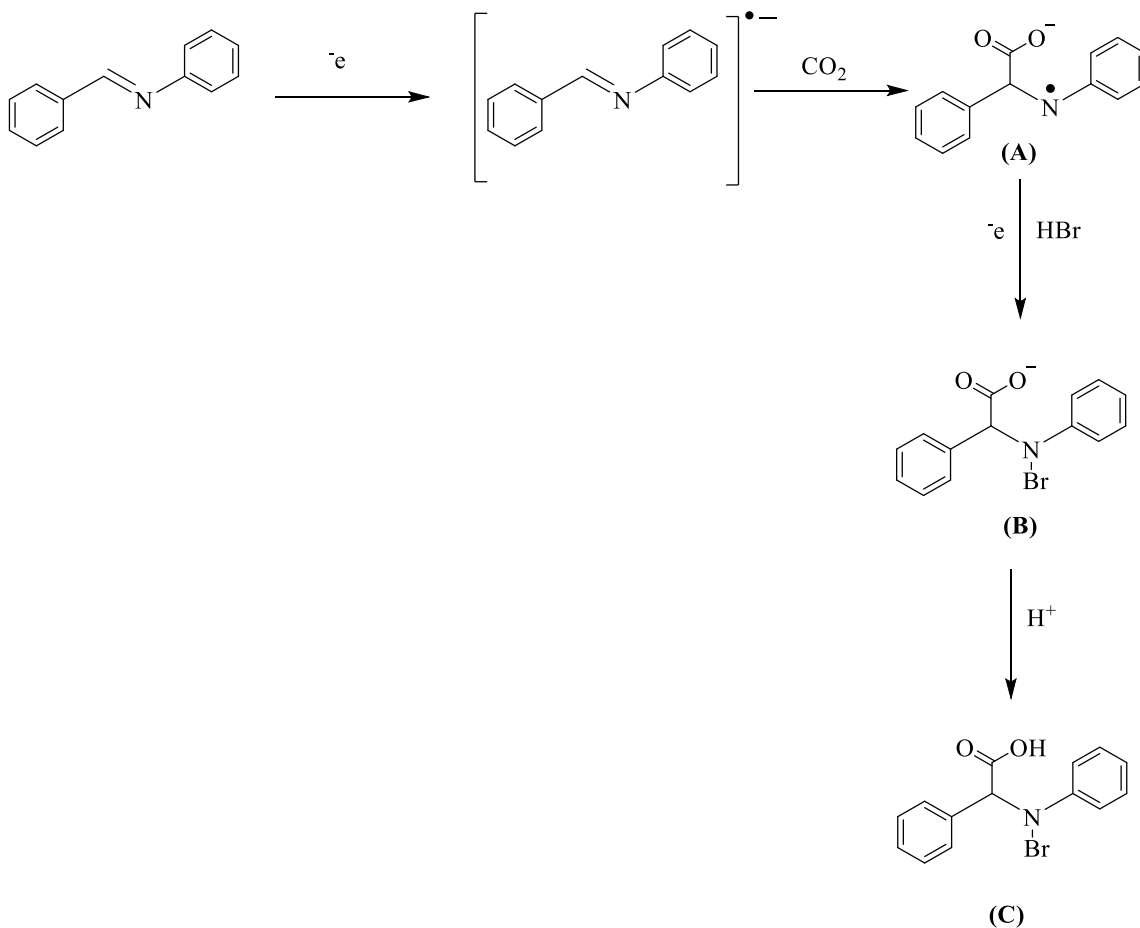
At the Cathode:

Scheme 17. *Shows the Benzylideneaniline electro-carboxylation mechanism* [23].

The initial step involves the reduction of benzylideneaniline to form a radical anion at the

cathode. This radical anion then reacts with carbon dioxide, resulting in the formation of

carboxylate anion A. Subsequently, A is further reduced to compound B through

protonation will produce C. Existing literature suggests that the proton necessary for this

step could be sourced from residual water, ammonium salts, or the DMF solvent.

In 2019, the research conducted by Irene et al. [24]. elucidated the electrochemical reduction characteristics of 4-halo benzonitrile compounds. They employed glassy carbon and silver as cathodes within a carbon dioxide-rich environment. By subjecting 4-halobenzonitriles to controlled potential electrolysis under a CO_2 atmosphere, they successfully achieved substantial yields of both mono- and di-carboxylated organic compounds. This electrolysis process took place in CO_2-saturated dimethylformamide solutions containing 0.1M of tetrabutylammonium tetrafluoroborate. Remarkably high yields, particularly in terms of di-carboxylated products, were achieved through the implementation of Ag as a cathode, showcasing notable electrocatalytic effects. This innovative technique presents an environmentally conscious pathway for synthesizing diverse phthalate derivatives. These derivatives hold promise as building blocks for the eco-friendly production of plastic polymers (Scheme 18 (1)).
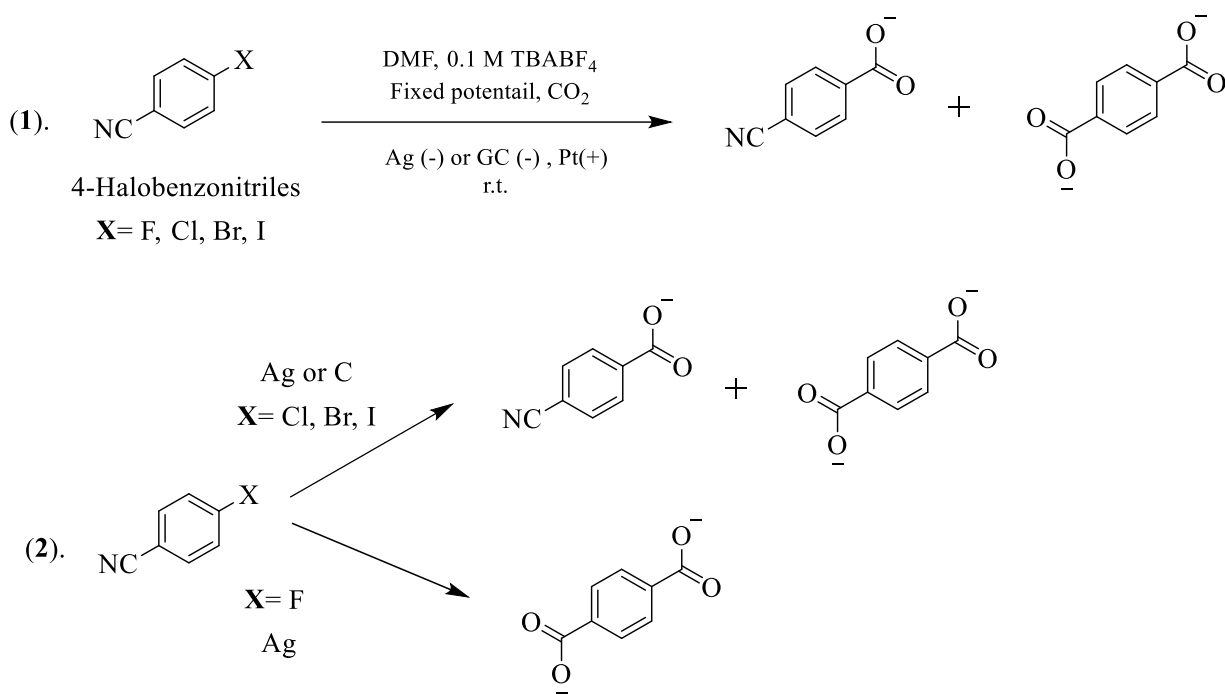
Scheme 18. *(1) The general scheme of electro-carboxylation of 4-halo benzonitrile, and (2) the final product(s) after electro-carboxylation of 4-halo benzonitrile based on the halide substituted group* [24].

It is expected that the mechanism will take a different route for (X=Cl, Br, or I) in comparison to X=F. Scheme 19 describes the mechanism of reaction for 4-chloro, bromo, or iodo benzonitrile (1) and 4-flouro benzonitrile (2).

Upon analyzing the aforementioned outcomes, it becomes reasonable to posit a mechanism for the integration of CO_2 into 4-halobenzonitriles (A) (where X = Cl, Br, and I) as depicted in Scheme 19 (1). The initial step involves the reduction of the 4-halobenzonitrile, yielding the corresponding radical anion (B), which promptly undergoes

cleavage, generating the benzonitrile radical (C) along with the corresponding halide ion. Subsequently, the radical undergoes further reduction at the electrode surface, resulting in the formation of the benzonitrile anion (D). This anion can then interact with CO_2 in an environment saturated with CO_2, leading to the formation of the 4-cyanobenzoate anion (E).

Conversely, the anion radical derived from fluorobenzonitrile reacts with CO_2 instead of undergoing dimerization, resulting in the creation of a carboxylated derivative of benzonitrile, as illustrated in Scheme 19 (2). However, this derivative proves unstable during highly negative reduction processes, undergoing further reductions following the same mechanism previously described for the other halobenzonitriles (X = Cl, Br, or I). Nonetheless, another notable effect arises from the potential incorporation of their lone pair. This effect governs their inclination to gain electrons and undergo reduction in the following order: I > Br > Cl > F. This order suggests that the halogen's lone pair can be integrated into conjugated systems, thereby influencing the reduction potential values. In addition, the nature of cathode electrode is investigated in this study stating that if graphite carbon is used as a working electrode, there will be dimerization of two 4-flourobezonnitrile to give 4,4-biphenyldicarbonitrile and 4,4-dicyanobibenzene. When employing silver (Ag) foil as the working electrode, benzonitrile and its dimer derivatives are also generated. In this context, it appears that the electrochemical reduction mechanism is consistent in both scenarios. However, the utilization of silver appears to promote the de-cyanidation of the resulting products, likely attributable to the adsorption of reduction intermediates on the electrode surface. The presence of 4-

hydroxybenzonitrile can be attributed to the reactivity of the initial reactant (4-F-benzonitrile) within the electrolyte medium following electrolysis. It can be deduced that for benzonitrile derivatives containing Cl, Br, and I, the electrocarboxylation process likely proceeds through a nucleophilic interaction between the benzonitrile anion and CO_2. Conversely, in the case of 4-F-benzonitrile, the electrocarboxylation process appears to be initiated by a reaction between the 4-F-benzonitrile radical anion and CO_2. The idea of the existence of halogen substituents in aromatic compounds, which are electron-withdrawing due to their greater electronegativity, facilitates their reduction. That means fluoro compound has the most electronegativity among other halo benzonitrile compounds, which will lead the fluoro compound to take a different route.
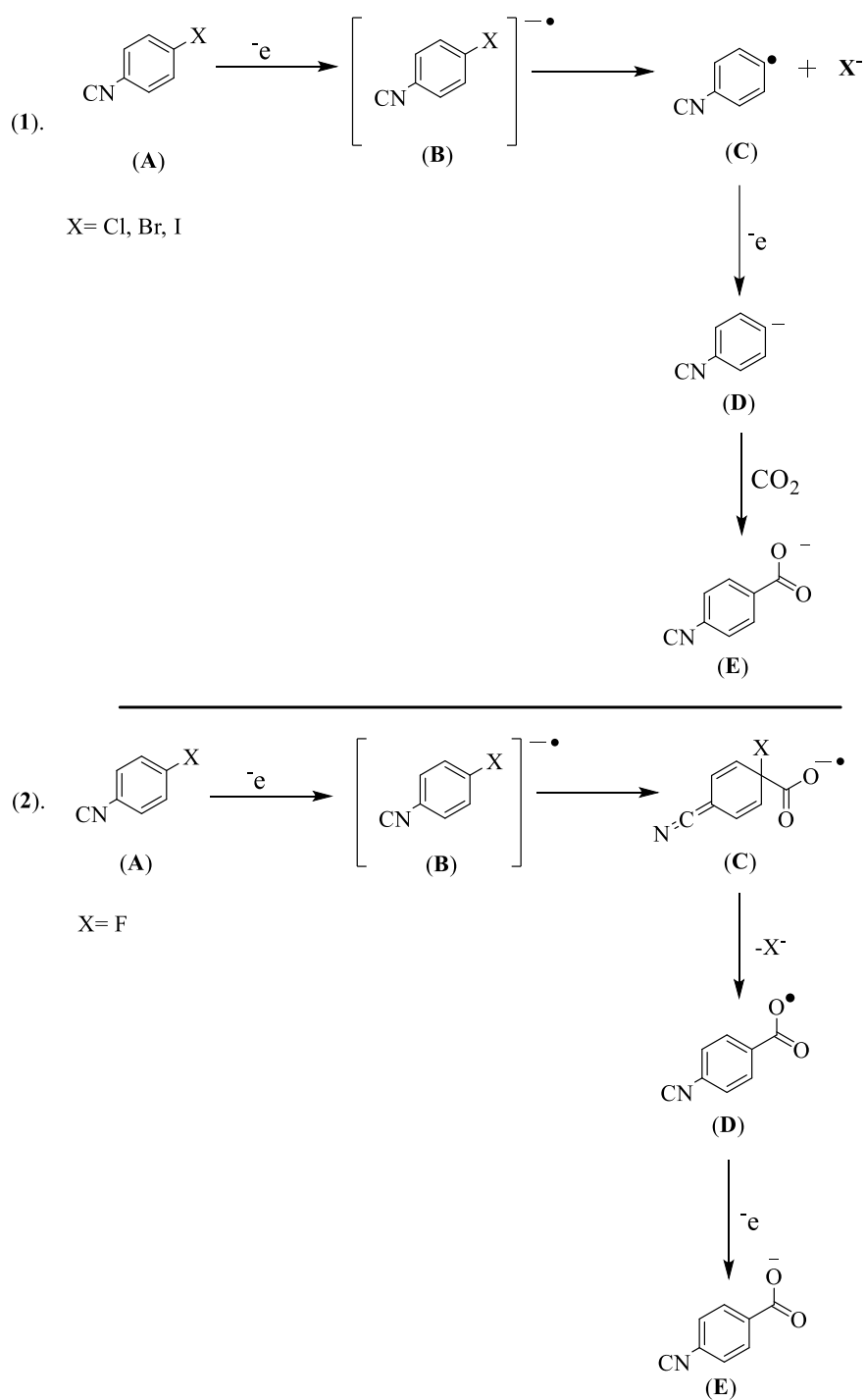
Scheme 19. *Shows (1) electro-carboxylation of 4-halo benzonitrile (X=Cl, Br, or I), (2)*

illustrates the final product(s) after electro-carboxylation of 4-fluoro benzonitrile [24].

A summary of these results is given in Table 1 [24]:

Table 1. *Shows the obtained product(s) distribution in the electrolysis of 10 mM of 4-halobenzonitriles (X= F, Cl, Br, I).*

Cathode	Entry	Halo benzonitrile (X)	Applied (E vs SCE)	Yield of Carboxylated Products	
				Mono	Di
Ag	1	F	-2.75	0	40
	2	Cl	-2.05	31	49
	3	Br	-1.90	1	87
	4	I	-1.80	39	67
Carbon	5	Cl	-2.15	15	23
	6	Br	-2.10	27	18
	7	I	-2.10	16	12

Furthermore, it is worth noting that numerous compounds incorporate halides as substituent functional groups and have been used as a substrate in the electro-carboxylation and reduction of carbon dioxide [24].

In the work by Wu et al. in 2018 [25], they unveiled a simple yet highly effective electrocatalytic method for converting methyl benzyl chloride into carboxylic acids using CO_2. This cutting-edge process occurs within a solitary electrolysis chamber, utilizing a copper foam cathode alongside a magnesium sacrificial anode, all while operating at room temperature and under a 1 atm CO_2 atmosphere. No supplementary catalysts are required,

eliminating the necessity for noble metals. The study (Scheme 20) involves examining the effect of different substituted positions on the reaction of the three isomers o-, m-, and p) of methyl benzyl chloride. To further understand the effect of substituent group position and improving the para-position yield, an electron-donating group ($-OCH_3$) or an electron-withdrawing group ($-CF_3$) was placed at the para position (Scheme 20). A lower yield was obtained with the electron-donating group (methoxy), while a higher yield was achieved with the electron-withdrawing group (trifluoroethane), as having an electron withdrawing group makes the substrate easier to reduce.

0.1 M TEAI, MeCN
2 F/mol, CO_2

Cu (-) , Mg (+)
r.t.

(83 %)

o- Methyl benzyl Chloride

(85 %)

m- Methyl benzyl Chloride

(87 %)

p- Methyl benzyl Chloride

(72 %)

(76 %)

(88 %)
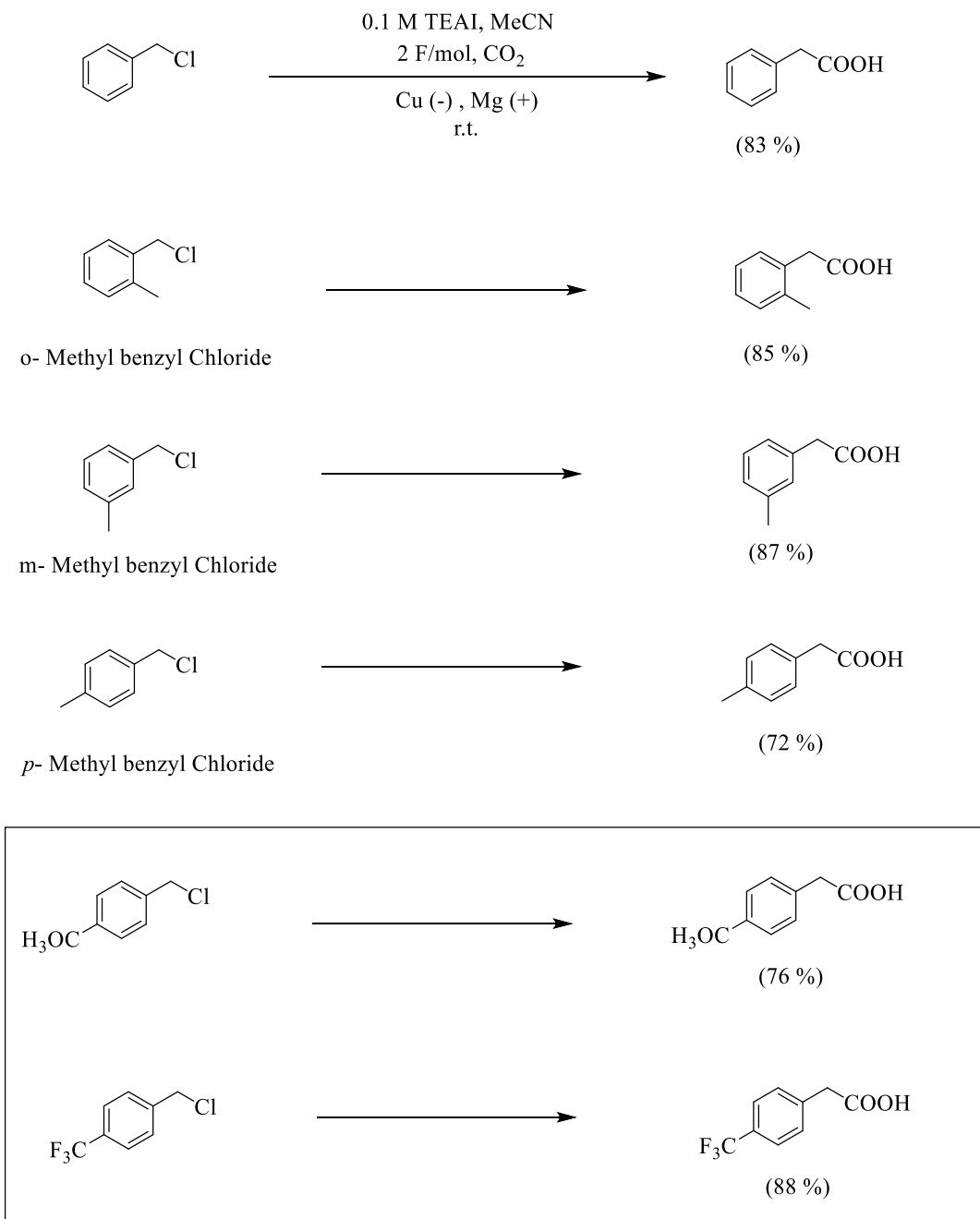
Scheme 20. *Shows the electro-carboxylation of benzylic halides* [25].

In a study conducted by Yang and colleagues in 2019 [25], they demonstrated a straightforward and effective electrochemical carboxylation method for benzylic C−N bonds utilizing CO_2 under ambient conditions. This technique proved successful for both primary and secondary benzylic C−N bonds.

In 2011, Senboku [26] reported a study clarifying the electro-carboxylation mechanism of 2-alloloxybromobenzene. When the electrochemical reduction of 2-alloloxybromobenzene (referred to as compound A in Scheme 21) was conducted in DMF, an undivided cell was employed. The cell featured a platinum cathode and a magnesium anode. This reduction took place in the presence of carbon dioxide and 0.5 equivalents of methyl 4-tert-butylbenzoate, which served as an electron transfer mediator. This process led to the specific formation of the corresponding aryl radical (B). Subsequently, this radical underwent cyclization to produce compound C. This transformation was followed by an electron transfer event, resulting in the formation of compound D. Notably, carbon dioxide was effectively incorporated during this series of reactions, leading to the successful generation of 2,3-dihydrobenzo[*b*]furan-3-ylacetic acid (referred to as compound E in Scheme 21) with an impressive yield of 82% [26].
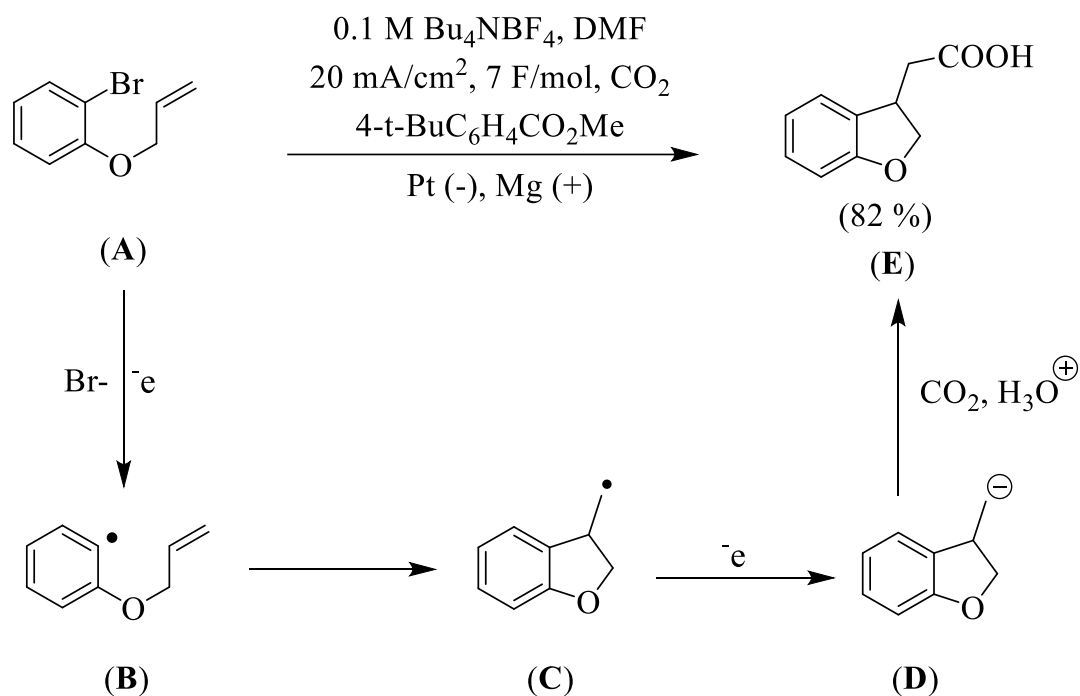
Scheme 21. *Demonstrates the electrochemical carboxylation of 1-(Allyloxy)-2-bromobenzene* [26].

Wang et.al. 2022 [27]. presents an effective and straightforward method for synthesizing valuable β-hydroxy acid derivatives using easily accessible aryl epoxides and CO_2, demonstrating notable chemo- and regioselectivity. This is achieved under gentle and environmentally sustainable electrochemical conditions (Scheme 22).
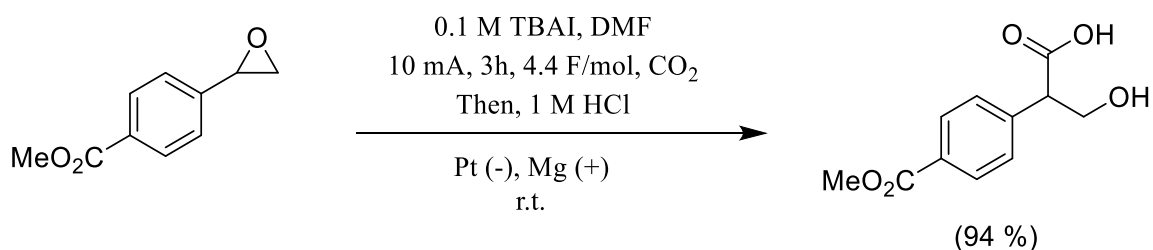
Scheme 22. *Shows the electro-carboxylation of aryl epoxides* [27].

The proposed reaction mechanism is explained as follows (Scheme 23).
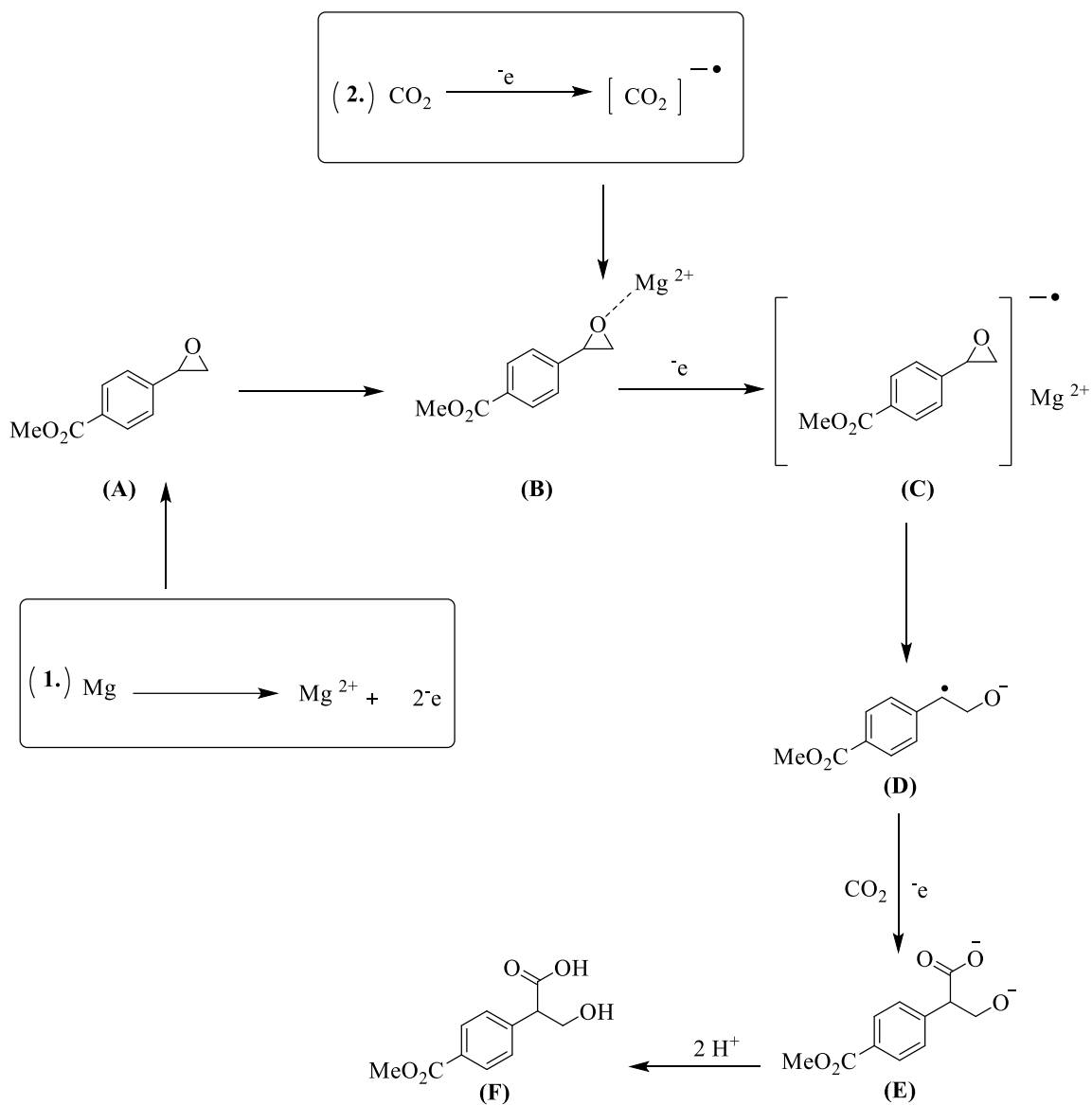
Scheme 23. *Displays how methyl 4-(oxiran-2-yl) benzoate undergoes electro-*

carboxylation. with carbon dioxide [27].

Magnesium ions were continuously generated on the anode and these then associated with the epoxide (A), providing intermediate (B). Two possible pathways were proposed in the next step. (1) Direct electrochemical reduction occurred predominantly for substrates with more positive reduction potentials, furnishing intermediate (C). On the other hand, the electrochemical reduction of CO_2 generated a CO_2 radical anion through a one-electron reduction process (2). As an alternative pathway, the generated CO_2 radical anion gives one electron to the epoxide to give intermediate (C). Then, intermediate (C) underwent C-O bond cleavage to give the C-centered radicals (D). Subsequently, another one-electron reduction and C-nucleophilic attack of CO_2 resulted in intermediate (E), which finally yielded β-hydroxy acids (F) after work-up with aqueous HCl.

Additionally, electrochemical carboxylation of benzyl carbonates has been examined and studied (Scheme 24) [1].

Reaction conditions above arrow: 0.1 M Bu_4NBF_4, CH_3CN, 45 mA/cm^2, 10 F/mol, CO_2, Pt (-), Mg (+), r.t.

R= Me OR Et

R= Me (89 %)
R=Et (93 %)
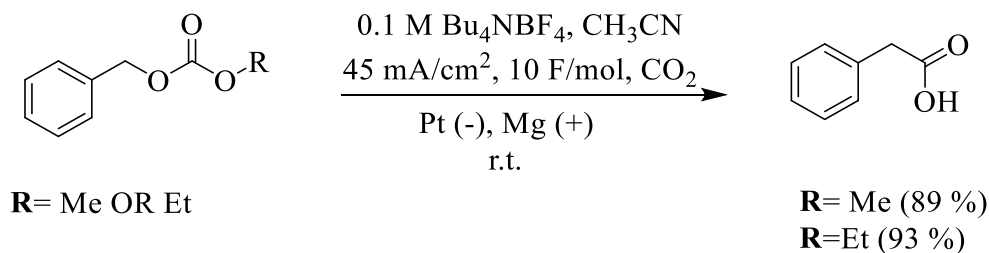
Scheme 24. *Shows the electro-carboxylation of benzyl carbonate* [1].

Flavones have been investigated within this domain as one of the chemical substrates by many scientists. One of these works is Senboku et.al., 2011 [28], where flavones underwent reductive carboxylation at the C_2 position in a remarkably regioselective

fashion to produce flavanone-2-carboxylic acids. This transformation was achieved

through constant current electrolysis of flavones in DMF containing 0.1 M Bu_4NBF_4,

with the presence of CO_2, utilizing a one-compartment cell equipped with a Pt cathode

and an Mg anode.

reaction conditions:
0.1 M Bu_4NBF_4, DMF
15 mA/cm^2, 4 F/mol, CO_2
Pt (-), Mg (+)
0 ^{O}C

(78 %)
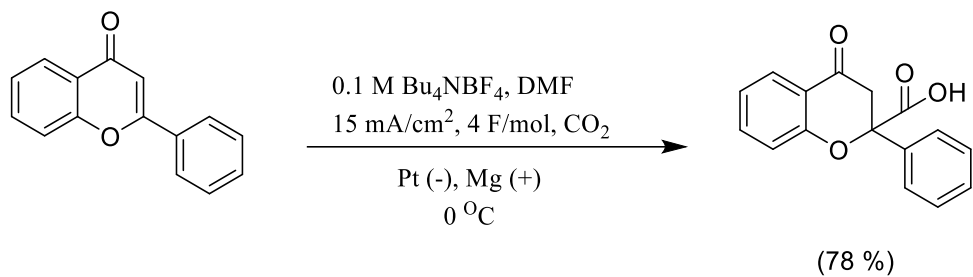
Scheme 25. *Shows the electro-carboxylation of Flavones* [28].

At the Anode:

$$Mg \longrightarrow Mg^{2+} + 2\,^-e$$
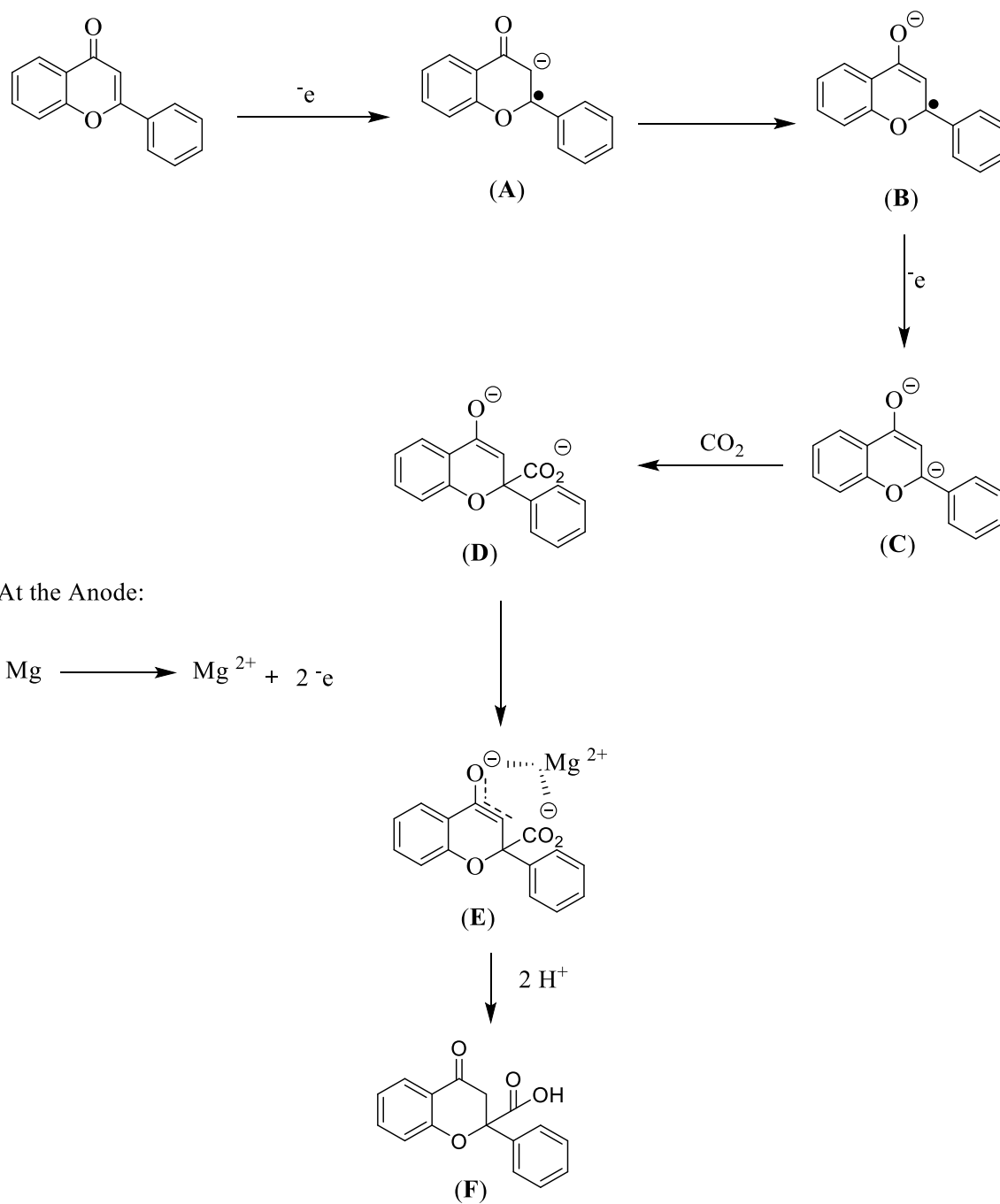
Scheme 26. *Illustrates the mechanism of Flavones electro-carboxylation* [28].

Scheme 26 illustrates potential reaction pathways. When considering the cathode, the favored process involves a one-electron reduction of flavone, leading to the formation of a radical anion (A). This (A) species can resonate into a more stable enol form (B), followed by an additional one-electron reduction, resulting in a dianion (C). By selectively targeting the C_2 position, CO_2 can be incorporated, forming the carboxylate ion (D). The reason of targeting the C_2 position is that the enolate moiety within dianion C exhibits lower reactivity compared to the anion present at the C_2 position of C. As a result, CO_2 engages in a reaction with dianion C specifically at its C_2 position. Conversely, at the anode, magnesium metal dissolution occurs, producing magnesium ions. The carboxylate ion (D) can readily captu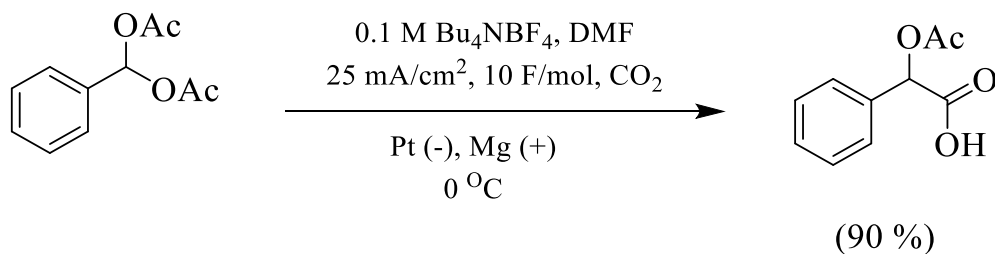re these magnesium ions, forming a salt (E), which, upon exposure to an acidic treatment, transforms into a carboxylic acid (F).

As mentioned previously, the use of carbon dioxide as a carbon source for carboxyl groups would provide a novel environmentally benign synthesis of many chemical products that can be used in many applications. One of these products is Mandel acid, 2-hydroxy-2-phenylacetic acid, and its derivatives are useful and important as synthetic intermediates biologically active compounds. Senboku et.al., 2019 found an efficient synthesis of Mandel acetates by electrochemical carboxylation of benzal diacetates (Scheme 27) [29].

$$\text{0.1 M Bu}_4\text{NBF}_4\text{, DMF}$$
$$25 \text{ mA/cm}^2\text{, 10 F/mol, CO}_2$$
$$\text{Pt (-), Mg (+)}$$
$$0\,^{\circ}\text{C}$$

(90 %)

Scheme 27. *Illustrates the electro-carboxylation of benzal diacetate* [29].

Senboku et.al. (2019) gave two possible routes of formation of the intermediate carboxylated compound (Scheme 28).

At the Anode:

$$Mg \longrightarrow Mg^{2+} + 2\ ^-e$$
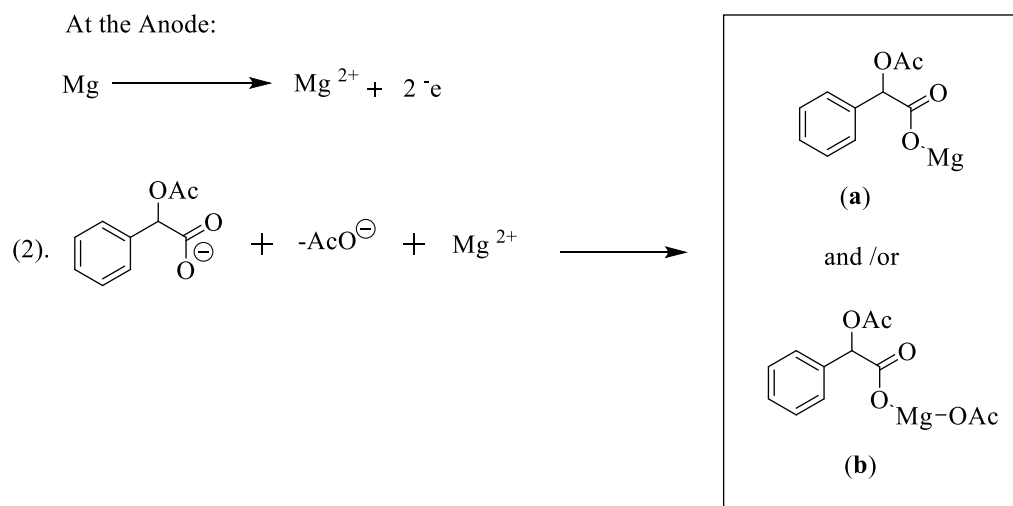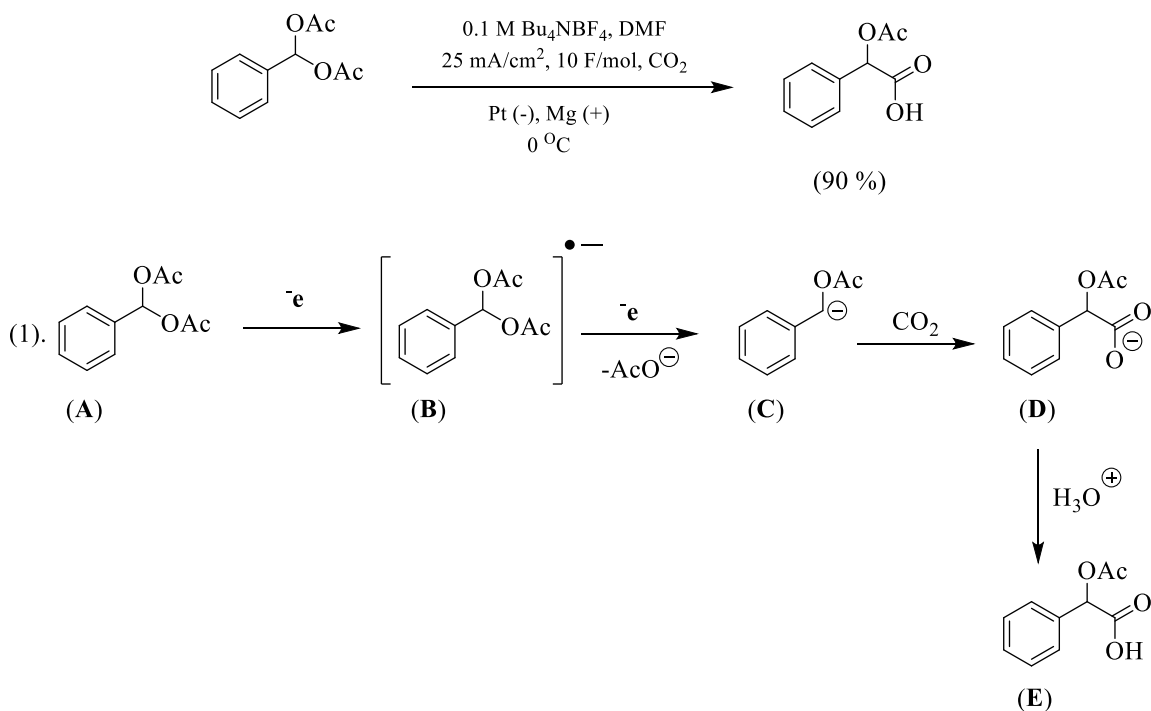
Scheme 28. *Illustrates the electro-carboxylation mechanism of benzal diacetate* [29].

In Scheme 28 there is a one electron reduction of A at the cathode, generating the corresponding radical anion B. Further one-electron reduction and elimination of one acetate ion at the benzylic position generates the corresponding benzylic carbanion C, which reacts with carbon dioxide to give the corresponding carboxylate ion D. On the other hand, at the anode, the dissolution of an anode metal, magnesium, takes place to generate Mg^{2+}. In the reaction medium, the metal ions and carboxylate ions D exist as metal salts (a and/or b). Acid treatment in work-up gives carboxylic acid E.

In addition, there are many papers published on the electro-carboxylation reduction of alkenes as one of the chemical substrates which is investigated in this field [30].

(a)   (b)   (c)   (d)
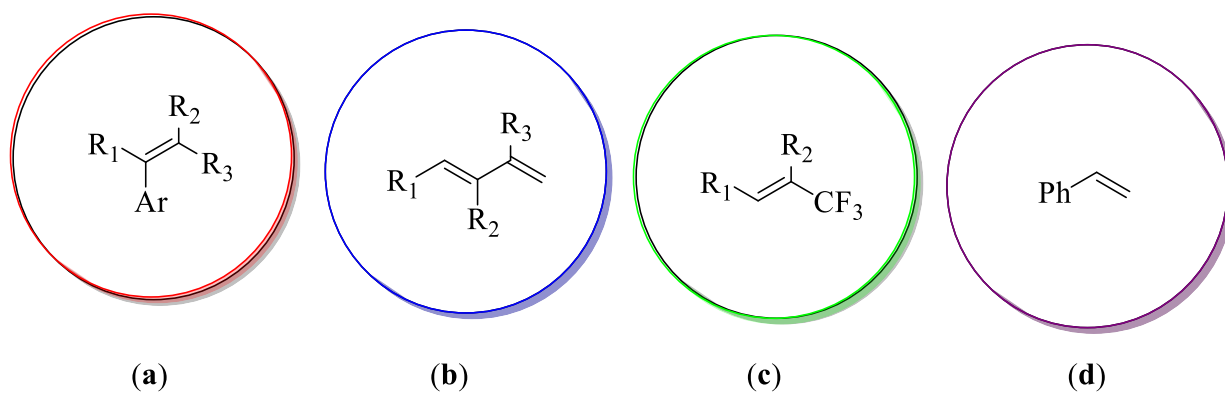
Scheme 29. *Illustrates some alkenes examples which is been investigated the electro-carboxylation field* [31].

a. **Electrochemical carboxylation of Phenyl substituted Alkenes.**
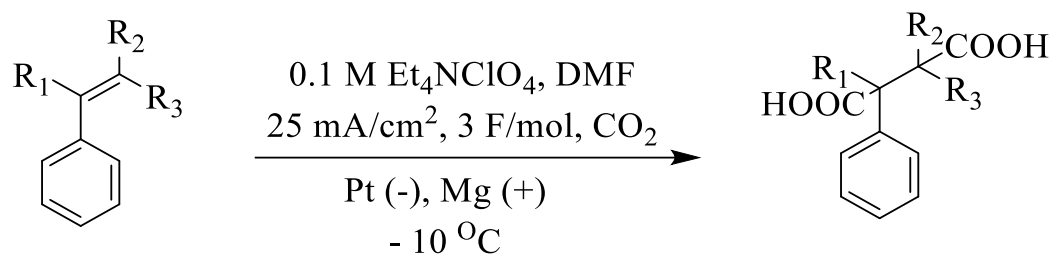
Scheme 30. *Illustrates the electrochemical carboxylation of phenyl substituted*

alkenes [30].
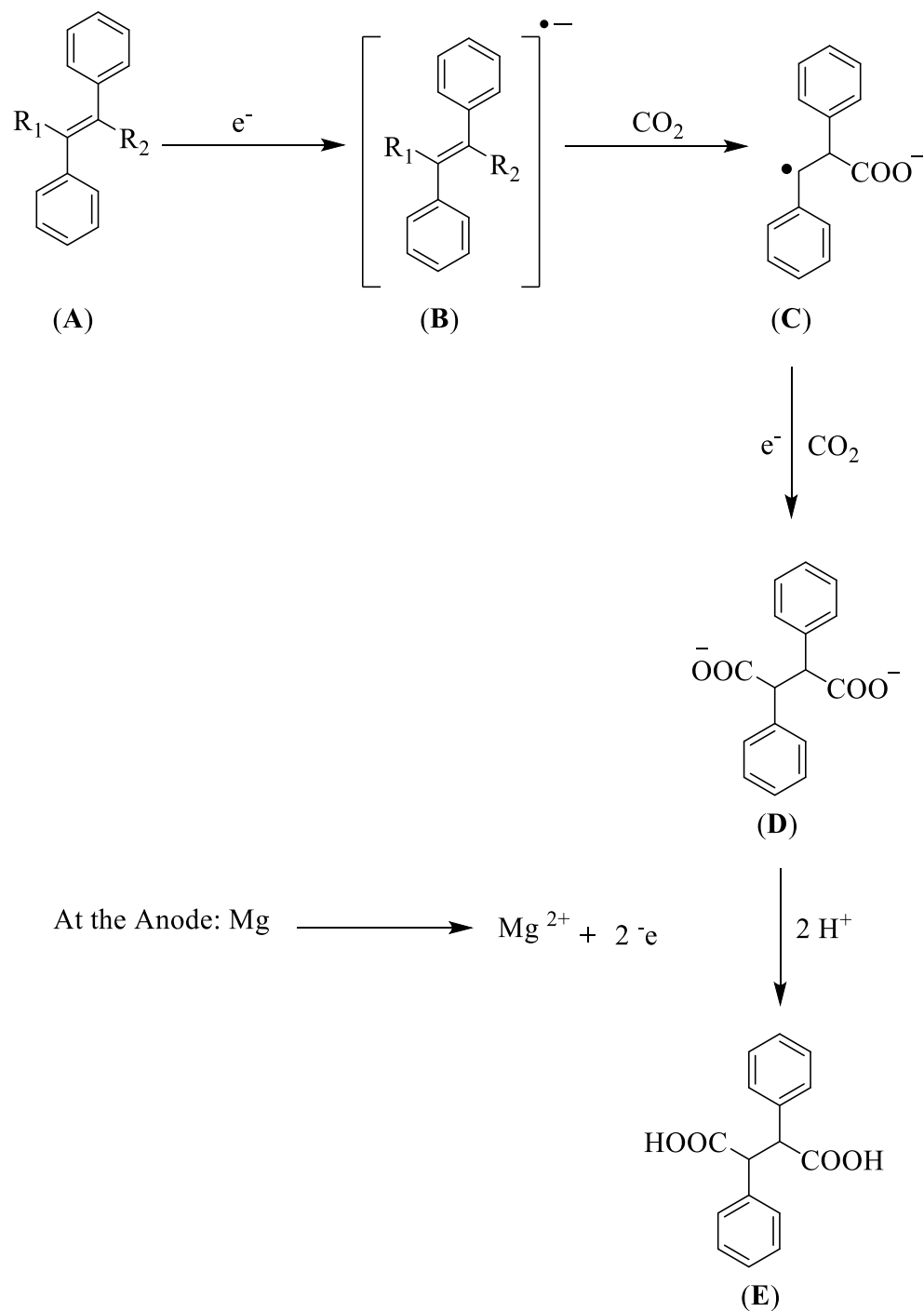
Scheme 31. *Illustrates the electrochemical carboxylation mechanism of phenyl substituted alkene* [30].

The electrochemical carboxylation of E-stilbene A (Scheme 31) would start at reduction of A and then formation of the corresponding alkene radical. The reason for this is because E-stilbene's reduction potential is the same or slightly more positive than that of carbon dioxide. The final product of trans-stilbene electro-carboxylation is 2,3 diphenyl succinic acid. However, Senboku et.al., 2001 discussed the possibility of another pathway when it comes to styrene derivatives (note that this will be discussed in Scheme 37). The results of reaction with various substrates are summarized in Table 2.

Table 2*. Shows the obtained carboxylated product(s) from electroreduction of phenyl substituted alkenes in the presence of CO_2 [30].*

Entry	Alkene	Product	Yield %
1	Styrene	Phenylsuccinic acid	66 %
2	α-Methyl Styrene	2,2-Disubstituted succinic acids	68 %
3	E-β-Methyl Styrene	2-Methyl-3-phenylsuccinic acid	77 %
4	Z-β-Methyl Styrene	2-Methyl-3-phenylsuccinic acid	70 %
5	1,1 Dipheylethylene	2,2-Disubstituted succinic acids	91 %
6	E-Stilbene	2,3-Diphenylsuccinic acid	84 %
7	Z-Stilbene	2,3-Diphenylsuccinic acid	84 %

Senboku et al's 2001 study can be summarized as follows:

1- Trans and Cis chemical structures of the same species did not make much

   difference in terms of the yield of the products which contained 2 phenyl rings

   e.g., stilbene.

2- Beta's (β) chemical structures had a high yield in comparison to alpha (α) for the

   same chemical substrate (Methyl styrene).

3- Substitution by two phenyl rings at the same carbon will give the highest yields

   for instance: 1,1-diphenylethylene, with 91% yield at low temperature [30].

b. Electrochemical carboxylation of dienes.
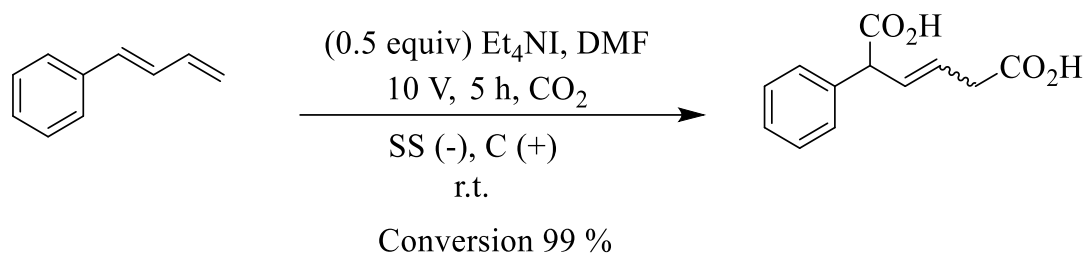
Scheme 32. Illustrates the electro-carboxylation conditions of *1-phenyl- 1,3- butadiene*

[32].
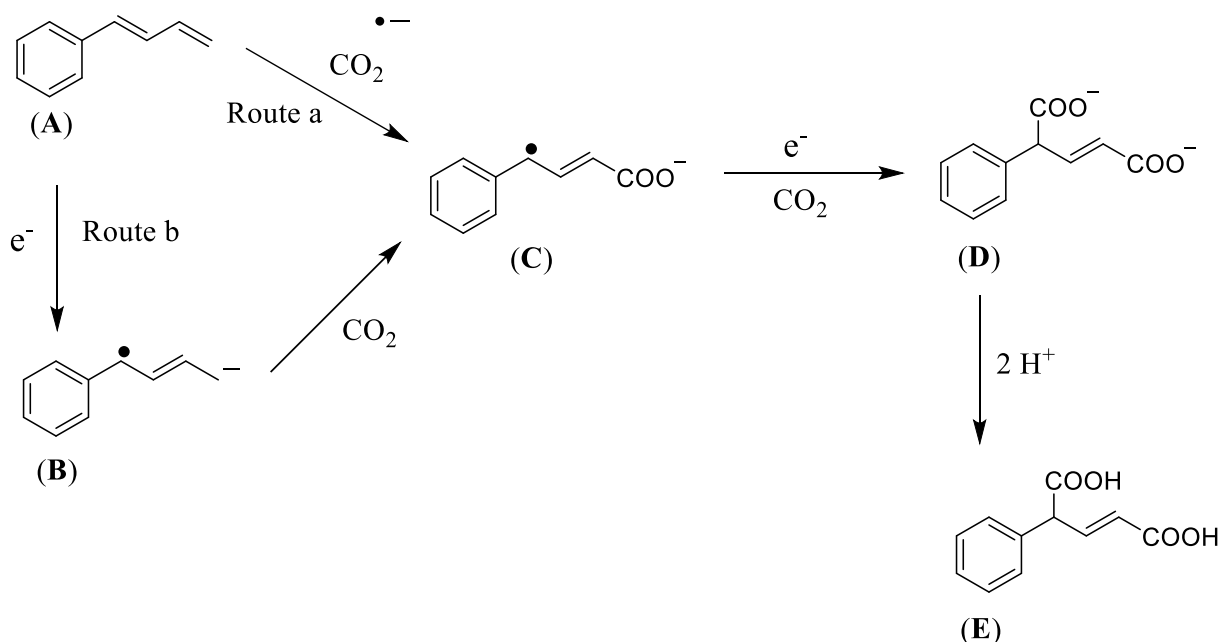
Scheme 33. *Illustrates the mechanism of 1-phenyl-1,3-butadiene electro-carboxylation* [32].

The mechanism could take two routes a, and b. First, 1-phenyl-1,3-butadiene A could react with a carbon dioxide radical, reduced previously at the electrode. Afterward, C is formed. A further one-electron reduction in the presence of carbon dioxide leads to D. Then, the formation of final product E occurs after protonation. However, the reduction could also take another route b, where 1-phenyl-1,3-butadiene is reduced to its radical and then reacts with carbon dioxide.

c. **Electrochemical defluorinative carboxylation of α-CF$_3$ alkenes.**
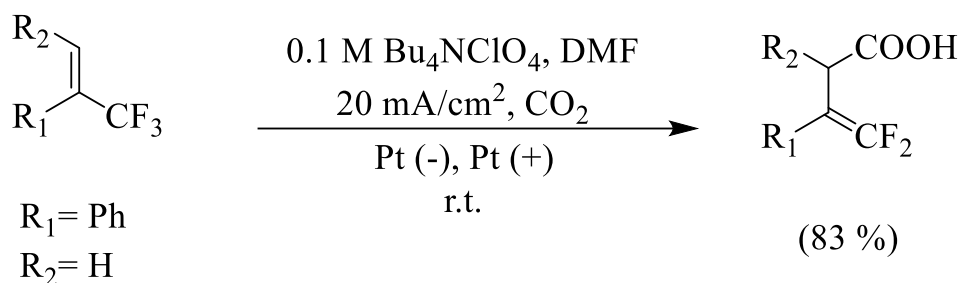
Scheme 34. *Illustrates electrochemical defluorinative carboxylation of α-CF₃ alkenes* [33].
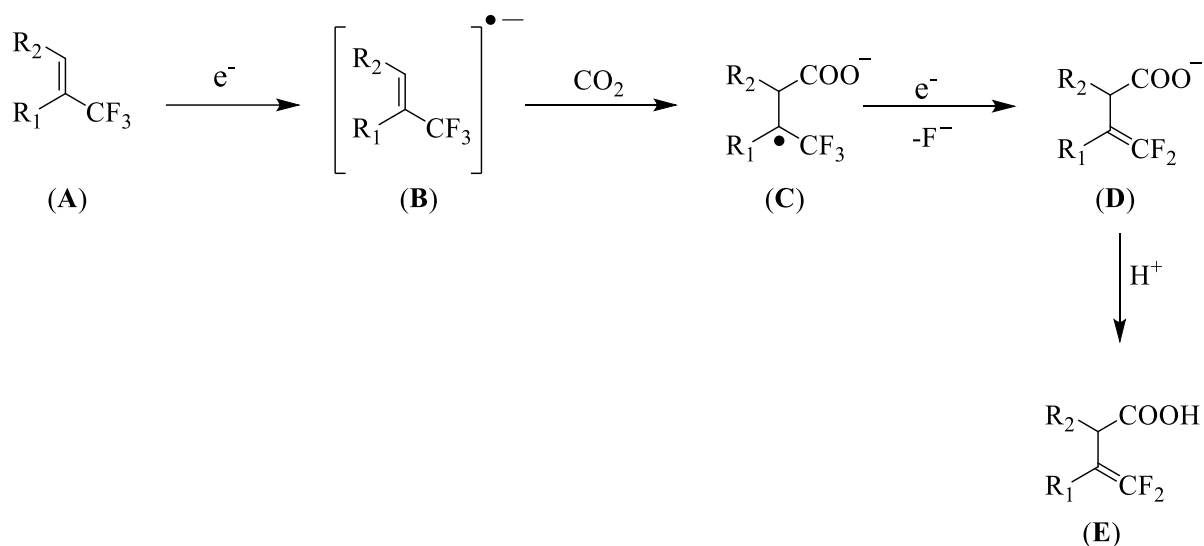
Scheme 35. *Depicts the electrochemical mechanism of trifluoromethyl alkene carboxylation.* [33].

α-CF₃ alkenes undergoes reduction by one electron to form radical B. Then it reacts with carbon dioxide to form C. A further electron reduction will defluorinate the species (-F⁻) and will form the intermediate D which will be protonated afterward and form the final products E.

d. **Electrochemical Carboxylation of styrene derivatives.**

$$0.1 \text{ M TEABr, CH}_3\text{CN}$$
$$16 \text{ mA/cm}^2, 3 \text{ F/mol, CO}_2$$
$$\overline{\text{Ti (-), Mg (+)}}$$
$$0 \,^O\text{C}$$

(80 %)
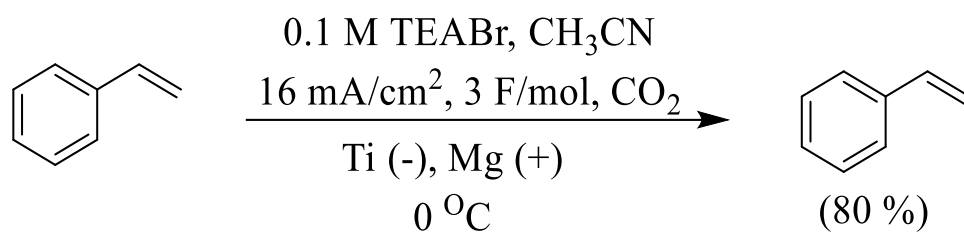
Scheme 36. *Illustrates* electrochemical carboxylation of Styrene [34].

(A) e⁻ (B) CO₂ (C) e⁻ (D)

CO₂

(E)

2 H⁺

(F)
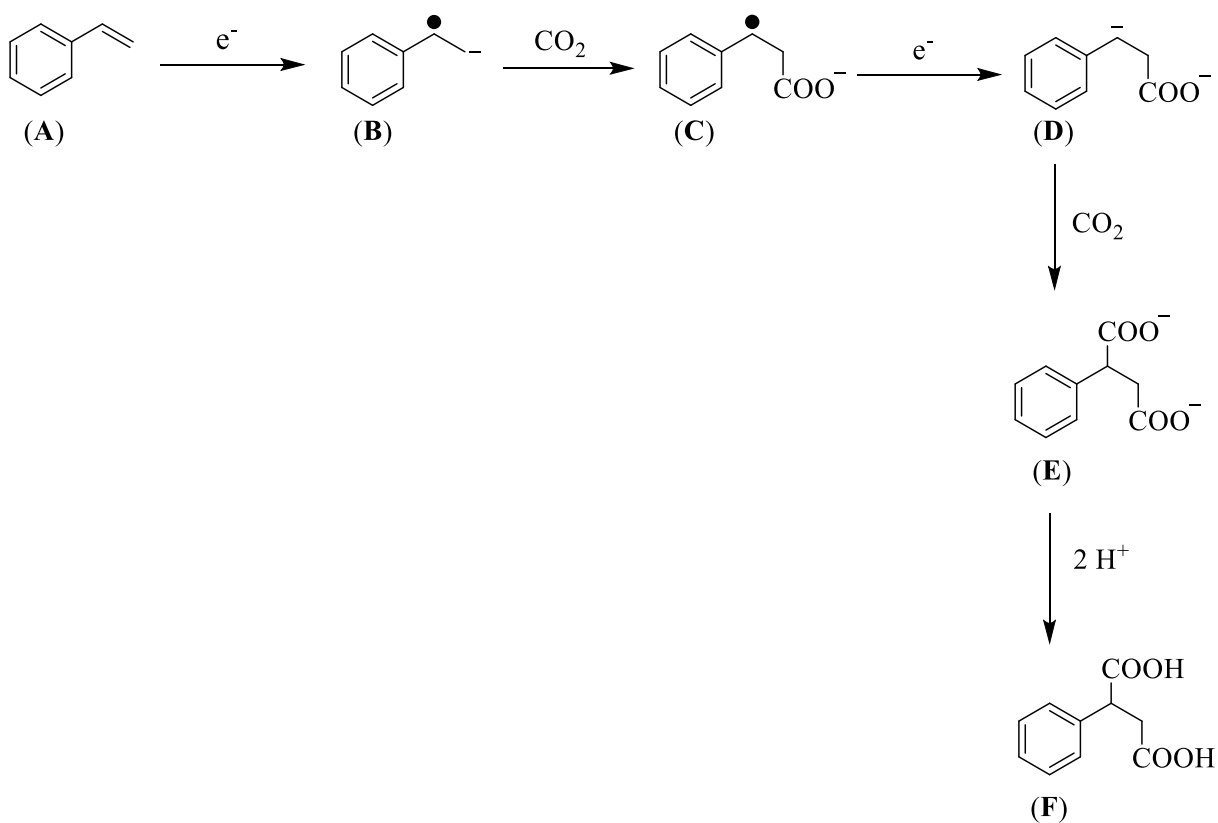
Scheme 37. *demonstrates how styrene undergoes electrochemical carboxylation.*[34].

Styrene A undergoes a direct one-electron reduction, resulting in the formation of its

anion radical B. The reaction between B and CO_2 produces an intermediate known as

monocarboxylated C. Subsequent one-electron reduction, followed by a reaction with

CO_2, results in the creation of the dicarboxylation product E. During the electrolysis

process, Mg metal dissolves, leading to the presence of Mg^{2+} ions at the anode. These

magnesium ions readily interact with carboxylate ions E, forming stable magnesium

carboxylate complexes. Upon undergoing an acid treatment, these complexes yield the

dicarboxylic acid 2-phenylsuccinic acid F.

Yuan et.al., 2008 [35]. have studied the electro-carboxylation of varied phenyl substituted

alkenes including styrene and stilbene derivatives. One of the styrene derivatives which

has been investigated in this study was 4-methoxy styrene to produce 2-(4

methoxyphenyl) succinic acid, Scheme 38.
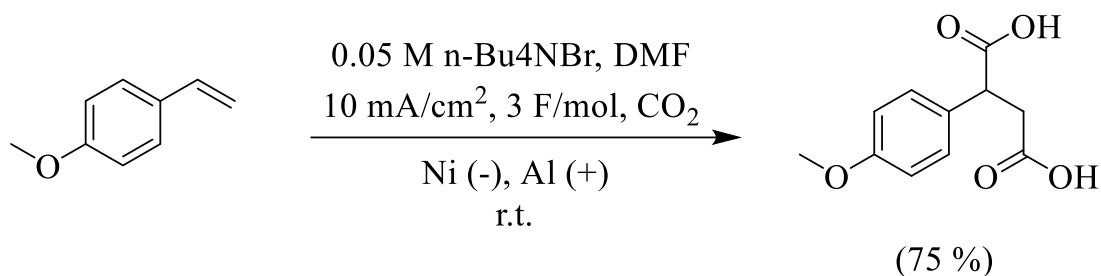
Scheme 38. *Shows the electrochemical carboxylation of 4-methoxy styrene* [35].

Yuan et.al., 2008 also examined many substituted styrenes to produce a variety of

succinic acids in high yields at room temperature, Scheme 39.
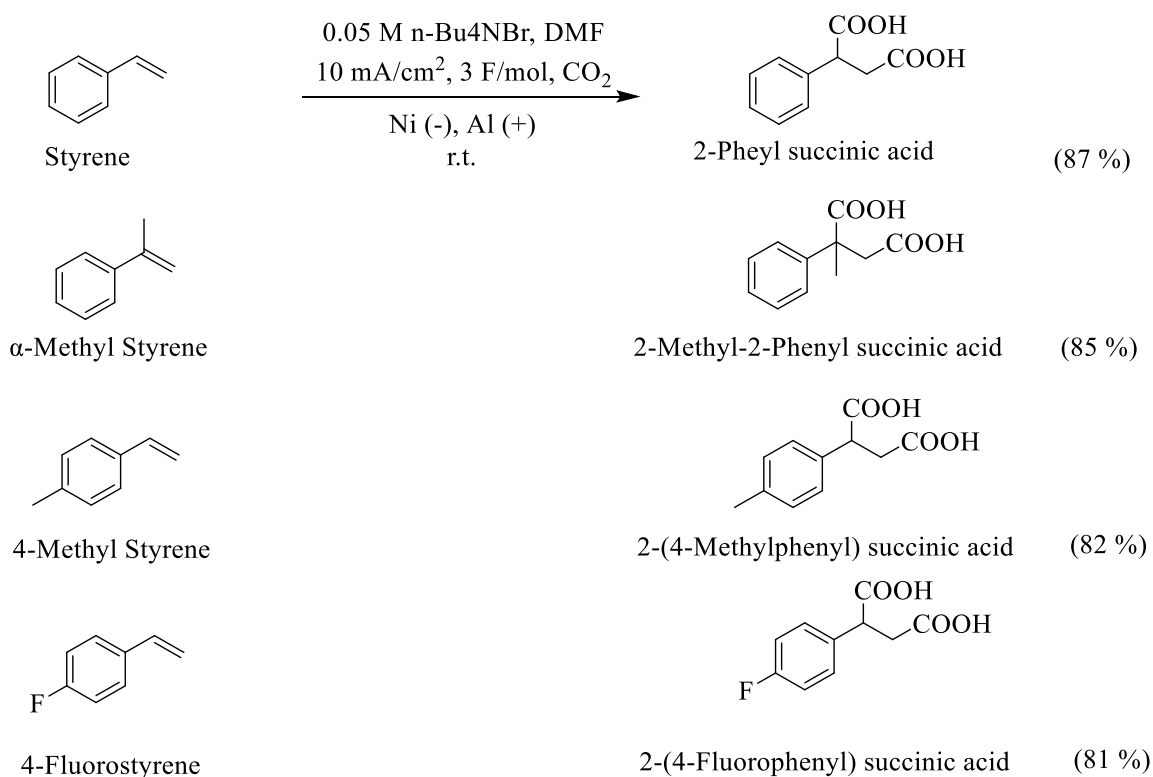
Scheme 39. *Shows the* electrochemical carboxylation of varied substituted alkenes under carbon dioxide [35].

In comparison to Senboku et al. (2001) and Yuan et al. (2008), it can be seen that both studies have used totally different reaction conditions. Yuan et al. (2008) used Ni a cathode and Al as anode, while Senboku et.al. (2001) used Pt cathode and Mg as an anode [30, 35]. Another different reaction condition is the temperature in Senboku et.al.,2001 he applied -10 ^{O}C, while Yuan et.al.,2008 proven that the selectivity of the products after electro carboxylation may differ as the rection kinetics would change based on the applied temperature during the electrolysis. For example, when styrene is electro-carboxylated in Senboku et.al.,2001, (Table 2) the obtained phenyl succinic acid yield as the only product is 66%, while in Yuan et.al.,2008 the obtained yield for the same product

is 87% Scheme 39. In Yuan et.al.,2008 there is evidence of some by-products when the reaction conditions were examined such as changing reaction temperature, carbon dioxide pressure, or current density.

Senboku et.al.,2001 also studied 1,2-dihydronaphthalene as one of the phenyl alkenes scheme 40.
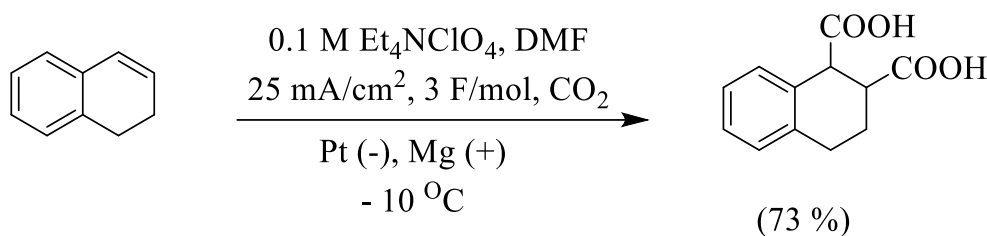
Scheme 40. *Shows the electrochemical carboxylation of 1,2-dihydronaphthalene* [30].

In Scheme 7, we discussed the electro-carboxylation of naphthalene compounds, which resulted in the fixation of two carboxylic groups in different positions. This differs from Scheme 40 presented by Senboku et al. in 2001, where one of the rings had only one double bond. Specifically, the electrocarboxylation of naphthalene yielded 1,4-dihydro-1,4-naphthalenedicarboxylic acid as the product, while the electrocarboxylation of 1,2-dihydronaphthalene resulted in 1,2,3,4-tetrahydro-1,2-naphthalenedicarboxylic acid [18, 30].

However, our work is based on alkenes substrates, specifically, phenyl-substituted alkenes. There will be a deep experimental investigation of the previous phenyl-substituted alkenes in Chapter 3 (a and d, scheme 29, Chapter 1).

The focus of this project will include substrates with one phenyl aromatic ring (styrenes) and two phenyl aromatic rings (stilbenes), see Scheme 41, and some of their derivatives.
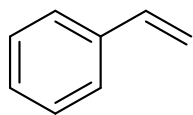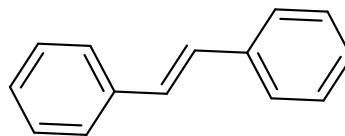
(a) **(b)**

Scheme 41. *Shows chemical structures of (a) Styrene; and (b) Stilbene compounds.*

Nevertheless, the activation and effective utilization of CO_2 presents ongoing challenges primarily because it exists as the most oxidized form of carbon, exhibiting both thermodynamic stability and kinetic inertness in specific desired reactions.

This concept prompted the integration of carbon dioxide capture into the electrochemical reaction using electrode mesh. The aim was to prolong its presence on the working electrode surface to ensure the reduction of CO_2 and its reaction with the selected substrates. This approach lays the groundwork for future investigations into different electrode meshes and their impact on yield and product selectivity. However, this thesis will primarily focus on the utilization of nickel mesh as a starting point. Some discussion on the choice of nickel is done in (chapter 3) will show the benefits of choosing Ni mesh electrode.

References

[1]. Senboku, H. Electrochemical Fixation of Carbon Dioxide: Synthesis of Carboxylic Acids. *Chem. Rec.*, **21** (9), 2354–2374 (2021).

[2]. Saputra, R., Khalid, M., Walvekar, R., & Pariatamby, A. Circular carbon economy. In *Emerging carbon capture technologies* (pp. 427-462). Elsevier, (2022).

[3]. Hansen, J., Kharecha, P., Sato, M., Masson-Delmotte, V., Ackerman, F., Beerling, D. J., & Zachos, J. C. Assessing "Dangerous Climate Change": Required Reduction of Carbon Emissions to Protect Young People, Future Generations and Nature. *PloS one*, **8** (12), e81648, (2013).

[4]. Pradhan, S., & Das, S. Recent Advances on the Carboxylations of C(sp3)–H Bonds Using CO2 as the Carbon Source. *Synlett*. (2023).

[5]. Oh, Y., Vrubel, H., Guidoux, S., & Hu, X. Electrochemical Reduction of CO2 in Organic Solvents Catalyzed by MoO2. *Chem. Commun.*, **50** (29), 3878–3881 (2014).

[6]. Liu, Q., Wu, L., Jackstell, R., & Beller, M. Using Carbon Dioxide as a Building Block in Organic Synthesis. *Nat. Commun.*, **6** (1), 5933 (2015).

[7]. Liu, X. F., Zhang, K., Tao, L., Lu, X. B., & Zhang, W. Z Recent Advances in Electrochemical Carboxylation Reactions Using Carbon Dioxide. *Green Chem. Eng.*, **3** (2), 125–137 (2022).

[8]. König, M., Vaes, J., Klemm, E., & Pant, D. Solvents and Supporting Electrolytes in the Electrocatalytic Reduction of CO2. *Iscience*, **19**, 135-160., (2019).

[9]. Chaplin, R. P. S., & Wragg, A. A. Effects of Process Conditions and Electrode Material on Reaction Pathways for Carbon Dioxide Electroreduction with Particular Reference to Formate Formation. *J. App. Electrochem.*, **33**, 1107-1123, (2003).

[10]. Wang, S., Feng, T., Wang, Y., & Qiu, Y. Recent Advances in Electrocarboxylation with CO2. *Chemistry - An Asian Journal*, **17** (17), e202200543 (2022).

[11]. Zhang, X., Guo, S. X., Gandionco, K. A., Bond, A. M., & Zhang, J. Electrocatalytic Carbon Dioxide Reduction: From Fundamental Principles to Catalyst Design. *Materials Today Advances*, *7*, 100074 (2020).

[12]. Dell'Amico, L., Bonchio, M., & Companyó, X. Recent Advances in Electrochemical Carboxylation of Organic Compounds for CO2 Valorization . *CO2 as a Building Block in Organic Synthesis*, *3*, 225–252 (2020).

[13]. Cauwenbergh, R., Goyal, V., Maiti, R., Natte, K., & Das, S. Challenges and Recent Advancements in The Transformation of CO2 into Carboxylic Acids: Straightforward Assembly with Homogeneous 3D Metals. *Chem. Soc. Rev.*, **51** (22), 9371–9423 (2022).

[14]. Duñach, E., Dérien, S., & Périchon, J. Nickel-Catalyzed Reductive Electrocarboxylation of Disubstituted alkynes. *J. Organomet. Chem*, **364** (3), C33-C36 (1989).

[15]. Dérien, S., Clinet, J. C., Duñach, E., & Périchon, J. Electrochemical Incorporation of Carbon Dioxide into Alkenes by Nickel Complexes. *Tetrahedron*, **48** (25), 5235-5248 (1992).

[16]. Sock, O., Troupel, M., & Perichon, J. Electrosynthesis of carboxylic acids from organic halides and carbon dioxide. *Tetrahedron letters*, *26*(12), 1509-1512 (1985).

[17]. Senboku, H., Yoneda, K., & Hara, S. (2015). Electrochemical direct carboxylation of benzyl alcohols having an electron-withdrawing group on the phenyl ring: one-step formation of phenylacetic acids from benzyl alcohols under mild conditions. *Tetrahedron Letters*, *56*(48), 6772-6776.

[18]. Yuan, G., Li, L., Jiang, H., Qi, C., & Xie, F. Electrocarboxylation of Carbon Dioxide with Polycyclic Aromatic Hydrocarbons Using Ni as The Cathode. *Chin. J. Chem.,* **28** (10), 1983–1988 (2010).

[19]. Sheta, A. M., Alkayal, A., Mashaly, M. A., Said, S. B., Elmorsy, S. S., Malkov, A. V., & Buckley, B. R. Selective Electrosynthetic Hydrocarboxylation of α,β-Unsaturated Esters with Carbon Dioxide**. *Angew. Chem. Int. Ed.* **60** (40), 21832–21837 (2021).

[20]. Senboku, H., Yamauchi, Y., Fukuhara, T., & Hara, S. Electrochemical Carboxylation of Aliphatic Ketones: Synthesis of β-keto Carboxylic Acids. *Electrochem.*, **74** (8), 612–614 (2006).

[21]. Silvestri, G., Gambino, S., & Filardo, G. Electrochemical Carboxylation of Aldehydes and Ketones with Sacrificial Aluminum Anodes. *Tetrahedron Lett.*, **27** (29), 3429–3430 (1986).

[22]. Seidler, J., Roth, A., Vieira, L., & Waldvogel, S. R. Electrochemical CO2 Utilization for The Synthesis of α-Hydroxy Acids. *ACS Sustain. Chem. Eng.*, **11** (1), 390–398 (2023)

[23]. Li, C. H., Song, X. Z., Tao, L. M., Li, Q. G., Xie, J. Q., Peng, M. N., & Xu, M. F. Electrogenerated-Bases Promoted Electrochemical Synthesis of N-Bromoamino Acids from Imines and Carbon Dioxide. *Tetrahedron*, **70** (10), 1855-1860 (2014).

[24]. Reche, I., Mena, S., Gallardo, I., & Guirado, G. Electrocarboxylation of Halobenzonitriles: An Environmentally Friendly Synthesis of Phthalate Derivatives. *Electrochimi. Acta.*, 320, 134576 (2019).

[25]. Wu, L. X., Sun, Q. L., Yang, M. P., Zhao, Y. G., Guan, Y. B., Wang, H., & Lu, J. X. Highly Efficient Electrocatalytic Carboxylation of 1-Phenylethyl Chloride at Cu Foam Cathode. *Catal.*, **8** (7), 273 (2018).

[26]. Senboku, H., Michinishi, J. Y., & Hara, S. Facile synthesis of 2, 3-dihydrobenzofuran-3-ylacetic acids by novel electrochemical sequential aryl radical cyclization-carboxylation of 2-allyloxybromobenzenes using methyl 4-tert-butylbenzoate as an electron-transfer mediator. *Synlett*, **2011** (11), 1567-1572 (2011).

[27]. Wang, Y., Tang, S., Yang, G., Wang, S., Ma, D., & Qiu, Y. Electrocarboxylation of Aryl Epoxides with CO2 for The Facile and Selective Synthesis of β-Hydroxy Acids. *Angew. Chem.*, **134** (38), e202207746 (2022).

[28]. Senboku, H., Yamauchi, Y., Kobayashi, N., Fukui, A., & Hara, S. Electrochemical Carboxylation of Flavones: Facile Synthesis of fFavanone-2-Carboxylic Acids. *Electrochem.*, **79** (11), 862-864 (2011).

[29]. Senboku, H., Sakai, K., Fukui, A., Sato, Y., & Yamauchi, Y. Efficient Synthesis of Mandel acetates by Electrochemical Carboxylation of Benzal Diacetates. *ChemElectroChem*, **6** (16), 4158-4164 (2019).

[30]. Senboku, H., Komatsu, H., Fujimura, Y., & Tokuda, M. Efficient Electrochemical Dicarboxylation of Phenyl-Substituted Alkenes: Synthesis of 1-Phenylalkane-1,2-Dicarboxylic Acids. *Synlett*, **2001** (3), 418–420 (2001).

[31]. Zhong, W., Huang, W., Ruan, S., Zhang, Q., Wang, Y., & Xie, S. Electrocatalytic Reduction of CO2 Coupled with Organic Conversion to Selectively Synthesize High-Value Chemicals. *Chem. Eur. J.,* **29** (20), e202203228 (2023).

[32]. Sheta, A. M., Mashaly, M. A., Said, S. B., Elmorsy, S. S., Malkov, A. V., & Buckley, B. R. Selective α, δ-Hydrocarboxylation of Conjugated Dienes Utilizing CO2 and Electrosynthesis. *Chem. Sci.*, **11** (34), 9109-9114 (2020).

[33]. Gao, X. T., Zhang, Z., Wang, X., Tian, J. S., Xie, S. L., Zhou, F., & Zhou, J. Direct Electrochemical Defluorinative Carboxylation of α-CF 3 Alkenes with Carbon Dioxide. *Chem.Sci.*, **11** (38), 10414-10420 (2020).

[34]. Wang, H., Lin, M. Y., Fang, H. J., Chen, T. T., & Lu, J. X. Electrochemical Dicarboxylation of Styrene: Synthesis of 2-Phenylsuccinic Acid. *Chin. J. Chem.*, **25** (7), 913-916 (2007).

[35]. Yuan, G. Q., Jiang, H. F., Lin, C. & Liao, S. J. Efficient Electrochemical Synthesis of 2-Arylsuccinic Acids from CO2 and Aryl-Substituted Alkenes with Nickel as The Cathode. *Electrochim. Acta.*, **53** (5), 2170–2176 (2008).

Chapter 2: Overview of the Techniques Used

Synopsis

In this chapter, we will provide a concise overview of the primary techniques utilized in Chapters 3 and 4, encompassing both electrochemical and analytical methods. Additionally, we will present a theoretical foundation to familiarize readers with these techniques before encountering them in the subsequent sections of the text.

1. Electrochemistry.

Electrochemistry is a field of study that focuses on the investigation of chemical processes involving the movement of electrons. This electron movement, often referred to as electricity, arises from the transfer of electrons between different elements or species in a chemical reaction known as an oxidation-reduction (or "redox") reaction [1].

1.1. Oxidation.

Oxidation refers to the process in which a molecule, atom, or ion loses electrons during a chemical reaction. This loss of electrons leads to an increase in the oxidation state of the respective species.

Figure 1. *Shows Oxidation process.*

1.2. Reduction.

Reduction occurs when there is a gain of electrons by an atom, molecule, or ion, resulting in a decrease in the oxidation state of the species involved.

It is very important to mention that both reduction and oxidation can occur in the same system; this can be termed a "redox reaction" as it involves both reactions.
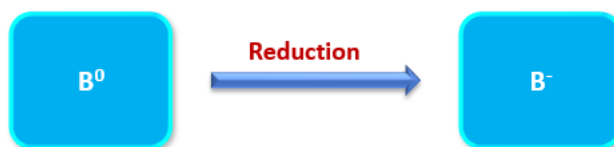
Figure 2. *Shows Reduction process.*

2. Reaction Reversibility.

Chemical reversibility refers to the property of a reaction where the conversion of reactants to products and the conversion of products back to reactants can occur simultaneously. In other words, a reversible reaction is one that can proceed in both the forward and reverse directions under certain conditions. This implies that the reaction reaches a state of dynamic equilibrium, where the rates of the forward and reverse reactions are equal. While, in an irreversible reaction, the consumed products cannot return back to reactants [1].

3. Electron Transfer and Energy levels.

In electrochemistry, the Fermi level is a concept used to describe the energy levels of electrons in a material or at the interface between an electrode and an electrolyte solution. The Fermi level represents the highest occupied energy level of electrons at absolute zero temperature (0 Kelvin) in a system.

When an electrode is immersed in an electrolyte solution, the Fermi level of the electrode and the Fermi level of the solution will interact. The relative positions of

these Fermi levels determine the movement of electrons between the electrode and the solution, influencing electrochemical processes. This can be summarized in two possible steps:

1- The Fermi level at the electrode refers to the energy level at which electrons are located within the electrode material. It represents the energy required for an electron to move from the electrode to the solution or vice versa. The exact position of the Fermi level within the electrode depends on factors related to the electrode composition, electronic structure, and doping.

2- Similarly, the second possibility is related to the Fermi level in the electrolyte solution corresponding to the energy level of the highest occupied electronic states within the solution. It represents the energy at which electrons in the solution are available for participation in electrochemical reactions or electron transfer processes [1].

However, it is worth mentioning the difference in Fermi levels between the electrode and the solution, often referred to as the electrode potential or electrochemical potential, which influences the movement of electrons as it was mentioned previously. This leads to thinking about the electron movement directions possibilities. First possibility: if the Fermi level of the electrode is lower than that of the solution, electrons tend to move from the solution to the electrode, resulting in an oxidation process. Conversely, the second possibility is if the Fermi level of the electrode is higher than that of the solution, electrons tend to move from the electrode to the solution, leading to a reduction process. This allows the Fermi levels to be

manipulated by application of an external voltage, allowing control over the direction

and rate of electron transfer reactions in electrochemical systems (Figure 3).
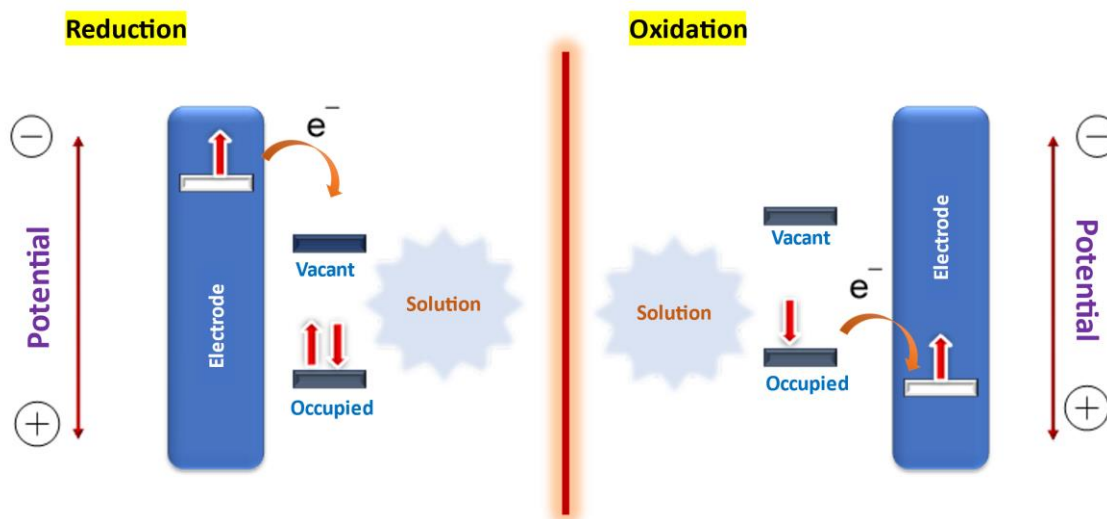
Figure 3. *General Scheme explaining the electron transfer process between electrode and*

solution [1].

Of course, changing the electrode potential will change the electrode polarization, which

then changes the movement of electrons in the electrode Fermi level, and charge

accumulation, or depletion occurs, leading to an electrochemical polarization. It is also

known that the polarization of an electrode is the deviation of its potential from the

equilibrium potential, while depolarization is the process of returning the electrode to its

equilibrium potential. This phenomenon is called "Heterogeneous electron transfer".

Nevertheless, electrode polarization can be categorized into two types:

1- Faradaic Polarization: involves charge transfer reactions at the electrode surface. For example, during the reduction of a species, the buildup of positively charged species at the electrode-electrolyte interface causes a decrease in the electrode potential.

2- Non-Faradaic Polarization: This phenomenon occurs as current passes through the system and the charge progressively accumulates. This accumulation arises from the fact that ions or other species that enter the electrode become trapped and cannot exit. This situation occurs in different situations: when there is no electrode reaction at all, when the electrode reaction involves atoms that are part of the electrode structure itself, or when the reacting species undergoes oxidation or reduction within the electrode but remains "Stuck" (or absorbed on the surface) without the ability to escape to the medium [2].

3.1. Heterogenous Electron Transfer.

Heterogeneous electron transfer refers to the movement of electrons between species residing in different phases or interfaces. Generally, one species exists in the solution phase, while the other occupies a solid electrode or remains insoluble.

3.2. Homogenous Electron Transfer.

Homogeneous electron transfer encompasses electron exchange between species existing within the same phase, often in a solution. In this scenario, both the oxidizing and reducing species are present in a shared medium, capable of freely moving and interacting. The transfer of electrons transpires through molecular or ionic species

dissolved in a solvent. For example, in an aqueous solution, the oxidizing and reducing species manifest as solvated ions in the liquid phase. Homogeneous electron transfer primarily occurs in solution-based reactions. This would appear when the undivided cell is used and the chemical species in the medium have a possibility to react with each other. Noting that will increase the chance of side reactions occurring [1].

4. Electrochemical System arrangements.

There are two main types of electrode systems: two and three-electrode systems (Figure 4). A three-electrode configuration includes the Working electrode (WE), Counter electrode, and reference electrode.
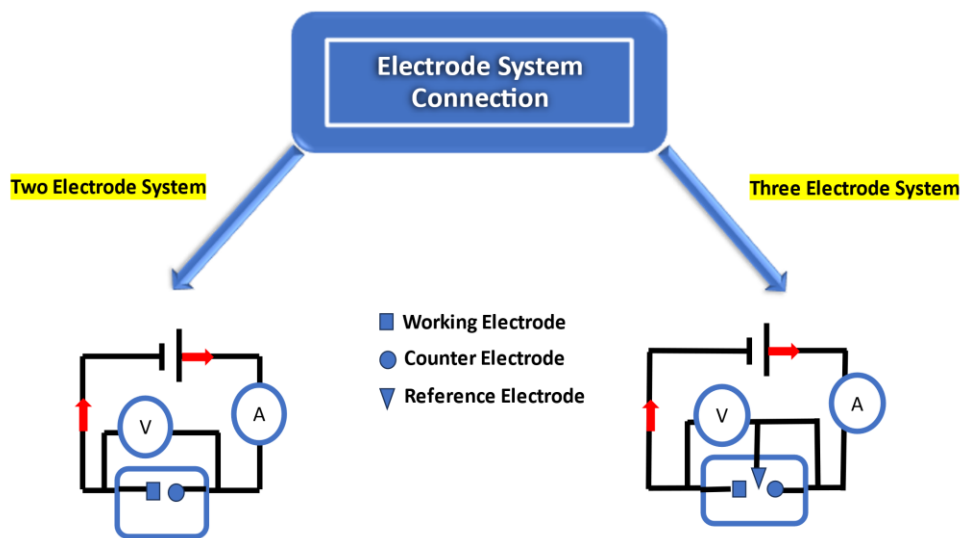

Figure 4. Two-electrode vs three-electrode systems.

As many types of electrodes are mentioned above, it is worth defining each electrode and explaining its role during the electrochemical process.

4.1. Electrodes.

Electrodes can come in various shapes, including plates, foils, rods, wires, or meshes. The choice of electrode shape depends on the specific requirements of the experiment or application. For example, plate or foil electrodes are often used when a larger surface area is needed, while rod or wire electrodes are suitable for smaller-scale experiments or precise measurements. Mesh electrodes offer high surface area and are commonly employed in applications such as electroplating or electrosynthesis.

Furthermore, it is generally preferred to have a comparable surface area between the working electrode and the counter electrode e.g., two electrode system. Balancing the surface areas ensures that the electron transfer and reaction rates at both electrodes are similar, preventing any significant concentration gradients or disparities in the current density. This equal surface area ratio helps maintain a well-controlled and uniform electrochemical reaction throughout the cell. On the other hand, there are some exceptions to this role, which is using a rotating disk electrode where the current density can be controlled and disturbed equally without any side mechanical or electrical effect.

4.1.1. Working Electrode (WE).

The working electrode is the electrode where the electrochemical reaction under investigation occurs. It serves as the focal point of the experiment, and its behavior and response are studied and measured. Various materials can be used to construct the

working electrode, including metals, carbon, or other conductive substances. Often, the surface of the working electrode is modified or tailored to optimize specific reactions or enhance selectivity.

4.1.2. Auxiliary or Counter Electrode (CE).

The auxiliary electrode, also known as the "Counter" electrode, completes the electrical circuit within the electrochemical cell. This electrode provides a pathway for the flow of current and balances the electron transfer occurring at the working electrode. Typically composed of inert materials like platinum or graphite, the counter electrode does not participate in the specific electrochemical reaction under investigation (i.e. it is a non-sacrificial electrode). Sacrificial counter electrodes can also be used, however, such as the magnesium counter electrode used in this thesis. In the current case, the magnesium forms complexes with the products and actively participates in the reaction.

4.1.3. Reference Electrode (RE).

The reference electrode's primary function is to establish a fixed potential against which the potential of the working electrode (the electrode under investigation) can be measured. The choice of the reference electrode, whether a saturated calomel electrode, silver/silver nitrate, or silver chloride electrode, or some other electrode, all depends on the environmental nature of the electrochemical cell involving electrolyte, solution, and other species. From this point, reference electrodes have two main types:

- Aqueous Reference Electrodes
- Nonaqueous Reference Electrodes.

The response observed at the reference electrode should exhibit reversibility, enabling the calculation of the system potential using the Nernst equation (see section 5.1.1., Equation 1). Additionally, it should possess the ability to restore its potential following the application of current stress. The following chart presents some reference electrode examples (Figure 5) [3].

Reference Electrode Types [vs. NHE (mV)]

Hydrogen

For Example:
- **Standard Hydrogen Electrode**
Potential **0 mV** (1 M H$^+$)

$2H^+ + 2e^- \rightleftharpoons H_2$

Mercury

For Example:
- **Calomel**
1- SCE (Saturated KCl) **+240 mV.**
2- SSCE (Saturated NaCl) **+236 mV.**
3- NCE (1M KCl) **+280 mV.**

$Hg_2Cl_2 + 2e^- \rightleftharpoons 2Hg + 2Cl^-$

Silver

For Example:
- **Silver Chloride e.g., KCl**

Potential **+197 mV.**

$AgCl + e^- \rightleftharpoons Ag + Cl^-$
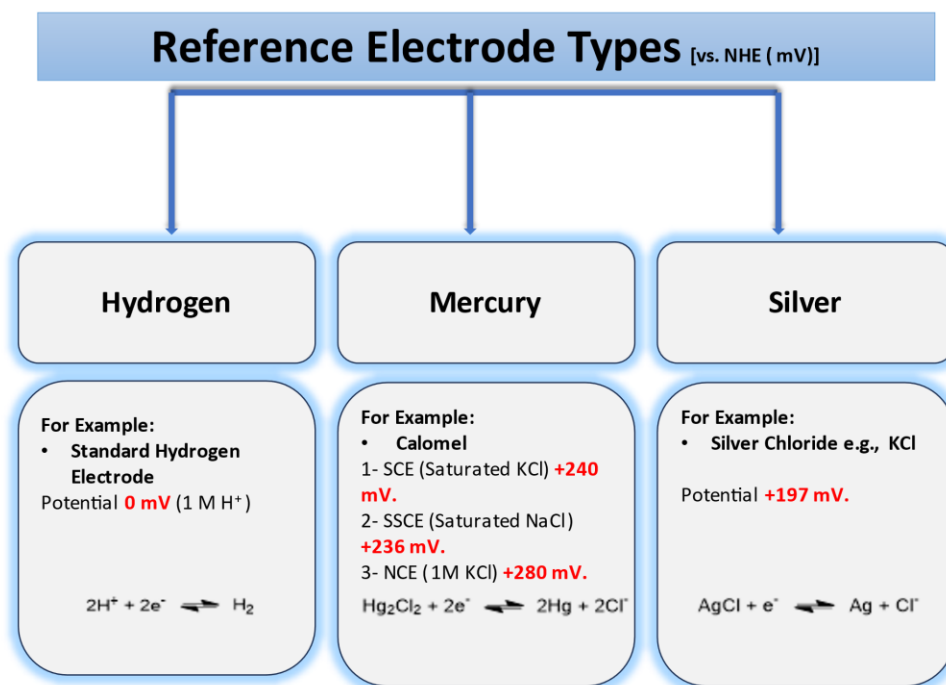
***Figure 5.** Some Reference electrode types vs. Normal Hydrogen Electrode (NHE).*

Teflon cap/
active electrode
holder

Filling
port
with cap

Active Electrode

Filling
solution

Ceramic frit
sealed into glass (shown)
or
Vycor frit with
Teflon heat shrink

Glass
body

Brass pin
soldered to
silver wire

Teflon
end-cap

Silver wire

Anodic AgCl
coating

Glass tube

Filling
solution

Teflon
heat shrink

Vycor frit

H_2

H_2

Pt - glass
seal

Platinized
Electrode
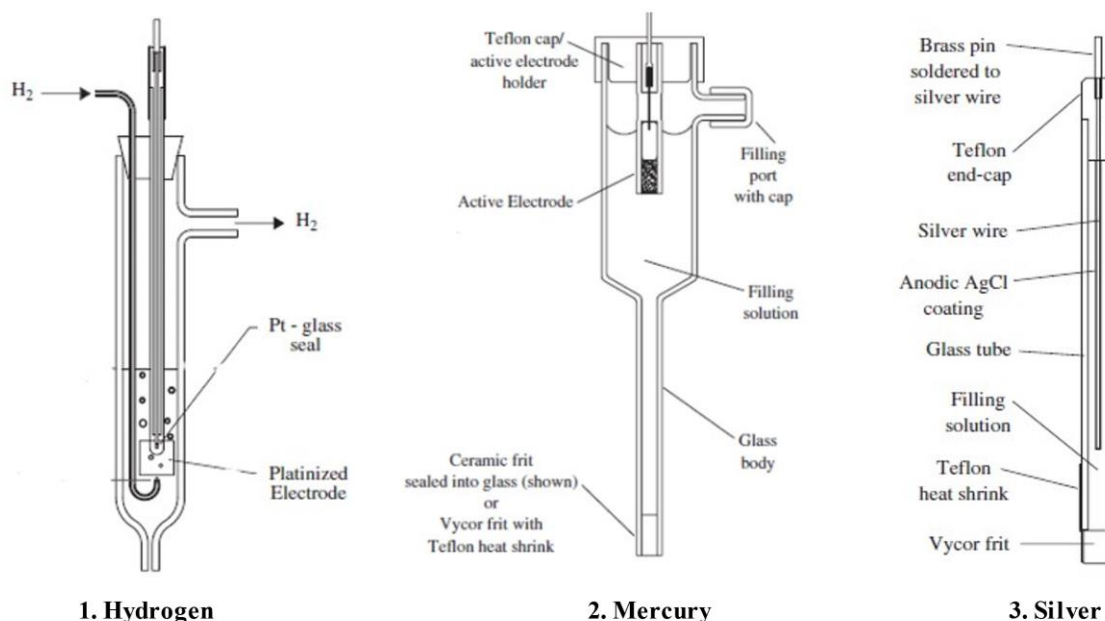
1. Hydrogen

2. Mercury

3. Silver

Figure 6. *Illustrates contentment of each 1. Hydrogen Reference electrode, 2. Mercury Reference electrode, and 3. Silver Reference electrode* [4].

4.2. Electrochemical Cell System and Types.

Divided and undivided cells are two types of electrochemical cells that differ in their electrolyte configurations and the movement of species within the cell. The main difference between them lies in how they handle the transport of reaction products and the prevention of unwanted reactions.

4.2.1. Undivided Cell.

In an undivided cell, there is no physical barrier or separator between the working electrode and the counter electrode. They share the same electrolyte solution. This

configuration allows for unrestricted movement of all species (reactants and products) between the two electrodes.

Undivided cells are commonly used when the reactants and products do not interfere with each other or when their crossover or mixing does not affect the desired electrochemical process.

However, undivided cells can suffer from side reactions or unwanted reactions at the counter electrode due to the direct contact between the two electrodes (Figure 7).

4.2.2. Divided Cell.

In a divided cell, a physical barrier or separator is placed between the working electrode and the counter electrode, effectively separating the two compartments. The separator is typically a porous material that allows the movement of ions while preventing direct contact between the electrodes and slowing down the mixing of the reactant species. Divided cells are used when it is necessary to prevent the mixing of reactants or to minimize unwanted reactions.

The separator ensures that the reaction products generated at the working electrode are confined to that compartment and do not interfere with the counter electrode or undergo unintended reactions. Divided cells are commonly employed in applications where selective reactions are desired, such as in certain electrolysis processes or in studying specific redox reactions (Figure 7) [5].
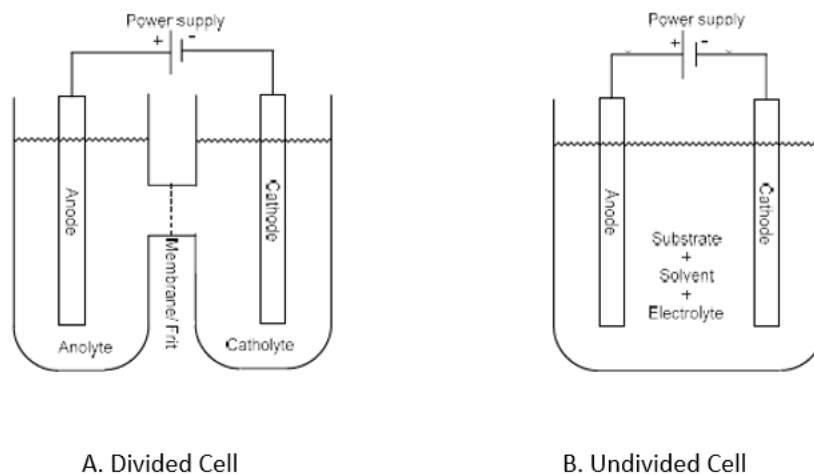
Figure 7. *Illustrates Cell types: (A) Divided Cell, and (B) undivided Cell.*

The choice between a divided and undivided cell depends on the specific requirements of the electrochemical system and the desired control over the reactions taking place. Divided cells provide greater control over the movement of species and prevent undesirable interactions between the electrodes, while undivided cells offer simplicity and ease of setup.

4.3. Solvents.

For the purpose of facilitating electron transfer between electrodes or species, a medium is required. This medium commonly takes the form of a solvent, which can either be aqueous or non-aqueous (organic). The selection of the solvent is largely dependent on the specific objectives of the project at hand. Additionally, it is crucial to consider that the solvent must effectively dissolve the reactants and the resulting products to prevent potential mechanical and electrical complications that may arise during the process of

electrolysis. Another property that could be considered is the volatility of the solvent, especially when a long reaction takes place [6].However, the choice of solvent in electrochemical reactions profoundly influences the outcome. Beyond factors like intermediate stabilization and reagent solubility, several considerations are vital: solvent stability window, counter reaction promotion, intermediate stabilization, and intrinsic resistance (conductivity). For instance, DMF serves as a typical aprotic solvent, while alcohols are prototypical protic solvents. Generally, polar solvents are preferred in electrochemistry due to their lower resistance, leading to higher conductivity compared to non-polar solvents. Moreover, they typically dissolve electrolytes more effectively. The use of dry and degassed solvents is crucial to consider as it can impact product yield.

The solvent window denotes the potential range within which a solvent remains stable against oxidation and reduction. Its extent is influenced by electrode material, electrolyte species and concentration, among other factors. Ensuring solvent stability under electrochemical conditions is imperative. Degradation of the solvent under these conditions can dominate the primary reaction due to its higher concentration compared to the substrate, resulting in minimal substrate conversion. However, operating within the solvent window allows for the use of solvents with low degradation potential [6]. In this project, dimethylformamide (DMF) serves as the solvent due to its cost-effectiveness, low volatility, and its ability to dissolve electrolytes and other necessary species. Furthermore, we have observed that higher current densities can accelerate the degradation of DMF, particularly when the potential window is expanded, as determined in some experimental setups. However, our project has demonstrated that, despite efforts

to control factors like current density and potential window, DMF degradation still occurs within the chosen experimental parameters. This degradation, though anticipated, does not significantly impact the overall yield of products, which remains satisfactory. The experimental setup includes a nickel mesh working electrode, a saturated calomel electrode (SCE) as the reference electrode, and the chosen DMF medium.

4.4. Electrolyte.

The electrolyte can be defined as a solution medium that contains positive and negative ions and is capable of conducting electric current. When an electric potential is applied across the electrolyte, the ions within the solution become mobile and can move toward the oppositely charged electrodes. This movement of ions allows for the flow of electric current through the electrolyte, facilitating electrochemical reactions and processes [6].

5. Electrochemical Techniques.

From a scientific perspective, electrochemical techniques can be classified into four distinct categories, primarily determined by the variable that is chosen for manipulation and control:

1- **Controlled Potential,** for instance, cyclic voltammetry, and chronoamperometry.

2- **Controlled Current e.g.,** chronopotentiometry, and constant current electrolysis.

3- **Controlled Total Charge Passed** for example, coulometry, controlled-potential coulometry, and controlled-current coulometry.

4- **Impedance Techniques** such as electrochemical impedance spectroscopy (EIS) and impedance voltammetry

In this section, we will provide a concise explanation of the electrochemical techniques employed in this thesis. Special attention will be given to the insights they offer, the experimental setup(s) utilized, and the scenarios where one technique proves more advantageous than the others [1].

5.1. Voltammetry.

Potentiodynamic techniques are a subset of electrochemical methods where the potential applied to the electrode is varied within a specific voltage range known as the "Potential window." This variation in potential influences the polarization of the electrode. It is important to note that electrode polarization can occur in two main scenarios:

1. Application of a voltage proportional to the charge passed: This method facilitates electrode polarization and is commonly referred to as an ideal polarized electrode.

2. Occurrence of a redox reaction: In this case, the polarization of the electrode is effectively canceled out, resulting in a non-polarized electrode. In other words, two distinct categories of electrodes are recognized: polarizable and non-polarizable electrodes, each possessing unique traits and purposes. A polarizable electrode is distinguished by its capability to experience a notable shift in its electrochemical potential (voltage) in response to an external electrical potential. This alteration in potential occurs as a result of charge buildup at the interface between the electrode and the electrolyte, leading to a state of polarization. Conversely, a non-polarizable electrode remains relatively unchanged in its electrochemical potential when exposed to an external electrical potential. These electrodes

exhibit minimal accumulation of charge at the electrode-electrolyte interface compared to their polarizable counterparts [1].

The specific response of the working electrode, whether it can be effectively polarized or depolarized, depends on its chemical nature, particularly if it is inert or susceptible to polarization. It is important to mention that the reference electrode is non-polarizable, but it is affected by the polarization of the working electrode. In addition, any current results from the process can be shown in a voltammogram.

Voltammetry stands out as one of the most widely used electrochemical techniques due to its capacity to provide both qualitative and quantitative data within a short timeframe. It achieves this by examining the redox activity of the species under investigation across a range of applied potentials. In other words, in this technique, a time-dependent potential excitation signal is applied to the working electrode, causing its potential to vary in relation to the fixed potential of the reference electrode. Linear Sweep Voltammetry (LSV) and Cyclic Voltammetry (CV) are the two most common types of voltammetry techniques. In this thesis, only cyclic voltammetry was implemented and will be discussed further.

5.1.1. Cyclic Voltammetry

Cyclic voltammetry (CV) stands out as one of the most widely used electrochemical techniques due to its capability to generate both qualitative and quantitative data swiftly, by investigating the redox behavior of the species under examination across a range of applied potentials. In a typical CV experiment, the variation in current response of the

species is observed as the potential of the working electrode is incrementally changed at a constant rate, known as the scan rate [7].

The aim of this voltametric technique is to have an introductory idea about the behavior of the species in the medium before starting the main electrolysis. However, applying cyclic voltammetry can have many purposes.

First, cyclic voltammetry allows the determination of kinetic parameters such as electron transfer rates and reaction mechanisms. By analyzing the shape and position of peaks in the voltammogram, information about the rate of electron transfer, diffusion coefficients, and reaction mechanisms can be obtained, to name but a few. In cyclic voltammetry, alterations in scan rate can significantly impact the determination of rates and diffusion coefficients, primarily due to their influence on the kinetics of the redox process and the mass transport of electroactive species. Here's an elaboration on the various additional factors at play [1]:

First, changes in scan rate modify the pace at which potential is swept across the working electrode, directly affecting the kinetics of the electrochemical reaction. Higher scan rates may prevent the reaction from reaching equilibrium, leading to non-reversible behavior and distorted peaks in the voltammogram. Analyzing the variation of peak currents with scan rate offers valuable insights into the reaction kinetics. Second, scan rate adjustments impact the transport of electroactive species to and from the electrode surface. Faster scan rates can exacerbate mass transport limitations, where species diffusion to the electrode surface lags behind the changing potential. This phenomenon often manifests as peak

broadening and altered peak shapes. Conversely, slower scan rates allow for more effective mass transport, mitigating these effects. Third, the diffusion coefficient of an electroactive species reflects its mobility within the electrolyte solution, crucially influencing its rate of diffusion to the electrode surface and hence the electrochemical reaction rate. Fourth, changes in scan rate also affect the rate constants governing the redox reaction at the electrode surface. Faster scan rates may accentuate the impact of kinetic limitations, whereas slower scan rates enable the system to approach equilibrium more closely. Finally, variations in scan rate can induce shifts in peak potentials, attributable to kinetic effects, ohmic drop, and double-layer charging phenomena [1].

Second porpose of applying this technique is that, cyclic voltammetry provides insights into redox chemistry, including the characterization of redox couples, identification of oxidation and reduction potentials, and determination of the reversibility of redox reactions. This information is important for understanding the behavior of electroactive species and their reactivity. Third, cyclic voltammetry can be used to study the modification of electrode surfaces. By measuring the changes in the voltammogram before and after surface modification, the effectiveness of different electrode coatings, films, or functionalization strategies can be evaluated. This is important in various fields such as catalysis. Fourth, cyclic voltammetry can be employed as an analytical technique for the detection and quantification of analytes in a sample. The relationship between the current response obtained from the cyclic voltammogram and the concentration of the analyte in solution is directly linked. When the concentration of the analyte rises, the current response

similarly increases, despite the nature of this relationship - whether linear or nonlinear - depending on the specific characteristics of the system under investigation generally. Furthest, this technique has applications in fields such as environmental analysis, pharmaceutical analysis, and food science, etc. While in the subject, it is important to understand the voltammogram shape. Herein, ideal voltammogram is explained in (Figure 8).
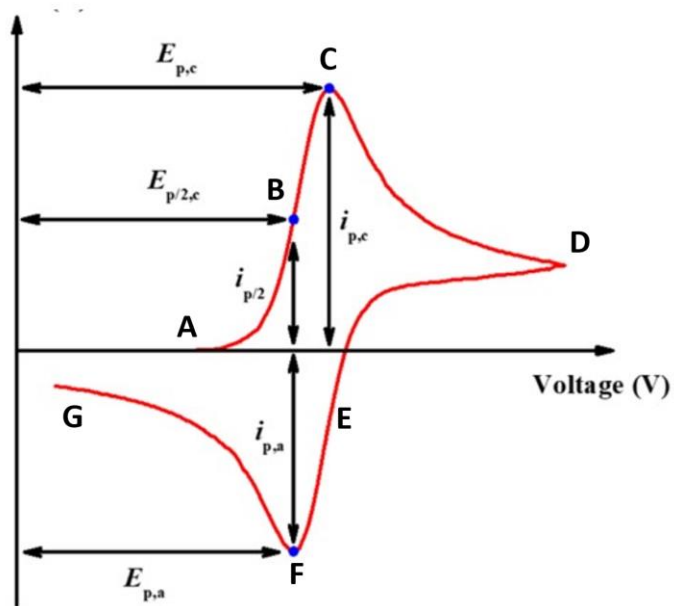

Figure 8. An idealized Cyclic Voltammogram [7].

Cyclic voltammetry can take many shapes based on the potential window range, which is inserted through software connected to the electrical instrument. In addition, it depends on the research interest and the electrode's and species' chemical nature, whether they are reversible or irreversible. Moreover, the involved peak(s) can be shifted based on many factors such as scan rate. The typical shape for cyclic voltammetry (the "Duck Shape") involves cathodic and anodic peaks that occur. The cathodic peak potential is labelled, E_{pc}, and anodic peak potential, E_{pa}, respectively. Each of them has a current i_{pc} (cathodic current, negative) and i_{pa} (Anodic current, positive) correspondingly. The average of these two potentials will be E_0 (sometimes also called $E_{1/2}$). Cyclic voltammetry provides insights into the kinetics, thermodynamics, and mechanism of electrochemical reactions [7,8].

While scanning the potential in a negative (cathodic) direction from point A to point D, the components near the electrode experience a gradual depletion as they undergo reduction, leading to the formation of oxidized species. At the juncture denoted as point C, where the peak cathodic current (ip,c) is evident, the current is governed by the influx of additional species through diffusion from the bulk solution.

Upon the initiation of reduction, certain oxidized species exit from the electrode's surface into the solution. Furthermore, as the potential progresses to more negative values, the pace of diffusion for oxidized species from the bulk solution to the electrode's surface diminishes, resulting in a decrease in the current as the scan continues (from C to D). Upon reaching the switching potential (point D), the direction of the scan reverses, and the potential begins to ascend in the positive (anodic) direction. During this time, while

the concentration of oxidized species at the electrode's surface had diminished, the concentration of neutral species at the electrode's surface witnessed an increase, conforming to the Nernst equation. The newly introduced neutral species at the electrode's surface undergoes oxidation as the applied potential becomes more positive. At positions B and E, the concentrations of neutral species and substrate at the electrode's surface achieve equilibrium, aligning with the Nernst equation, $E = E_{1/2}$. This equilibrium corresponds to the midpoint potential between the two observed peaks (C and F) and offers a direct approach to estimate E^0 for a reversible electron transfer. The separation of the two peaks is a result of the analyte's diffusion to and from the electrode (Figure 8). The Nernst (equation 1) establishes a connection between the potential of an electrochemical cell (E), the standard potential of a species (E^0), and the relative activities of the oxidized (Ox) and reduced analytes (Red) in the system when it's at equilibrium.

$$E = E^0 \frac{RT}{nF} + ln \frac{(Ox)}{(Red)} = E^0 \frac{RT}{nF} + 2.3026 \frac{(Ox)}{(Red)} \log 10 \frac{(Ox)}{(Red)} \qquad \textbf{\textit{Equation (1)}}$$

F represents Faraday's constant

R is the universal gas constant

n denotes the number of electrons

T represents the temperature.

On the other hand, when electron transfer faces a significant challenge (electrochemical irreversibility), the rate of electron transfer reactions slows down. This requires using more negative (or positive) potentials to observe reduction (or oxidation) reactions. As a result, a larger the difference between the anodic and cathodic peak (ΔE_p) emerges. Processes that can be easily reversed electrochemically, with fast electron transfers following the Nernst equation, are often labeled as "Nernstian."

5.1.2. Chronopotentiometry.

Chronopotentiometry is defined as a galvanostatic technique that involves maintaining a constant level of current at the working electrode for a specific duration. Throughout this period, the potential and current at the working electrode are systematically monitored and recorded over time. It can be used for electrode reactions, charge transfer kinetics, and electrochemical reaction mechanisms (See Results and Discussion, Chapter 3, and Chapter 4).

5.1.3. Chronoamperometry.

Chronoamperometry is defined as a potentiostatic technique and is used to measure the current as a function of time at a working electrode. It involves applying a constant potential to the working electrode and recording the resulting current over a specified period. This technique provides information about the electrochemical reactions

occurring at the electrode surface, including kinetics, diffusion processes, and charge

transfer mechanisms [9] (Figure 9).
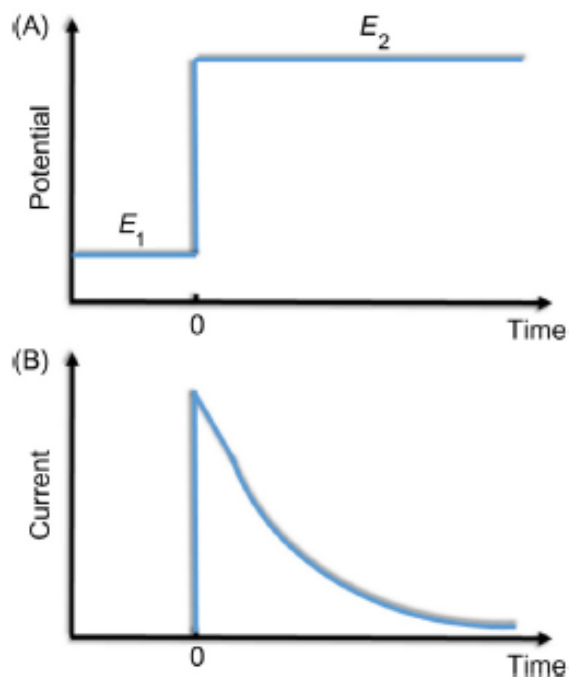
Figure 9. *Chronoamperometry (A) Shows the applied Potential vs Time, (B) Shows the*

recorded Current vs Time [9].

5.1.4. Chrono coulometry.

This technique shares a similar principle with chronoamperometry but focuses on the

relationship between charge and time rather than current and time. Unlike

chronoamperometry, where the current decreases over time, in chrono coulometry, the

charge increases as the experiment progresses. This difference in monitoring the charge

accumulation instead of the current flow is the key distinction between the two methods.

In this thesis, only Cyclic voltammetry is applied to have an introductory idea for the system and involved chemicals. Then, chronopotentiometry is applied for the reduction reaction (Chapters 3 and 4).

6. Analytical Techniques.

6.1. Nuclear Magnetic Resonance.

Nuclear Magnetic Resonance (NMR) is an analytical technique for identifying the chemical structure of a compound. In order to understand how this analytical method can do this, it is very important to understand the device parts. In this section of the thesis, there will be a simple explanation of the following:

A. Instrument parts.

The NMR device parts can be summarized as follows [10] :

1- Sample holder which will hold the NMR tube and then be placed in a queue.

2- A probe where the sample is positioned within the core of the magnetic field for the purpose of conducting the NMR experiment. Enclosed within the probe are radiofrequency (RF) coils, which are finely tuned to specific frequencies associated with atomic nuclei within the given magnetic field. Moreover, the probe encompasses essential hardware components responsible for controlling and monitoring the temperature of the sample.

3- Magnet: The instrument includes a powerful magnet, typically a superconducting magnet which will generate a magnetic field, which shall be referred to as the "External field, B_0".

4- Computer and Software: A computer equipped with specialized NMR software controls the instrument, acquires, and processes NMR data, and facilitates data analysis, interpretation, and visualization.

5- Nitrogen and Helium liquid: The instrument's maintenance requires filling constantly in the NMR instrument, so the desired temperatures can be maintained, ensuring the stability and performance of the magnet, and cooling the relevant components in the NMR instrument [9].
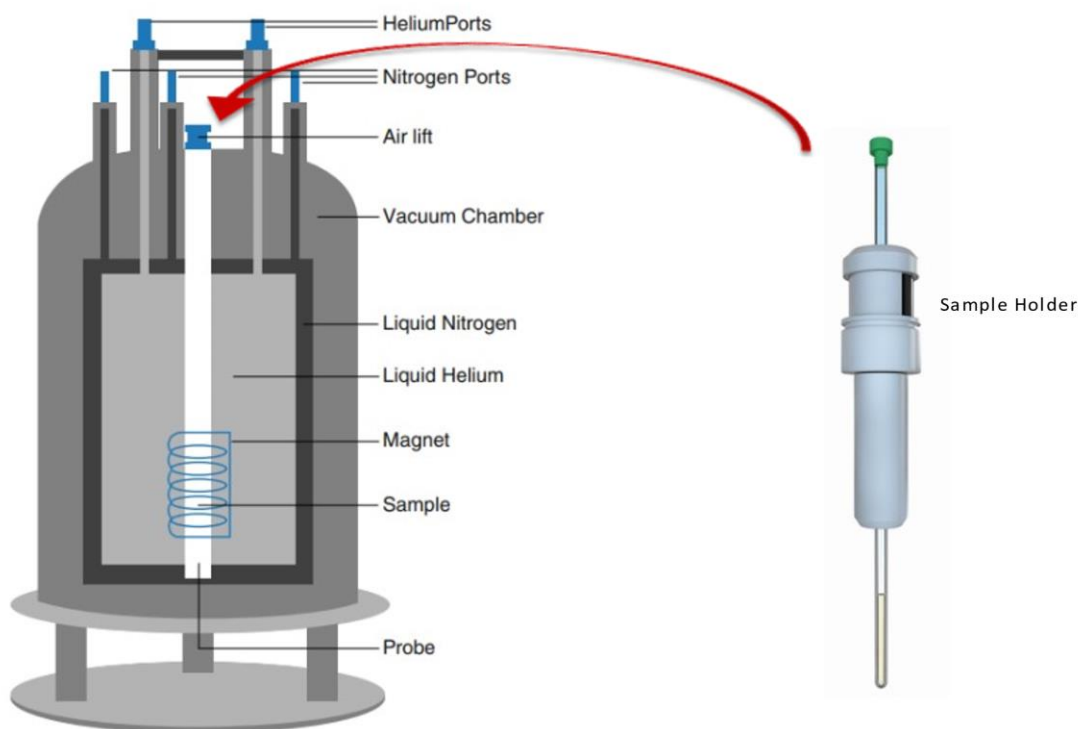
Figure 10. *Shows parts of Nuclear Magnetic Resonance (NMR) instrument* [11].

B. Nuclear Magnetic Resonance Theory [10].
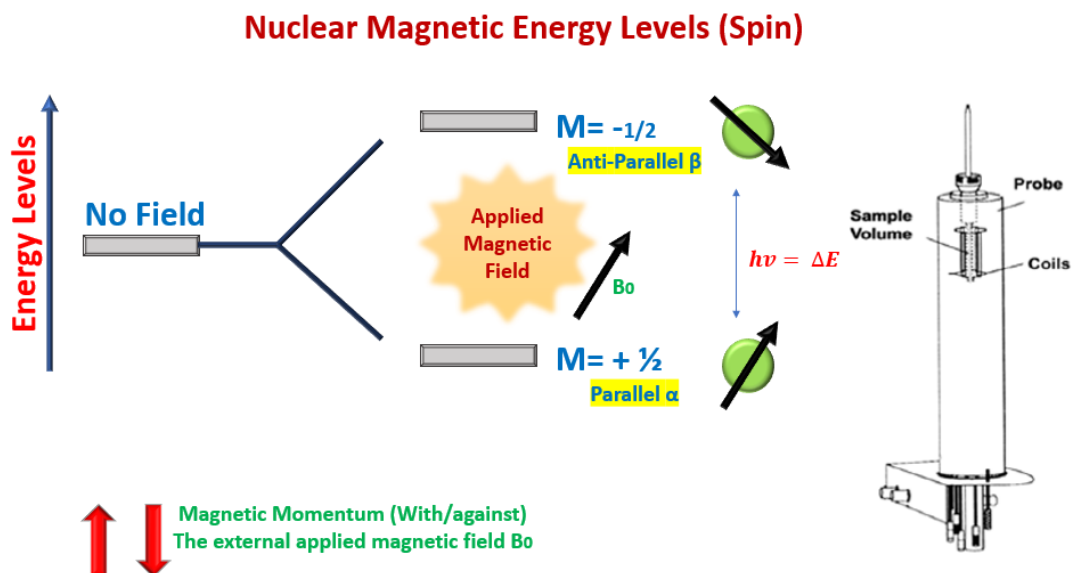
Figure 11. *Shows the theory of Nuclear Magnetic Energy (NMR).*

Nuclear magnetic resonance can be understood by considering the possible alignments of a nucleus's magnetic moment in relation to an external magnetic field. The coupling between protons and neutrons within a nucleus is characterized by three scenarios determined by the nuclear spin value, denoted as I.

$$\mu = I\gamma \frac{h}{2\pi} \qquad \textbf{\textit{Equation}} \ (\textbf{2})$$

I represent the quantum number associated with nuclear spin, which is determined by the composition of protons and neutrons within the nucleus.

γ denotes the gyromagnetic ratio, signifying the ratio of an entity's magnetic moment to its angular momentum.

'h' stands for Planck's constant."

First, when neutrons and protons are present in odd numbers within an atom, resulting in an odd total, the value of I yields half-integral numbers e.g., 1/2, 3/2. Conversely, in atoms with an even total of neutrons and protons, all spins pair up, resulting in I = 0. For instance, the 12C isotope exemplifies this scenario, rendering the atoms magnetically inert with no interaction with spectrometers. In another situation, where both neutrons and protons exist in odd numbers, *I* becomes an integer greater than 1/2, leading to the nucleus also possessing an electric quadrupole moment, denoted as Q. Consequently, the charge distribution deviates from spherical symmetry, potentially affecting NMR spectra. Despite this, analyzing such molecules remains technically feasible. In addition, the magnetic moment undergoes precession around the direction of B0, analogous to the spinning of a top. In the case of the 1H isotope (where I = 1/2), there exist two possible orientations: nuclei with m = +1/2 (α spin state) align parallel to the external field and possess lower energy compared to those with m = −1/2 (β spin state), which align against the magnetic field. The energy of interaction between the magnetic moment and the applied field depends on the angle between them (Figure 11, 12).

These distinct energy states facilitate spectroscopic analysis. Since the energy difference between the two states is minute (on the order of $10^{-5}/10^{-6}$), electromagnetic radiation in the form of radio waves is sufficient to induce transitions between them. The frequency required for these transitions can be determined using the Bohr relation (equation 3) or expressed in terms of the gyromagnetic ratio for NMR (equation 4).

$$hv = \Delta E \quad \textbf{\textit{Equation}} (\textbf{3})$$

$$v = B_0 \frac{\gamma}{2\pi} \quad \textbf{\textit{Equation}} \textbf{ (4)}$$

When the sample is exposed to the appropriate frequency of radiation, it absorbs energy equivalent to ΔE. As a result, a nucleus in a lower state (α proton) can undergo a "spin-flip" to transition to a higher energy state (β proton). This phenomenon occurs when the nuclei resonate with the applied radiation, giving rise to the term "nuclear magnetic resonance." Following the excitation, the nucleus reverts to its original lower state, releasing the absorbed energy. This process is referred to as relaxation. During this stage, a small burst of radiofrequency electromagnetic radiation is emitted, which is subsequently detected by the NMR machine.
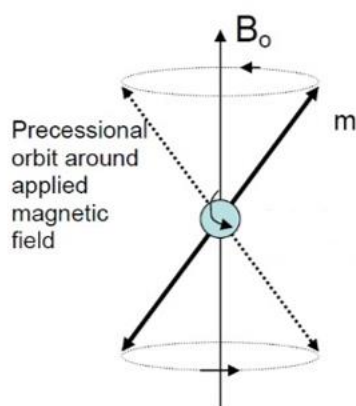
Figure 12. *Shows the magnetization affect spinning by external magnetic field (B_0).*

Nuclei in close proximity to each other can exert an influence on the effective magnetic field of one another. This is called spin-spin coupling or J coupling.

$$J\ Hz = \Delta\ ppm\ x\ instrument\ frequency \qquad \textbf{Equation (5)}$$

The chemical shift is a measure of the resonance frequency of a particular hydrogen nucleus relative to a reference compound, usually tetramethylsilane (TMS), which is assigned a chemical shift of 0 ppm. Chemical shifts are expressed in parts per million (ppm) and are influenced by the local electron distribution and magnetic environment around a proton. Different types of protons in a molecule experience different chemical shifts due to variations in their electron density and shielding effects from neighboring atoms. This information helps chemists deduce the structural features and functional groups present in the compound.

The chemical shift of a nucleus is defined as the disparity between the resonance frequency of the nucleus and a reference frequency, relative to the standard. This value is typically expressed in parts per million (ppm) and its symbol δ.

$$\delta = \frac{v_H - v_{reference}\ (Hz)}{frequency\ of\ the\ spectrometer\ (MHz)} \qquad \textbf{Equation (6)}$$

C. Interpreting the obtained Results [10].
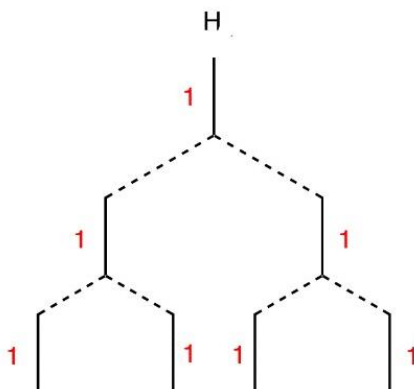
Figure 13. Shows the hydrogen splitting by hydrogen atoms neigboneighborsus.

Splitting, also known as multiplicity or coupling, occurs when the protons in a molecule are influenced by neighboring protons with different spin states. This effect arises from the magnetic interaction between the spins of adjacent protons, leading to a splitting of the resonance signal into multiple peaks.

The splitting pattern can be analyzed using the n+1 rule, where "n" is the number of adjacent, chemically distinct protons that are three bonds away from the proton being observed. The rule states that if there are "n" adjacent protons, the resonance signal will be split into "n+1" peaks. For example, if a proton has two adjacent protons, it will exhibit a triplet pattern (1+2 = 3 peaks) in the NMR spectrum. The size of the splitting (the spacing between the peaks) provides information about the coupling constants (J values), which in turn can reveal the type and number of neighboring protons. The most common patterns are doublet, triplet, quartet, etc. Each of these patterns corresponds to a specific number of neighboring protons contributing to the coupling (Figure 13).
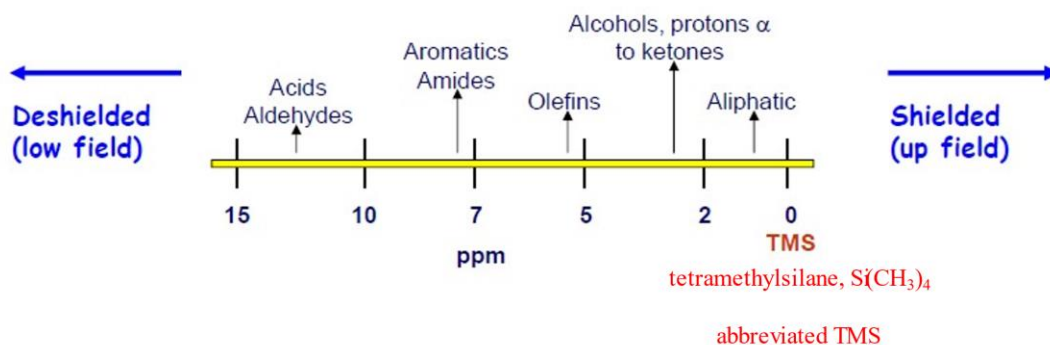
Figure 14. Shows up-filed and downfield scale in ppm of varied functional groups.

As a brief summary:

1- Nuclei movements will generate a current, magnetic field.

2- This magnetic field could be aligned or against the externally applied magnetic field.

3- When the sample is exposed to the external magnetic field, the electron magnetic field will go against the field direction.

3- This will allow the NMR instrument to produce signals. Briefly, NMR peaks become visible in the spectrum due to the interplay between the sample's nuclei and the magnetic field, coupled with the application of radio frequency pulses which is generated from the coil. These unique features of the peaks provide valuable insights into the sample's chemical structure, local environment, and molecular interactions.

4- The signals can be up-field or downfield (Figure 14) based on the following

• Functional groups in the chemical structure.

• The surrounding neighbor atoms which will shield other atoms.

However, it is well known that the atoms in the chemical structure have different positions from their neighbor's atoms. In this regard, NMR analysis can be divided into one dimensional (1D) experiment such as ^{1}H NMR and ^{13}C NMR. Also, two-dimensional NMR (2D) experiments such as HSQC, and HMBC are possible. In our thesis, only one dimension of NMR will be involved (Chapters 3 and 4).

6.2.Mass Spectrometry.

Mass spectroscopy is a scientific technique employed to identify species present in a sample by analyzing the mass-to-charge ratio (m/z) of ions generated through the ionization of chemical compounds. The process involves vaporizing the molecules within the sample and subjecting them to ionization by bombarding them with electrons or other ions. This ionization leads to the fragmentation, to name but few, of the molecules into charged fragments, which can then be separated and sorted based on their m/z ratio. These ions are subsequently detected by a specialized instrument capable of detecting charged particles.

[12] Only electrospray ionization (ESI) is used for analyzing products in this thesis.
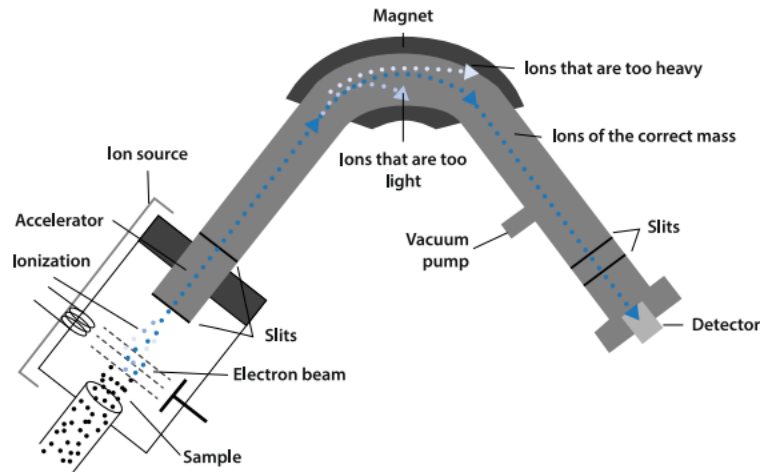
Figure 15. *Illustrates the main components of the mass spectrometer device* [11].

1- A sample will be evaporated before bombarding this with electrons or ions through a

source. Due to the electric charge carried by the ions, their movement through the

magnetic sector causes the ion beam to bend in an arc. This bending effect, described

by theradius (r) of this curved path, depends on factors such as the ion's momentum

(μ), charge (C), and the strength of the magnetic field (B).

$$r = \frac{\mu}{C \times B} \qquad \textbf{Equation (7)}$$

In other words, the substrate is subjected to an electron bombardment, leading to the

ionization of a portion of the substrate. This ionization can occur either through the

substrate capturing some of the bombarding electrons or more frequently through the

expulsion of its own electrons due to the high-velocity electron beam, resulting in the

formation of cations. These ions are subsequently steered in varying directions within

a magnetic field, a deflection that hinges on factors such as their charge, mass, and, in

certain mass spectrometry devices, their cross-sectional area. This area offers insight

into the effective "size" of an ion concerning its interaction with surrounding particles. Generally, larger ions possess larger cross-sectional areas, increasing the likelihood of collisions with other molecules. As a result, this can enhance the efficiency of ion fragmentation or activation processes.

2- Accelerator: accelerates the ions to high velocities before they enter the magnetic sector. This initial acceleration is necessary to ensure that the ions have enough kinetic energy to travel through the rest of the instrument. Another important role of the accelerator is to select certain ions which can be accelerated or decelerated, allowing for the separation of ions with different masses or energies. To sum up, ions are accelerated by establishing a voltage gradient that propels them forward, boosting their velocity. This process is pivotal for fine-tuning ion manipulation to attain precise mass analysis. By meticulously adjusting electric potential differences, mass spectrometers effectively segregate ions according to their mass-to-charge ratio or kinetic energy, thereby enabling accurate characterization of chemical compounds.

3- Magnet: the purpose of the magnet is to separate ions in a magnetic field according to the momentum and charge of the ion.

4- Detector: is responsible for capturing and measuring ion signals, which allows for the identification, quantification, and characterization of compounds based on their masses. It's important to note that in mass spectrometry, the actual mass isn't directly measured, despite the technique's name. Instead, it's the generated graph that determines the mass-to-charge ratio (m/z). [, 12] .

6.3. Infrared spectroscopy.

This analytical technique is used to study the presence of different functional groups such as C=O and O-H. To understand FTIR analysis, it would be better to start by mentioning the instrument parts which include the following [13]:

1- The Energy Source: There are many souces such as lap, laser, or globar These sources of energy play a critical role in generating the necessary infrared radiation for interacting with the sample and creating the distinctive absorption spectra examined in FTIR spectroscopy.this radiation will pass through an aperture that regulates photons quantity reaching the sample, ultimately reaching the detector.

3- The Interferometer: The infrared beam enters the interferometer, where it undergoes a process called "spectral encoding," leading to the creation of an interferogram signal that exits the interferometer.
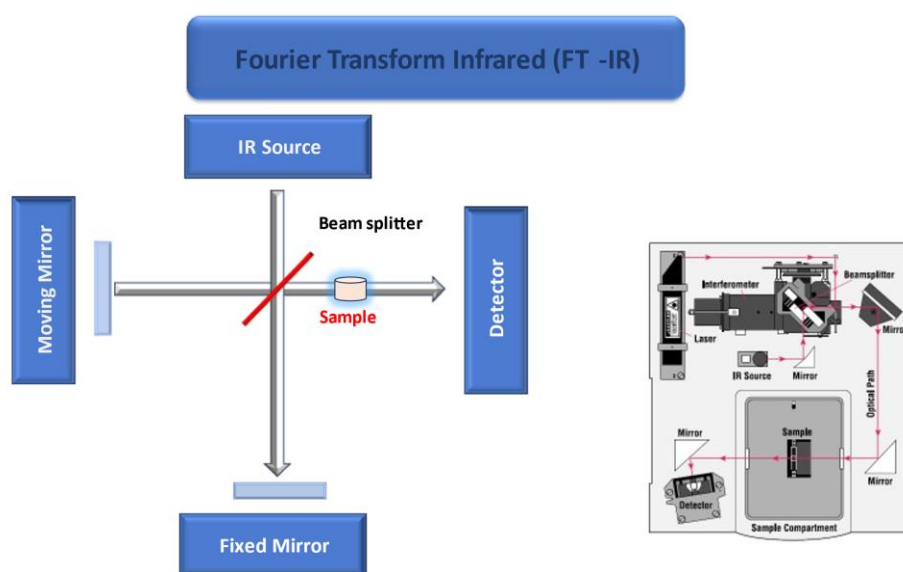
Figure 16. *Illustration of Fourier Transform Infrared (FTIR) instrument parts* [13, 14].

When the sample is placed under the infrared spectrum which acts as a unique identifier, it will resemble the fingerprint of that analyzed compound, with absorption peaks directly linked to the frequency of radiation that induces bond vibrations for the atoms in the molecule. Data in the form of "absorption versus wavenumber" or "transmission versus wavenumber" refers to the relationship between the amount of absorption or transmission of infrared radiation and the corresponding wavenumber. The wavenumber spectrum line regions can be categorized into the following [14] :
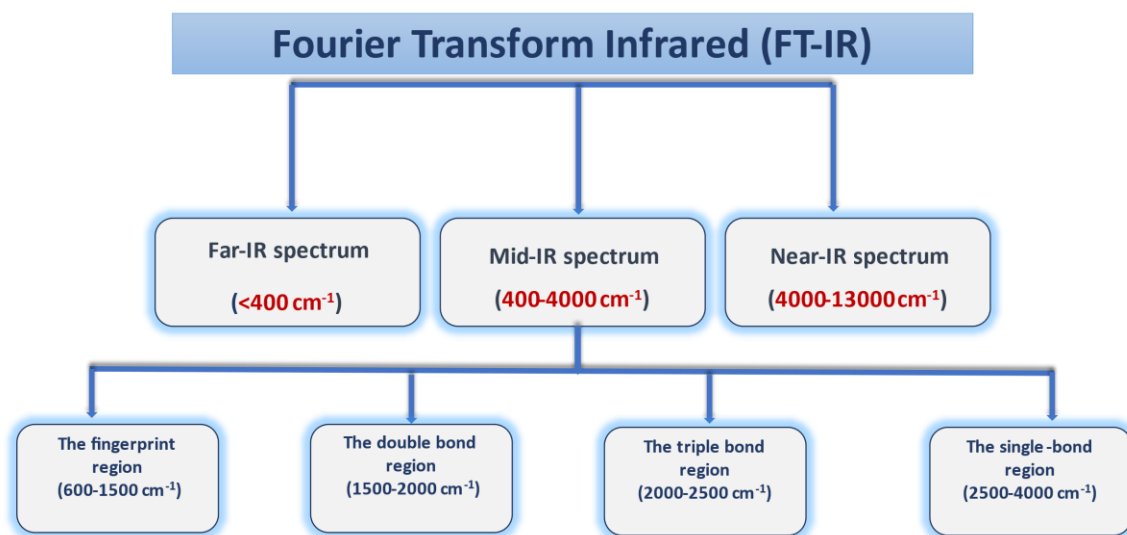
Figure 17. *Shows Fourier Transform Infrared (FTIR) spectrum, wavenumber regions.*

3- Sample Analysis: Within the sample compartment, the infrared beam interacts with the sample, either by transmitting through it or reflecting off its surface, depending on the specific analysis being performed. This stage enables the absorption of distinct frequencies of energy that are characteristic of the sample.

4- Detection: The beam then proceeds to the detector, where it is measured. The detectors employed in this process are specially designed to capture the unique interferogram signal.

5- Data Processing: The measured signal is digitized and sent to a computer system. Inside the computer, the signal undergoes a Fourier transformation, resulting in the generation of the final infrared spectrum. This spectrum is subsequently presented to the user for interpretation and any additional manipulation or analysis.

The process can be summarized as follows: By utilizing a beamsplitter, the incoming infrared beam can be divided into two optical beams. One of these beams reflects off a stationary flat mirror, while the other beam reflects off a flat mirror that is capable of moving a small distance away from the beamsplitter (typically a few millimeters). Once the beams reflect off their respective mirrors, they are recombined when they intersect at the beamsplitter. The key distinction between the two beams lies in the fact that while one beam follows a fixed path, the other beam's path continually changes due to the movement of its mirror. Consequently, the resulting signal that exits the interferometer emerges from the interference between these two beams. Known as an interferogram, this signal possesses a distinctive characteristic wherein each data point, contingent upon the

position of the moving mirror, contains information about every infrared frequency

originating from the source.
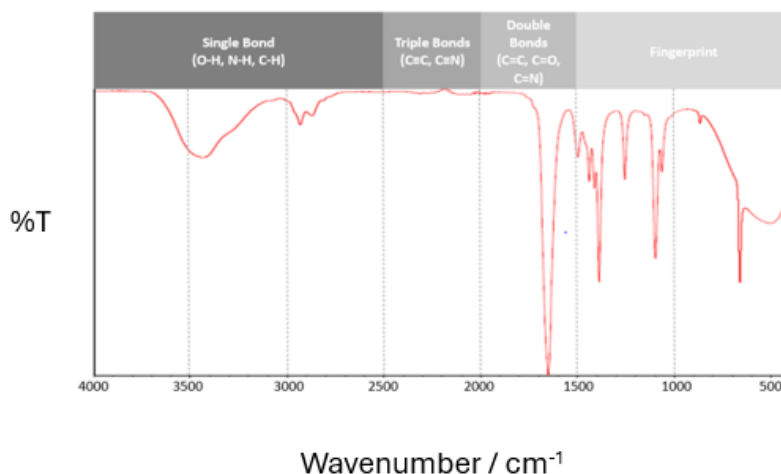
Figure 18. *Shows the mid-IR region, as used in this thesis* [14].

6.4. X-ray Diffraction analysis (Electrode surfaces).

X-ray diffraction (XRD) instruments are essential tools in the field of material science,

offering insights into the atomic and molecular structure of crystalline materials.

However, X-ray diffraction relies on the interaction between X-rays and the crystal lattice

of a material. When monochromatic X-rays are directed at a crystalline sample, the atoms

within the crystal scatter the X-rays. This scattering follows a specific pattern dictated by

Bragg's law [15]:

$$n\lambda = 2d\,sin(\theta) \qquad \textbf{Equation (8)}$$

Where:

n is an integer representing the order of diffraction.

λ is the wavelength of the incident X-rays.

d is the space between atomic planes within the crystal lattice.

θ is the angle between the incident X-ray beam and the scattered X-ray beam.

Moreover, the components of the X-ray diffraction (XRD) instrument can be summarized as follows:

1- X-ray Source: XRD instruments typically employ an X-ray tube as the source of X-rays. This tube generates X-rays when accelerated electrons collide with a target material, such as copper or cobalt. The result is monochromatic or nearly monochromatic X-rays.

2- Sample Holder: Crystalline samples under investigation are prepared as finely powdered or single-crystal specimens and securely placed on a sample holder to ensure even distribution.

3- Goniometer: A crucial element of XRD instruments, the goniometer allows precise control of the angles for both incident (θ) and scattered X-rays. Varying these angles permits the collection of diffraction data from various crystallographic planes. The X-ray tube generates a focused beam of X-rays with a specific wavelength such as Cu Kα radiation.

4- X-ray Detector: XRD instruments are equipped with detectors to measure the intensity of X-rays scattered at different angles. Common detector types include scintillation detectors, proportional counters, and solid-state detectors. These

detectors record the intensity of diffracted X-rays, forming the basis for creating a diffraction pattern.

5- Data Analysis Software: Modern XRD instruments are often connected to computers running specialized software for data analysis. This software processes the raw diffraction data, calculates crystal lattice parameters, and provides other structural insights about the sample.
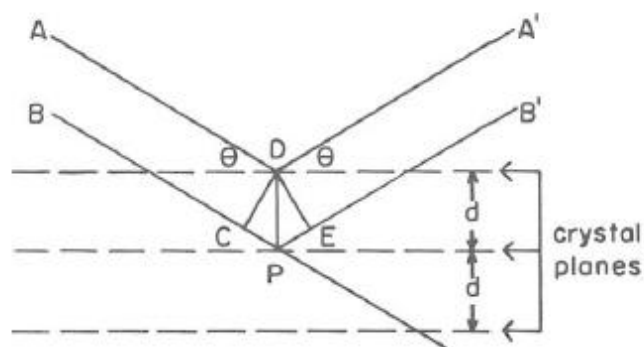
Figure 19. *Shows Diffraction from crystal planes, Bragg's idea* [15].

In this project, X-ray diffraction is used for studying nickel electrode (mesh). Nickel mesh analyzed using Rigaku Mini Flex with CuKα radiation. The scanning diffraction angle 2θ range was from 5 to 80° at a speed of 5° per minute. However, the idea of how this instrument works based on Bragg's law idea which illustrated in Figure 19.

6.5. Scanning electron microscope (SEM) and Energy Dispersion X-ray (EDX) Spectroscopy.

SEM represents an advanced microscopy method employed to capture highly magnified and detailed images of the surface morphology of specimens, while EDX is a technique

used in conjunction with electron microscopes (including SEM) to determine the elemental composition of a specimen.

Moreover, in this project, SEM equipped with EDX is used to give a detailed inspection of particle morphology and deliver precise analytical data with high sensitivity for individual particles.

The Scanning Electron Microscope (SEM) employs a concentrated electron beam, as opposed to visible light, to visualize the specimen and extract details regarding its structure and composition.

De Broglie introduced the wavelength equation for moving particles, specifically electrons, as

$$\lambda \ = \ h \ / \ (mv), \qquad \textbf{Equation (9)}$$

where:

λ represents the wavelength of the particles,

h denotes Planck's constant,

m signifies the mass of the particle (electron), and

v stands for the velocity of the particles.

The resolution of an optical microscope is the minimum distance between two points on a specimen that can still be discerned as distinct entities by either an observer or a camera system. The resolution (r) can be expressed as follows:

$$r = \lambda / (2NA) \quad \textbf{Equation } (\textbf{10})$$

Where,

λ represents the imaging wavelength.

NA stands for the numerical aperture of the objective.

EDX, or Energy Dispersive X-ray Spectroscopy, stands as a pivotal analytical technique frequently integrated within Scanning Electron Microscope (SEM) systems. This method gauges both the energy and intensity of X-rays generated when high-energy electrons from the SEM interact with the atoms within the sample, leading to the displacement of inner-shell electrons. Subsequently, these displaced electrons are replenished by electrons from outer shells, resulting in the emission of X-rays. The energy levels of these X-rays correspond to the specific elements found within the sample, while their intensity provides insights into the concentration of these elements. Furthermore, the EDX detector records the energy levels and the number of X-rays emitted by the sample. This dataset is harnessed to construct an elemental spectrum, which can be scrutinized to ascertain the elemental composition of the sample and gauge the relative proportions of these elements.
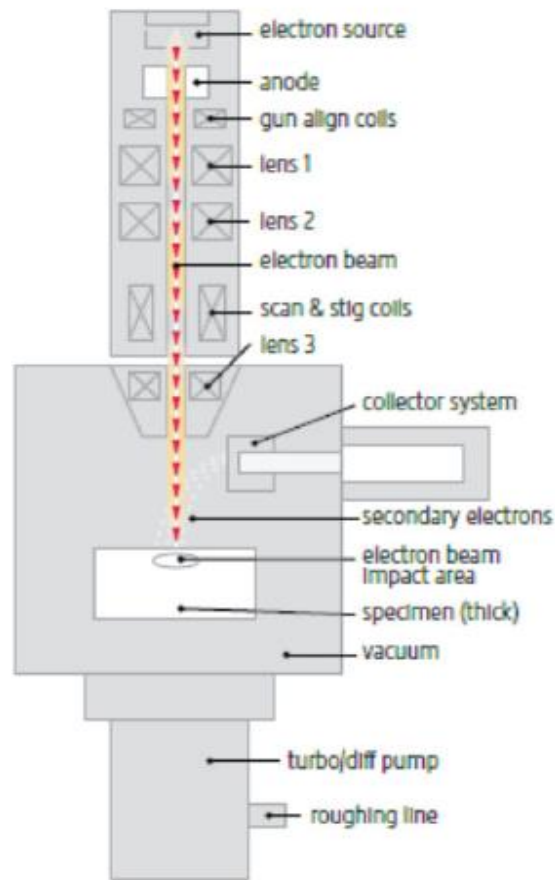
Figure 20. *Shows* Scanning electron microscope (SEM) instrument component [16].

The idea of this instrument Figure 20 starts when the electron gun generates an electron beam by heating a tungsten wire with an electrical current and then accelerating the electrons with the help of an anode.

This beam moves within a vacuum column, passing through electromagnetic fields and lenses that focus it onto the sample. To scan the sample's surface in a raster pattern,

deflection coils are used to guide the electron beam. Upon contact with the sample's surface, the incident beam generates various signals, including:

    a.   Secondary electrons (SE)

These electrons are characterized as low-energy emissions originating from the surface as a result of their interaction with the primary electron beam. They furnish valuable topographical data concerning the sample's surface, serving as the foundation for generating high-resolution images of the specimen [16].

    b.   Auger electrons (AES).

An incident high-energy electron from the SEM's electron beam interacts with an atom on the sample's surface. This collision transfers energy to one of the atom's inner-shell electrons, causing it to be excited and move to a higher energy level or be ejected from the atom entirely. When the inner-shell vacancy is filled, either by an outer-shell electron dropping down to the lower energy level or by another electron from a neighboring atom filling the vacancy, energy is released in the form of an Auger electron. The emitted Auger electron has a characteristic energy level, which is specific to the atom and energy level involved in the process. By measuring the energy of Auger electrons, researchers can identify the elements present in the sample and gain valuable compositional information.

    c.   Backscattered electrons (BSE).

High-energy electrons undergo backward scattering when they interact with the atoms within the sample. The intensity of these backscattered electrons is directly linked to the atomic number of the elements present in the sample, thereby imparting compositional contrast to the images.

Subsequently, these emitted signals are captured by electrical detectors, converted into digital images, and displayed on a screen. This digital imagery provides valuable information about the sample's elemental composition, structural variations, and morphology [16].

7. References

[1]   A. J. Bard and L. R. Faulkner, *Electrochemical Methods: Fundamentals and Applications*, John Wiley & Sons, New York., 2nd edn., (2001).

[2].   Biesheuvel, P. M., Porada, S., & Dykstra, J. E. The difference between Faradaic and non-Faradaic electrode processes. arXiv preprint arXiv:1809.02930 (2018).

[3].   Smith, T. J., & Stevenson, K. J. Reference Electrodes. In Handbook of Electrochemistry, *Elsevier*, 73-110 (2007).

[4].   Kahlert, H. Reference Electrodes. Electroanalytical Methods: Guide to Experiments and Applications, 291-308 (2010).

[5].   Leech, M. C., Garcia, A. D., Petti, A., Dobbs, A. P. & Lam, K. Organic Electrosynthesis: From Academia to Industry. *React Chem Eng.*, 5, 977–990 (2020).

[6]. Schotten, C., Nicholls, T. P., Bourne, R. A., Kapur, N., Nguyen, B. N., & Willans, C. E. (2020). Making electrochemistry easily accessible to the synthetic chemist. *Green Chemistry*, *22*(11), 3358–3375. https://doi.org/10.1039/d0gc01247e.

[7].   Kim, T., Choi, W., Shin, H. C., Choi, J. Y., Kim, J. M., Park, M. S., & Yoon, W. S. Applications of voltammetry in lithium-ion battery research. Journal of Electrochemical Science and Technology, 11(1), 14-25 (2020).

[8].   Bontempelli, G., Dossi, N. & Toniolo, R. Linear Sweep and Cyclic☆. Reference Module in Chemistry, Molecular Sciences and Chemical Engineering, *Elsevier*, https://doi.org/10.1016/B978-0-12-409547-2.12200-0. (2016).

[9].   Taherpour, A. A., & Mousavi, F. Carbon Nanomaterials for Electroanalysis in Pharmaceutical Applications. In Fullerens, Graphenes and Nanotubes, *William Andrew Publishing*, 169-225 (2018).

[10]. J.W.Akitt and B. E. Mann, *NMR and Chemistry: An introduction to modern NMR spectroscopy*, Cheltenham : Stanley Thornes, c2000, 4th edn., 2000.

[11]. Antcliffe, D., & Gordon, A. C. Metabonomics and intensive care. *Critical Care*, *20*(1). https://doi.org/10.1186/s13054-016-1222-8.(2016).

[12]. Van Bramer, S. E. An Introduction to Mass Spectrometry. Widener University, Department of Chemistry, One University Place, Chester, PA, 19013 (1998).

[13]. Thermo, N. Introduction to Fourier Transform Infrared Spectrometry. Thermo Nicolet Corporation. *Usa* 5 (2001).

[14]. Nandiyanto, A. B. D., Oktiani, R. & Ragadhita, R. How to Read and Interpret Ftir Spectroscope of Organic Material. *Indones. J. Sci. Technol*. 4, 97–118 (2019).

[15]. Whittig, L. D., & Allardice, W. R. X-ray Diffraction Techniques. *Methods of Soil Analysis: Part 1 Physical and Mineralogical Methods*, 5, 331-362 (1986).

[16] Kannan, M. Scanning Electron Microscopy: Principle, Components and Applications. *A textbook on fundamentals and applications of nanotechnology*, 81-92 (2018).

Chapter 3: Electro-carboxylation of phenyl-substituted Alkenes using Nickel cathode.

Synopsis

In this chapter, we will discuss the obtained results from electro-carboxylation reactions using Nickel as a cathode under simple reaction conditions. The product samples were analyzed using NMR, MS, and IR. Nickel cathode and Magnesium anode were analyzed using SEM-EDX, and XRD.

1. Introduction

Carbon dioxide emissions from burning fossil fuels are a major contributor to climate change, which is having increasingly serious environmental impact [1, 2]. At the same time, carbon dioxide is a valuable potential building block for the production of synthetic value-added chemicals [3, 4]. Electrochemical methods for the reduction of carbon dioxide (and/or its incorporation into substrate materials) are very appealing in this regard, as electrochemical technologies are inherently scalable [5, 6], whilst also offering the ability to couple directly to renewable energy sources [7, 8].

One avenue for employing carbon dioxide in synthesis via electrochemical means is the reduction of alkene substrates in the presence of CO_2, leading to addition of carboxylate units across the C=C bond and yielding highly desirable mono- and di-substituted carboxylic acids [9]. The exploration of this field has garnered significant attention in recent years and a selection of key reports in this area is summarized in Table 1. For example, Filardo et al. [10] studied the reduction of carbon dioxide at a graphite electrode in *N,N*-dimethylformamide (DMF) solvent containing tetrabutylammonium bromide (Bu_4NBr) as the supporting electrolyte at applied potentials between -2.45 to -2.50 V(vs. Ag/AgI) in a tank cell and obtained a mixture of 3-phenylpropionic and phenylsuccinic acids (Table 1, entry 1). Some of the same authors subsequently explored a wider range of potentials and reported somewhat altered product distributions [11] (Table 1, entry 2).

Most studies in this area appear to have been conducted under fixed current regimes, rather than at fixed potential. To this end, Dérien et al. explored the use of Ni complexes as catalysts for the electrochemically-driven addition of CO_2 to alkenes (Table 1, entry 3), again using a carbon-based working electrode [12]. A range of substrates were tested (styrene, α-methyl styrene, E-

β-methyl styrene and 1,1-diphenylethylene) and in some cases excellent yields of the substituted products were obtained.

Senboku and co-workers (Table 1, entry 4) examined a wider range of substrates still, and also replaced the carbon working electrode for a metal one (in their case, Pt). Their conditions led to a significant improvement in the conversion of the alkene substrates (essentially complete conversion in many cases), whilst still maintaining good-to-excellent yields for the functionalized substrates [13].

In 2008, Yuan et al. investigated the electrosynthesis of 2-aryl succinic acids by reacting carbon dioxide with a variety of aryl-substituted alkenes in an undivided electrochemical cell. These authors also employed their CO_2 at pressures above atmospheric (4 MPa) and comparatively modest current density (10 mA/cm^2). Of particular note, the authors compared the effect of using a Pt working electrode with using a Ni working electrode and were able to prepare the 2-aryl succinic products in fair to good yields (50-87%) with high selectivity (Table 1, entry 5) [14].

More recently, Alkayal et al. have studied the effect of using non-sacrificial counter electrodes during the electrolysis. In the vast majority of studies, a sacrificial anode is used, usually magnesium, such that Mg^{2+} ions are released into solution during the electrolysis which then binds to the acid products as they form. Alkayal et al. studied the use of copper working electrodes with both aluminum and carbon anodes at 50 °C in an undivided cell and developed a highly regioselective process for the formation of β-hydrocarboxylated products from substituted alkene substrates with potentially considerable synthetic utility (Table 1, entry 6) [15].

Inspired by these earlier studies, herein we report a study on the electrochemically-driven addition of CO_2 to a range of alkene substrates at nickel working electrodes at room temperature

(20 °C) and under 1 atm of carbon dioxide in a simple undivided cell in DMF, using the electrochemically inert electrolyte tetrabutylammonium hexafluorophosphate (nBu_4NPF_6). Our results show that there is still much that remains unknown about the process(es) by which CO_2 adds to alkenes under such electrochemical conditions, and that much remains to be optimized. Of particular note, we show a bias in favor of forming mono-substituted acid products, where the carbon dioxide adds exclusively to the position β to the aromatic ring in the substrates we examine, possibly as a result of using an Ni working electrode. We also provide direct evidence that the pathway whereby the alkenes are reduced at the electrode surface and then react with dissolved CO_2 is operating, adding credence to some of the mechanisms previously proposed for this class of reaction.

Table 1: *A selection of conditions, conversions and yields for the electro-reduction of alkenes in the presence of CO_2 from the literature.*

Entry	Alkene	Reaction Conditions	Conversion	Products and Yield	Ref
1	Styrene	Working electrode: Graphite electrode Counter electrode: Aluminum electrode Medium: DMF, Bu$_4$NBr, and continuously bubbling CO_2 Technique: Controlled potential electrolysis (−2.45 to 2.50 V vs Ag/AgI), Current density 24-12 mA/ cm^2. Cell type: diaphragmless tank cell Reaction temperature: Room temperature	60%	3-phenyl propionic acid (29%) Phenylsuccinic acid (60%)	[10]
2	Styrene	Working electrode: Graphite electrode Counter electrode: Aluminum electrode Medium: DMF, Bu$_4$NI, and continuously bubbling CO_2 Technique: Controlled potential electrolysis (−2.7 V vs Ag/AgI). Cell type: diaphragmless tank cell Reaction temperature: Room temperature	87%	Phenylsuccinic acid (40%) Phenylpropionic acid (35%) 3,4-diphenyl adipic acid (10%)	[11]
3	Styrene	Working electrode: Carbon fiber electrode	40%	Phenylsuccinic acid (85%)	[12]
	α-Methyl Styrene	Counter electrode: Magnesium electrode	35%	2,2-Disubstituted Succinic acid (71%)	
	E-β-Methyl Styrene	Medium: DMF, tetrabutylammonium tetrafluoroborate, CO_2 (1 atm)	45%	Mono and Dicarboxylic acids (44%)	
	1,1-Diphenylethylene	Technique: Current intensity 50 mA, 5-7 h Cell type: single-compartment cell Reaction temperature: 20 °C Catalyst: Ni complexes with several pentamethyl diethylene triamines	25%	2,2-Disubstituted Succinic acid (95%)	
4	Styrene	Working electrode: Platinum plate	73%	Phenylsuccinic acid (66%)	[13]
	α-Methyl Styrene	Counter electrode: Magnesium rod	98%	2,2-Disubstituted succinic acids (68%)	

	E-β-Methyl Styrene	Medium: DMF, tetraethylammonium perchlorate, CO_2 (1 atm)	98%	2-Methyl-3-phenylsuccinic acid (77%)	
	Z-β-Methyl Styrene	Technique: Constant current electrolysis (25 mA/cm^2)	98%	2-Methyl-3-phenylsuccinic acid (70%)	
	1,1-Diphenylethylene	Cell type: 2-Compartment cell	93%	2,2-Disubstituted succinic acids (91%)	
	E-Stilbene	Reaction temperature: −10 °C	84%	2,3-Diphenylsuccinic acid (84%)	
	Z-Stilbene	Styrene was electrolyzed in the presence of 4-methoxyphenol.	84%	2,3-Diphenylsuccinic acid (84%)	
5	Styrene	Working electrode: Nickel plate Counter electrode: Zinc plate Medium: DMF, n-Bu$_4$NBr, and CO_2 4 MPa. Technique: Constant current (10 mA/cm^2), two electrode set-up Cell type: high-pressure stainless-steel undivided cell Reaction temperature: Room temperature.	-	Phenyl succinic acid (50%)	[14]
		Working electrode: Nickel plate Counter electrode: Magnesium plate Medium: DMF, n-Bu$_4$NBr, and CO_2 4 MPa. Technique: Constant current (10 mA/cm^2), two electrode set-up Cell type: high-pressure stainless-steel undivided cell Reaction temperature: Room temperature.	-	Phenyl succinic acid (85%)	
		Working electrode: Nickel plate Counter electrode: Aluminum plate Medium: DMF, n-Bu$_4$NBr, and CO_2 4 MPa. Technique: Constant current (10 mA/cm^2), two electrode set-up Cell type: high-pressure stainless-steel undivided cell Reaction temperature: Room temperature.	-	Phenyl succinic acid (87%)	

		Working electrode: Platinum plate Counter electrode: Aluminum plate Medium: DMF, n-Bu$_4$NBr, and CO$_2$ 4 MPa. Technique: Constant current (10 mA/cm^2), two electrode set-up Cell type: high-pressure stainless-steel undivided cell Reaction temperature: Room temperature.	-	Phenyl succinic acid (89%)	
	α-Methyl Styrene	Working electrode: Nickel plate Counter electrode: Aluminum plate Medium: DMF, n-Bu$_4$NBr, and CO$_2$ 4 MPa. Technique: Constant current (10 mA/cm^2), two electrode set-up Cell type: high-pressure stainless-steel undivided cell Reaction temperature: Room temperature.	-	2-Methyl-2-phenyl succinic acid (85%)	
6	Styrene	Working electrode: Copper electrode Counter electrode: Carbon electrode Medium: DMF, n-Bu$_4$NI (0.04 M), triethylamine (0.04 M); triethanolamine (0.04 M), CO$_2$ (1 atm). Technique: Constant current at 60 mA, 24 hours Cell type: undivided cell, two-electrode set-up Reaction temperature: 50 °C	99%	3-Phenylpropanoic acid: 4-phenyl-1,3-dioxolan-2-one (3:1) ratio Phenylsuccinic acid: 3-phenylbutanoic acid (5:1).	[15]
		Working electrode: Copper electrode Counter electrode: Aluminum electrode Medium: DMF, n-Bu$_4$NI (0.04 M), and CO$_2$ (1 atm). Technique: Constant current at 60 mA, for 24 hours	-	2-phenylbutanoic acid (68%)	

		Cell type: undivided cell, two-electrode set-up Reaction temperature: 50 °C			
7	Styrene	Working electrode: Nickel Mesh Counter electrode: Magnesium rod	80 %	Phenylsuccinic acid (13%) 3-Phenylpropionic acid (53%)	This work
	α-Methyl Styrene	Medium: DMF, tetrabutylammonium hexafluorophosphate (TBA-PF$_6$), and	72 %	(S)-3-Phenylbutyric acid (68%)	
	E-β-Methyl Styrene	CO_2 (continuously supplied)	79 %	2-Methyl-3-phenylpropionic acid (69%)	
	Z-β-Methyl Styrene	Technique: Constant current electrolysis (35 mA) for 8 h	78 %	2-Methyl-3-phenylpropionic acid (68%)	
	1,1-Diphenylethylene	Cell type: undivided cell	75 %	2,3-Diphenylsuccinic acid (50%)	
	E-Stilbene	Reaction temperature: Room temperature.	74 %	2,3-Diphenylsuccinic acid (10%) 2,3-Diphenylpropionic acid (47%)	
	Z-Stilbene		84 %	2,3-Diphenylsuccinic acid (18%) 2,3-Diphenylpropionic acid (44%)	

2. Experimental Section

2.1. Materials:

Materials that are readily available for purchase (including supporting electrolytes, solvents, and alkenes) were used without undergoing any additional purification steps. Styrene (**1**, 99% purity), α-methyl styrene (**2**, 99% purity), trans-β-methyl styrene (**3**, 97% purity), cis-β-methyl styrene (**4**, >98% purity), 1,1-diphenylethylene (**5**, 98% purity), trans-stilbene (**6**, 98% purity) and cis-stilbene (**7**, 97% purity) were purchased from commercial sources and used as received. All the alkenes used in this study were purchased from Alfa Aesar, with the exception of Z-β-methyl styrene which was procured from TCI. The solvent used in this study, N,N-dimethylformamide, anhydrous, 99.8% purity, was obtained from Alfa Aesar and packaged under Argon. The supporting electrolyte, tetrabutylammonium hexafluorophosphate (98% purity) at a concentration of 0.1 M, was purchased from ThermoFisher Scientific. Carbon dioxide, with a purity of 99%, was purchased from BOC Ltd.

2.2. Electrochemical procedures:

A BioLogic SP-150 potentiostat was employed for all cyclic voltammetry and chronopotentiometry experiments. The electrochemical carboxylation of the alkenes was conducted using a one-compartment electrochemical cell with five necks (see Figure 1). The electrodes were situated in three of these necks, while the remaining two were designated for the gas inlet and outlet channels. The reference electrode utilized was a

saturated calomel electrode (CHI150, supplied by IJ Cambria Scientific Ltd), and the counter electrode (anode) was a magnesium rod measuring 6.35 mm in diameter and 25.4 mm in length, at a purity of 99.95% (metal basis) from Alfa Aesar. A nickel disc (BASi, 3.0 mm diameter) or a nickel mesh (0.35×2 cm^2, woven wire, 60 mesh, made from 0.18 mm wire, supplied by Alfa Aesar) were used as the working electrodes for cyclic voltammetry and bulk electrolysis respectively.
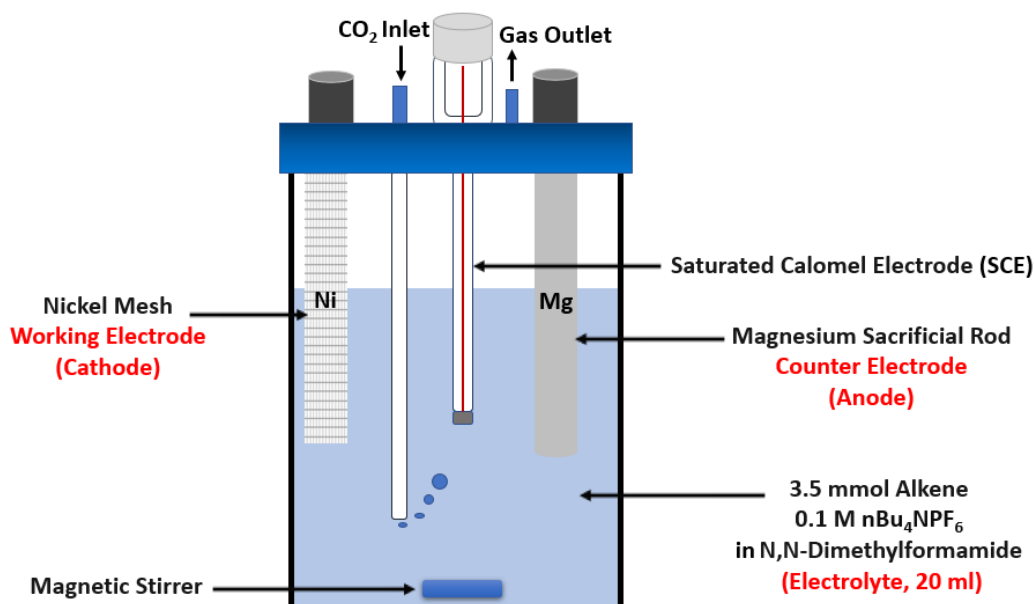
Figure 1: *An illustration of the cell set-up for both cyclic voltammetry and bulk electrolysis in this study.*

However, most of previous studies applied various of expensive working electrodes. In this work, we tend to use efficient and cheap electrode, which is nickel. In the matter of undivided cell choice, as primary study, we use this type of cells as most of previous studies investigated this field using undivided cell. In addition, few studies used mesh

electrodes to investigate the selectivity of products. Hence, this study is a further addition to the field.

However, prior to bulk electrolysis, the Ni mesh was sonicated in a sonication bath in 2 M HCl for 20 minutes and then rinsed with DMF. Meanwhile, the magnesium rod was sonicated in a sonication bath in DMF for 20 minutes. Both electrodes were then allowed to dry in the air. Bulk electrolysis was then initiated at room temperature (20 °C) with stirring under a constant stream of CO_2. In all cases, the electrolyte consisted of 0.1 M, tetrabutylammonium hexafluorophosphate (nBu_4NPF_6) in anhydrous N, N-dimethylformamide (volume = 20 mL). Into this volume of electrolyte, 3.5 mmol of alkene substrate was dissolved, giving a concentration of alkene substrate in the electrolyte of 0.175 M. For all bulk electrolyses, a fixed current of −35 mA was applied to the working electrode for 8 hours (corresponding to the passage of 3 *F* of charge relative to the number of moles of alkene present). The voltage required to deliver such currents was typically within the range −3 to −5.5 V vs SCE.

Although the range of voltage varied and increase during the electrolysis, but the mesh electrode geometry would be expected to selectively reduce good amount of the alkene into carboxylic acids. Moreover, the voltage range is approximately not too high in compared to other studies. If so, it is due to DMF degradation while products are consumed.

All cyclic voltammetry was performed under the same conditions and in the same cell as for bulk electrolysis, except using a Ni disc button working electrode (BASi, 3mm diameter). Cyclic voltammograms were recorded under Ar and under CO_2 for comparison (in both cases after bubbling for 20 minutes). The working electrode was polished between

experiments. Cyclic voltammetry was recorded at a scan rate of 10 mV/s over the range 0 V to −3 V vs. SCE, starting from 0 V.

2.3. Workup procedure:

The following procedure was adopted after bulk electrolysis for all the alkenes investigated. Firstly, the resulting electrolyte solution was placed in a round-bottomed flask, and the electrochemical cell and electrodes were washed with DMF and these rinsings added to the round-bottomed flask. The solvent was then removed under vacuum using a rotary evaporator. To the resulting residue was added 10 mL of 2.0 M hydrochloric acid (HCl) and the mixture stirred at room temperature for a duration of 3 hours. The purpose of this step was to fully protonate any carboxylic acids present, in order to facilitate their extraction into organic media. In the case of α-methyl styrene, cis-β-methyl styrene, and cis-stilbene, it was found that sonication for 30 minutes in an ice-filled sonication bath aided with breaking up the residue after addition of the HCl. After sonication, these mixtures were then stirred at room temperature for a duration of 3 hours as above. In all cases, the resulting mixture was then subjected to three successive extractions using diethyl ether, each with a volume of ether of 20 mL. It was found that chilling the aqueous phase prior to extraction was beneficial for improving the yield of products in the organic phase. The combined diethyl ether fractions were then combined and subjected to washing with saturated sodium chloride (brine solution). The organic phase was then dried using magnesium sulfate, filtered through filter paper, and evaporated using a rotary evaporator. Finally, the resulting solution was analyzed using nuclear magnetic resonance (NMR)

spectroscopy. NMR spectra were recorded at room temperature using a Bruker 400 MHz NMR spectrometer. The products were dissolved in CDCl$_3$ for analysis. The analysis procedure is summarized in Figure 2.
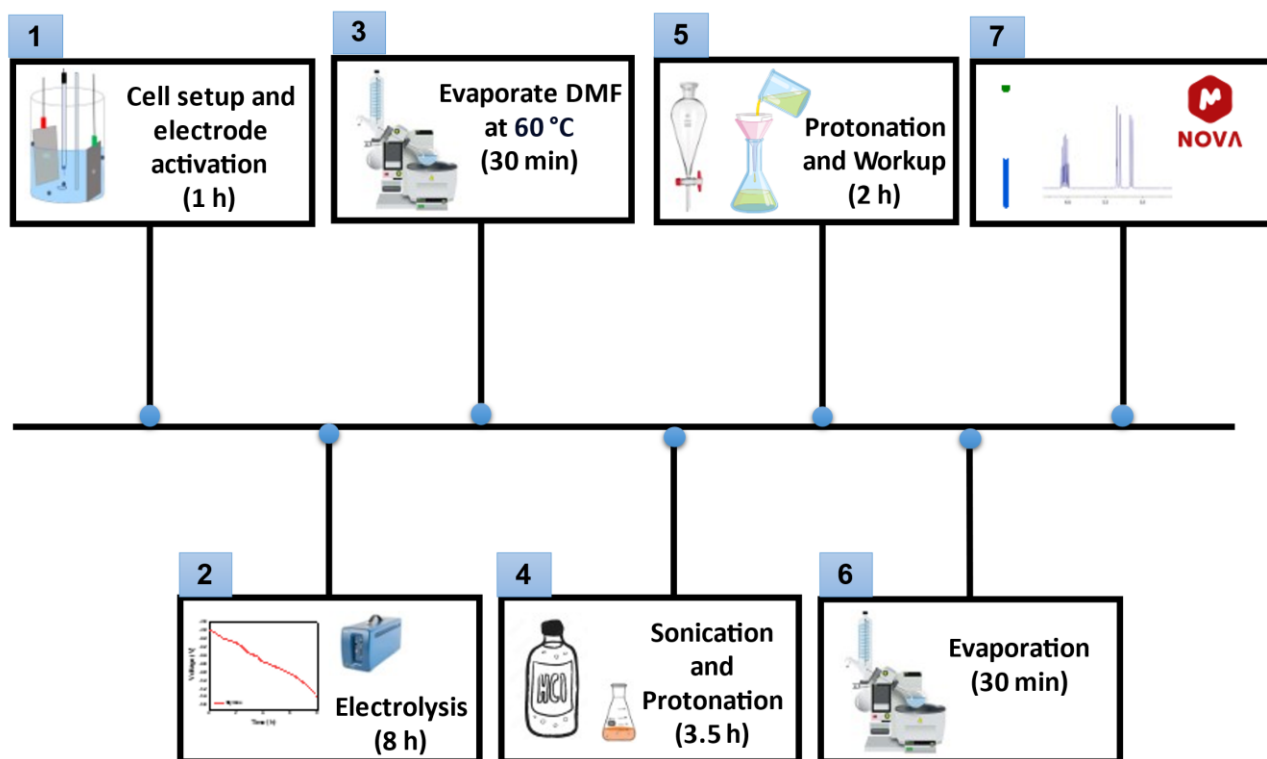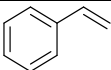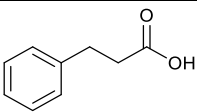
Figure 2: *An illustration of the extraction and analysis procedure used to isolate the products of electrolysis in this study.*
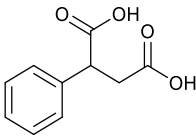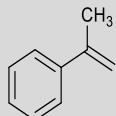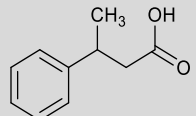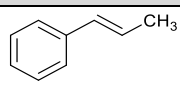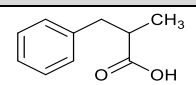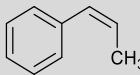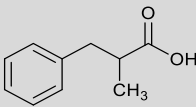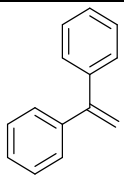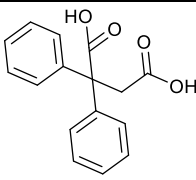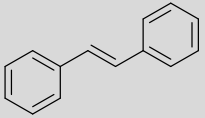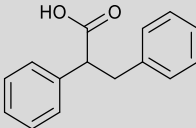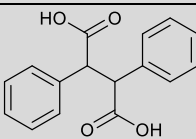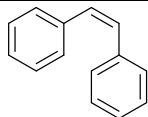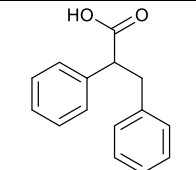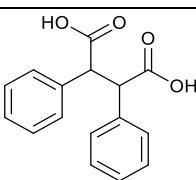
3. Results and Discussion

Table 1 shows conversions, isolated yields and Faradaic efficiencies for the production of various carboxylic acids from their parent alkenes under the conditions given in the experimental section, with the corresponding NMR, mass spectrometry and infrared spectroscopy data for all resulting products given in (Table 3). In all cases, substrate

conversion is good-to-excellent, indicating that the alkene starting materials are generally completely consumed during the reaction. However, in comparison to previous studies on electro-reduction of alkenes in the presence of carbon dioxide, the yields of mono-carboxylic acids are significantly higher and the yields of the di-carboxylic acids are correspondingly lower. For example, Senboku et al (Table 1, entry 4) obtained yields of the dicarboxylic acids of between 65 and 91% when operating at 263 K on a Pt cathode, with mono-carboxylic acids observed only in small amounts. In our study, this trend is reversed [1]. Campbell and Young have shown that Ni cathodes (such as were used here) are capable of hydrogenating activated double bonds to a much greater extent than cadmium, lead, amalgamated lead, copper or platinum cathodes [2]. This might explain the greater propensity towards the production of mono-carboxylic acids (where hydrogen has been added in preference to a second carbon dioxide molecule) compared to analogous studies on Pt cathodes [1].

Table 2: *conversions, isolated yields, and Faradaic efficiencies for the production of various carboxylic acids.*

Entry	Substrate	Substrate conversion (%)	Product	Isolated yield (%)	Faradic efficiency (%)
1		>99		53	36

Entry	Substrate	Conv. (%)	Product		
			2-phenylsuccinic acid	13	8
2	α-methylstyrene	>99	3-phenylbutanoic acid	68	46
3	(E)-β-methylstyrene	>99	2-methyl-3-phenylpropanoic acid	69	46
4	(Z)-β-methylstyrene	>99	2-methyl-3-phenylpropanoic acid	68	46
5	1,1-diphenylethylene	>99	2,2-diphenylsuccinic acid	67	44
6	(E)-stilbene	>99	2,3-diphenylpropanoic acid	62	41
			2,3-diphenylsuccinic acid	15	10
7	(Z)-stilbene	84	2,3-diphenylpropanoic acid	44	30
			2,3-diphenylsuccinic acid	18	12

In terms of the mono-carboxylic acids that are produced, it is striking that when non-symmetrical alkene substrates are employed, the monocarboxylic acids that are observed are all the anti-Markovnikov products (i.e. the carbon dioxide is found to add to the lesser-substituted of the two possible carbons from the alkene). The alternative arrangement (where CO_2 has added only to the more substituted carbon) is never observed. Figure 3 illustrates the three possible products that can be formed when carbon dioxide adds to a non-symmetrical substrate such as styrene. If carbon dioxide adds at both positions of the double bond, then 2-phenylsuccinic acid results. Conversely, if only mono-substitution occurs, then there are two possibilities for the products: 3-phenylpropionic acid (where the carbon dioxide adds to the terminal (β) position of the double bond, on the least substituted carbon) or 2-phenylpropionic acid (where the carbon dioxide adds to the more substituted (α) carbon).

Phenylbutyric acid   Phenyl Propionic acid   Phenyl Succinic acid
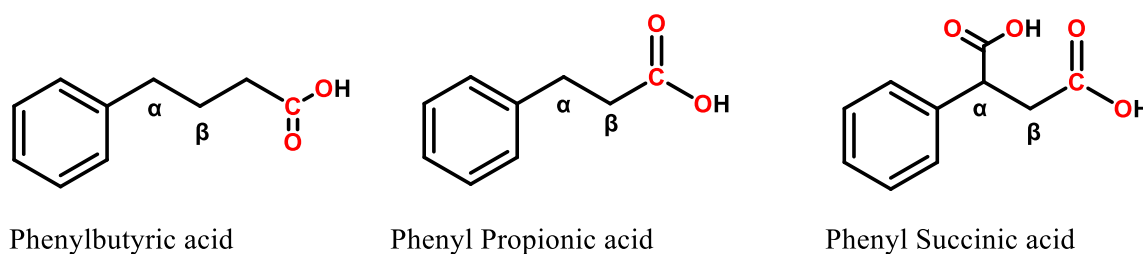
Figure 3: *The three possible structures that are possible after carboxylation of a phenyl-substituted alkene.*

These data show the position of the charge density when the alkene substrates in Table 2 are reduced by one electron to give the radical anions (see Figure 4 for possible

mechanisms). In all cases, the reactive unpaired electron on the radical anions is found at the β-carbon position. This appears to be a consequence of the aromatic ring syphoning electron density off the α-carbon through conjugation, leaving the more distant β-carbon with the larger electron density. The upshot is that carboxylate substitution at the β-carbon is preferred to substitution at the α-position for all the substrates that were examined. Previous studies on the electro-reductive addition of CO_2 to alkenes have proposed that both pathways shown in Figure 4 are possible, on account of the CO_2 and alkene reduction potentials being close to one another. However, the conditions used in this study, direct reduction of carbon dioxide at the electrode surface does indeed occur at approximately the same position as alkene reduction, implying that both pathways could operate in our case, at least in theory. However, to the best of our knowledge, direct evidence for either pathway has yet to be observed during the electro-reductive addition of CO_2 to alkenes.
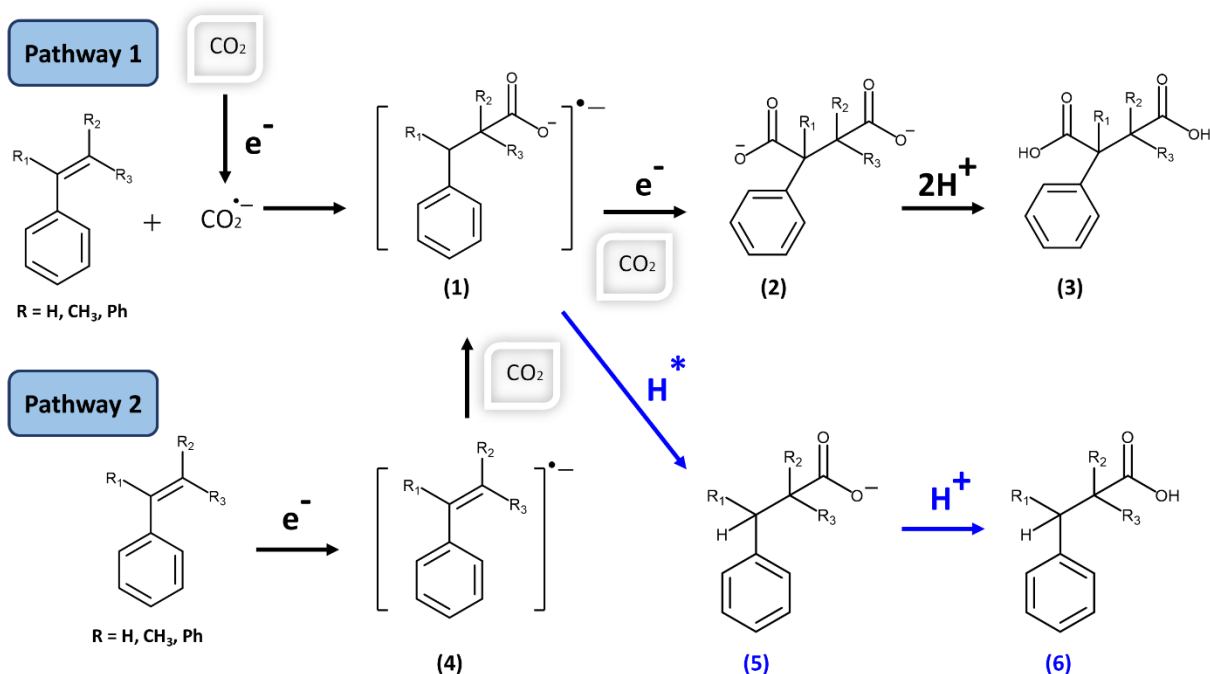
Figure 4: *The two suggested pathways for the electrochemically driven addition of CO_2 to alkene substrates: initial CO_2 reduction at the electrode, followed by addition (Pathway 1) and initial reduction of the alkene at the electrode, followed by reaction with CO_2 (Pathway 2). Arrows in black show the proposed route to the di-carboxylic acids; arrow in blue show the proposed route to the mono-carboxylic acids.*

Figure 4 depicts two potential reaction pathways that warrant consideration. The initial pathway, denoted as Pathway 1, commences with the reduction of carbon dioxide due to its higher reduction potential when compared to the alkene substrate. This reduction process generates a radical anion of carbon dioxide, which subsequently engages in a reaction with the alkene, forming an intermediate known as monocarboxylated compound (1). A subsequent electron reduction in the presence of carbon dioxide yields the dicarboxylation product (2). Following a protonation step, this product (2) is transformed

into a dicarboxylic acid. On the other hand, there might be side protonation process, which could come from the surrounding and presence of water. This creates a chance of producing mono acids as a main or side product. Another reason dis due to nickel as cathodic electrode tends to produce hydrogen during the reaction.

In the second pathway, Pathway 2, the alkene undergoes a direct one-electron reduction, leading to the formation of its anion radical (4). The interaction between (4) and CO_2 produces a monocarboxylated intermediate (1). Subsequent one-electron reduction, followed by a reaction with CO_2, culminates in the formation of the dicarboxylation product (2), which, after protonation, transitions into (3). Notably, there exists an alternative route for the intermediate monocarboxylated compound (1) if it undergoes protonation before experiencing further electron reduction. This alternative path leads to the formation of (5), which subsequently converts into (6) following another protonation step. In both of these pathways, during the electrolysis process, magnesium (Mg) metal dissolves, resulting in the presence of Mg^{2+} ions at the anode. These magnesium ions readily interact with carboxylate ions, forming stable magnesium carboxylate complexes. Through subsequent acid treatment, these complexes yield either mono or dicarboxylic acids.

The cyclic voltammograms of trans-stilbene and cis-stilbene in the presence and absence of CO_2 are instructive in this regard (Figure 11 and Figure 12 respectively). Figure 11 (red line) shows the cyclic voltammogram of electrolyte saturated with CO_2, while the blue line shows the cyclic voltammogram of electrolyte with 3.5 mmol trans-stilbene under argon. In the latter case, a quasi-reversible redox wave centered at around -2.3 V vs. SCE is

evident for the trans-stilbene. The green line then shows the effect of having both CO_2 and trans-stilbene present: the cyclic voltammogram very much resembles that of trans-stilbene in argon, but it now takes on features of a catalytic wave, with enhanced reductive current and a complete absence of any return oxidation wave for the redox event centered at −2.3 V vs. SCE. This implies that the reduced trans-stilbene is reacting with dissolved CO_2 chemically before it can be re-oxidized electrochemically at the electrode. This in turn suggests that a mechanism whereby the alkene is initially reduced at the electrode surface (with this then going on to react with carbon dioxide) is operating (Pathway 2 in Figure 4). Whilst these data do not exclude the possibility that Pathway 1 is operating simultaneously, they do at least provide evidence for the occurrence of Pathway 2, demonstrating directly for the first time that the "alkene first" route is a contributor in the electro-reductive addition of CO_2 to alkenes.

3.1. Cyclic Voltammetry
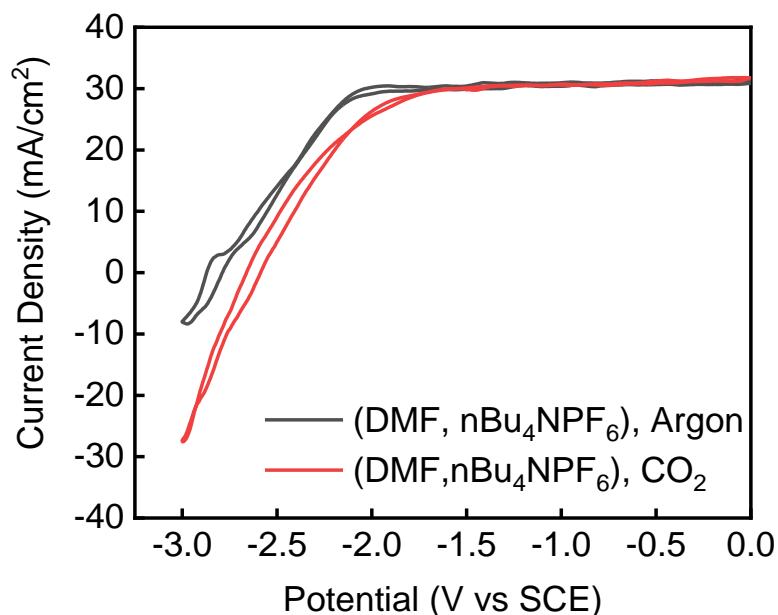
Figure 5: Cyclic Voltammetry of the electrolyte solution, 20 mL DMF containing 0.1 M nBu_4NPF_6 supporting electrolyte at room temperature, with scan rate of 10 mV/s. A Ni disc button (3 mm diameter) was used as the working electrode, a Mg rod was used as the counter electrode and an SCE electrode was used as the reference. Color code: electrolyte saturated with Ar (black line); electrolyte saturated with CO_2 (red line).

As a starting investigation point, a solution with just nBu_4NPF_6 supporting electrolyte in DMF at room temperature is run under argon Figure 5 (black trace) which indicates some irreversible background processes are occurring (e.g. breakdown of solvent). If the assumption that the system is fully isolated, then the breakdown of solvent should be the only effect on the occurrence of the negative current. This leads to lower the productivity percentage of the reaction due to some charges will be passed to degrades the DMF solvent.
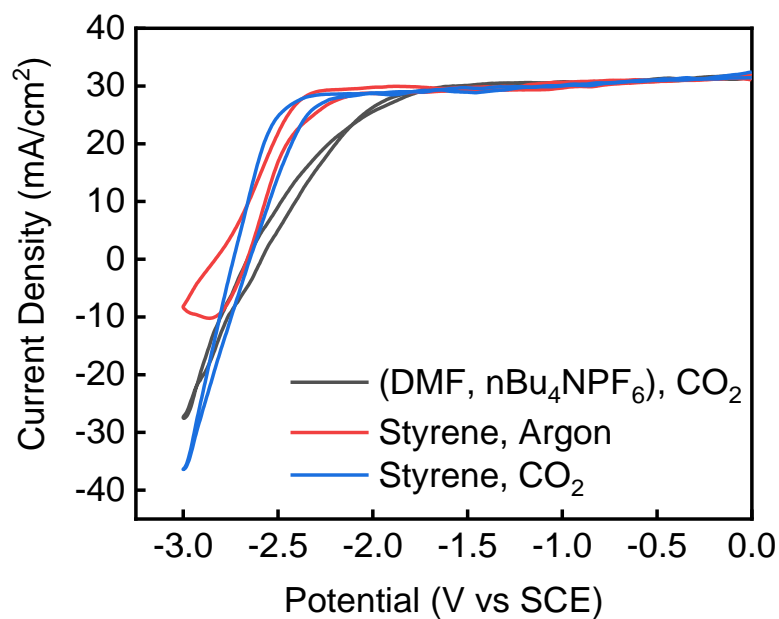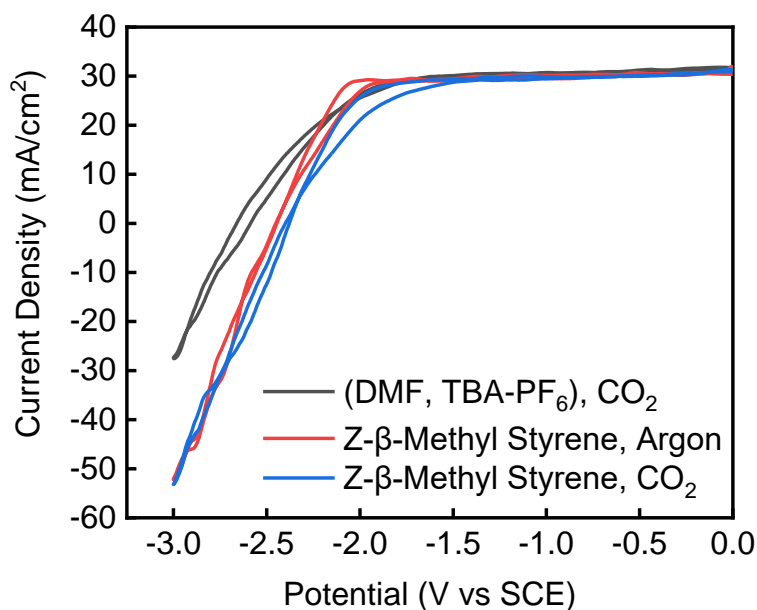
Figure 6: *Cyclic Voltammetry of 3.5 mmol solution of Styrene in 20 mL DMF containing 0.1 M nBu$_4$NPF$_6$ supporting electrolyte at room temperature, with scan rate of 10 mV/s. A Ni disc button (3 mm diameter) was used as the working electrode, a Mg rod was used as the counter electrode and an SCE electrode was used as the reference. Color code: electrolyte saturated with CO$_2$ (Black line), electrolyte plus 3.5 mmol of styrene saturated with Ar (Red line), electrolyte plus 3.5 mmol of styrene saturated with CO$_2$ (Blue line).*

Moreover, after adding styrene to the blank solution, the blue and black curves exhibit significant similarity, suggesting that in both cases, carbon dioxide reduction is occurring. At a potential of -3 V, there appears to be a slightly higher current for the combination of styrene and carbon dioxide. This observation hints at the possibility (-38 mA/cm^2) that, under these conditions, both styrene and carbon dioxide may be undergoing reduction processes.
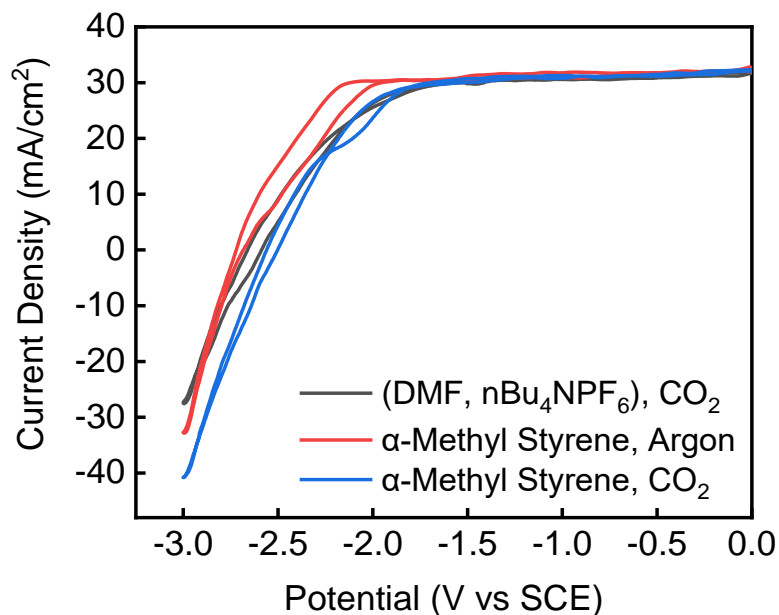
Figure 7: *Cyclic Voltammetry of a 3.5 mmol solution of α-Methyl Styrene in 20 mL DMF*

containing 0.1 M nBu₄NPF₆ supporting electrolyte at room temperature, with scan rate of

10 mV/s. A Ni disc button (3 mm diameter) was used as the working electrode, a Mg rod

was used as the counter electrode and an SCE electrode was used as the reference. Color

code: electrolyte saturated with CO₂ (Black line), electrolyte plus 3.5 mmol of α-Methyl

Styrene saturated with Ar (Red line), electrolyte plus 3.5 mmol of α-Methyl Styrene

saturated with CO₂ (Blue line).

Moreover, irreversible reaction occurs in (blue trace, Figure 7), and the current density for

both styrene Figure 6 and α-Methyl Styrene Figure 7 reached around -40 mA/cm^2 under
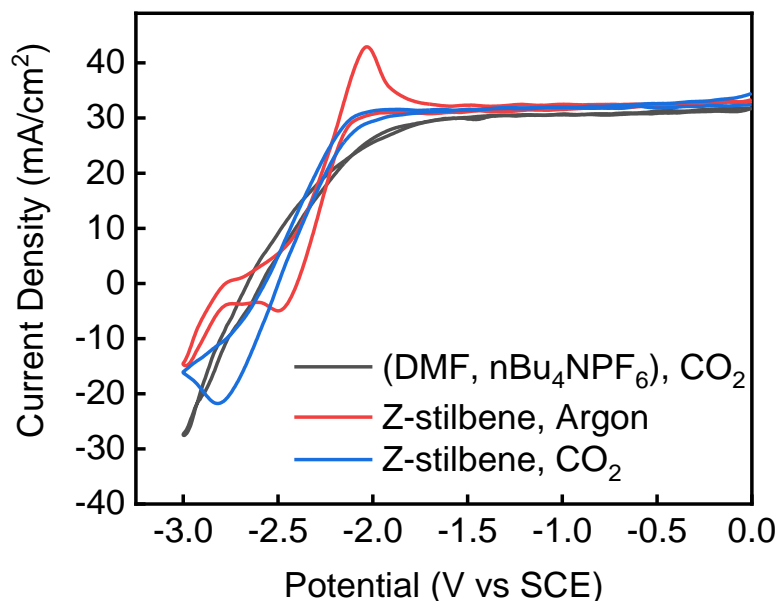
carbon dioxide.
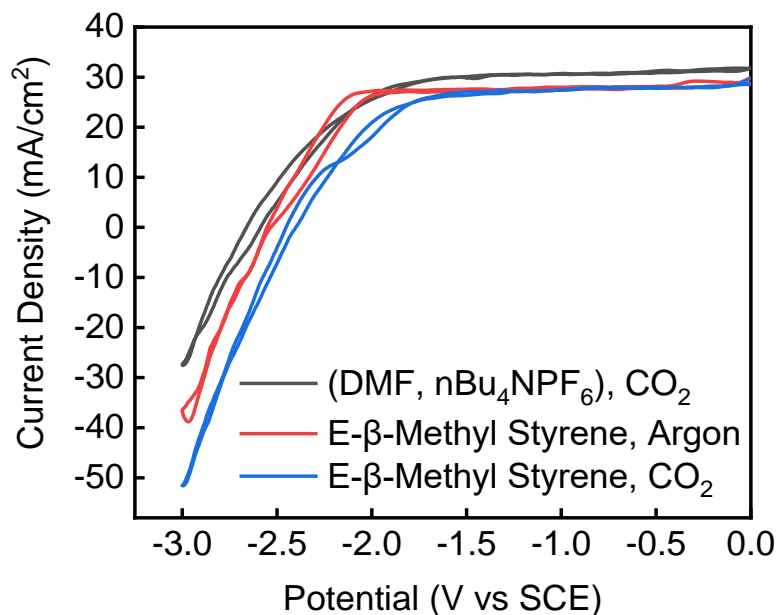
Figure 8: *Cyclic Voltammetry of a 3.5 mmol solution of E-β-Methyl Styrene in 20 mL DMF containing 0.1 M nBu₄NPF₆ supporting electrolyte at room temperature, with scan rate of 10 mV/s. A Ni disc button (3 mm diameter) was used as the working electrode, a Mg rod was used as the counter electrode and an SCE electrode was used as the reference. Color code: electrolyte saturated with CO_2 (Black line), electrolyte plus 3.5 mmol of E-β-Methyl Styrene saturated with Ar (Red line), electrolyte plus 3.5 mmol of E-β-Methyl Styrene saturated with CO_2 (Blue line).*

As a further investigation, E-β-methyl styrene is tested under argon Figure 8 (red trace) for a slightly more negative current than that of α-methyl styrene in Figure 7 (red trace). Interestingly, a negative current has a density of around -50 mA/cm² Figure 8 (blue trace) under carbon dioxide in compared to α-methyl styrene in Figure 7 (blue trace) where the

current density is around -40 Ma/cm^2. However, both α-methyl styrene and E-β-methyl styrene will take both mechanism rout in the same time.

Figure 9: *Cyclic Voltammetry of a 3.5 mmol solution of Z-β-Methyl Styrene in 20 mL DMF containing 0.1 M nBu$_4$NPF$_6$ supporting electrolyte at room temperature, with scan rate of 10 mV/s. A Ni disc button (3 mm diameter) was used as the working electrode, a Mg rod was used as the counter electrode and an SCE electrode was used as the reference. Color code: electrolyte saturated with CO$_2$ (Black line), electrolyte plus 3.5 mmol of Z-β-Methyl Styrene saturated with Ar (Red line), electrolyte plus 3.5 mmol of Z-β-Methyl Styrene saturated with CO$_2$ (Blue line).*

However, the cyclic voltammetry of the same compound in the form Cis (Z) will have the same result as trans of the same compound in form (E) β-methyl styrene mentioned above (Figure 8).
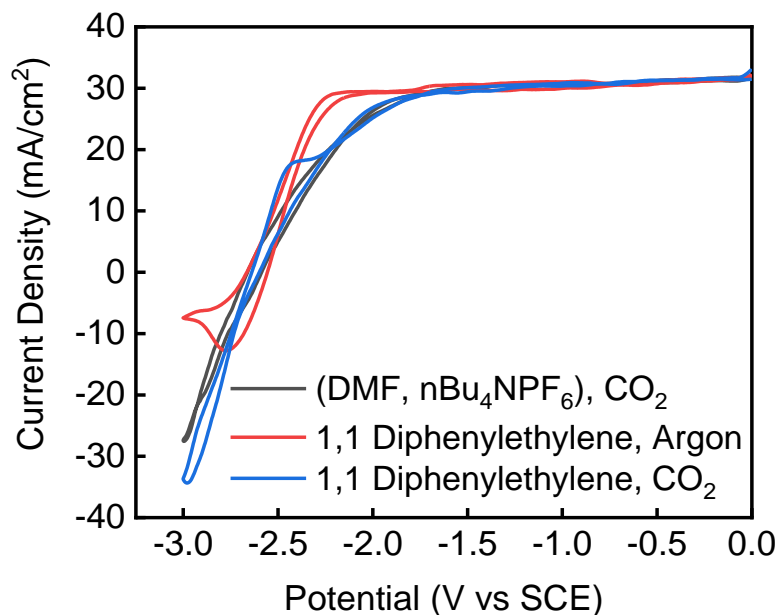
Figure 10: *Cyclic Voltammetry of a 3.5 mmol solution of 1,1-Diphenylethylene in 20 mL DMF containing 0.1 M nBu$_4$NPF$_6$ supporting electrolyte at room temperature, with scan rate of 10 mV/s. A Ni disc button (3 mm diameter) was used as the working electrode, a Mg rod was used as the counter electrode and an SCE electrode was used as the reference. Color code: electrolyte saturated with CO$_2$ (Black line), electrolyte plus 3.5 mmol of 1,1-Diphenylethylene saturated with Ar (Red line), electrolyte plus 3.5 mmol of 1,1-Diphenylethylene saturated with CO$_2$ (Blue line).*

Furthermore, to achieve a more comprehensive study, 1,1 diphenylethylene (two phenyl rings on one carbon atom) is examined by cyclic voltammetry Figure 10. It seems that Styrene Figure 6 is almost similar to the cyclic voltammetry of 1,1 Diphenylethylene.
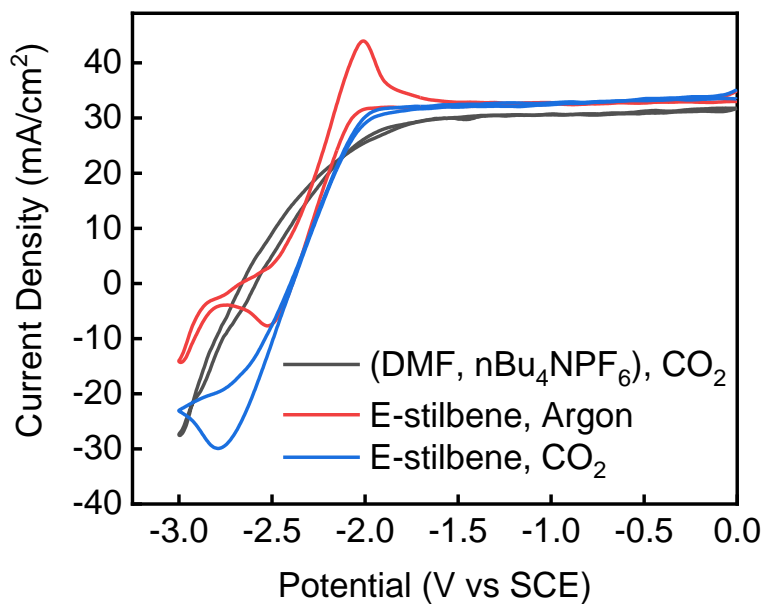
Figure 11: *Cyclic voltammetry of a 3.5 mmol solution of trans-stilbene in 20 mL DMF containing 0.1 M nBu₄NPF₆ supporting electrolyte at room temperature, with scan rate of 10 mV/s. A Ni disc button (3 mm diameter) was used as the working electrode, a Mg rod was used as the counter electrode and an SCE electrode was used as the reference. Color code: electrolyte saturated with CO₂ (black line), electrolyte plus 3.5 mmol of trans-stilbene saturated with Ar (red line), electrolyte plus 3.5 mmol of trans-stilbene saturated with CO₂ (blue line).*

Figure 12: *Cyclic Voltammetry of a 3.5 mmol solution of Z-Stilbene in 20 mL DMF*

containing 0.1 M nBu₄NPF₆ supporting electrolyte at room temperature, with scan rate of

10 mV/s. A Ni disc button (3 mm diameter) was used as the working electrode, a Mg rod

was used as the counter electrode and an SCE electrode was used as the reference. Color

code: electrolyte saturated with CO_2 (Black line), electrolyte plus 3.5 mmol of Z-Stilbene

saturated with Ar (Red line), electrolyte plus 3.5 mmol of Z-Stilbene saturated with CO_2

(Blue line).

Additionally, if phenyl ring is substituted in two different carbon atoms in the double bond

Figure 11 and 12, whether in the form of trans (E) and cis (Z), then the stilbene (two phenyl

ring) will re-oxidize, and the reaction will be quasi reversible (chemically) (red trace under

argon). The return peak disappears if the same alkene is under carbon dioxide, which means

the reaction between reduced stilbene and carbon dioxide is happening.

3.2. Chronopotentiometry.
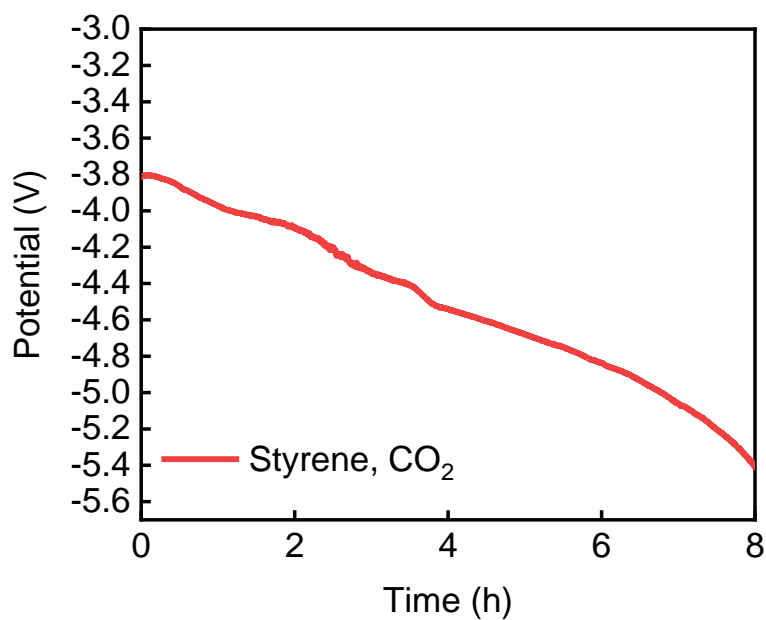
Figure 13: Chronopotentiometry of a 3.5 mmol solution of Styrene in 20 mL DMF containing 0.1 M nBu₄NPF₆ supporting electrolyte at room temperature, with fixed current -35 mA/cm² for 8 hours. A Ni mesh (2×0.35 cm²) was used as the working electrode, a Mg rod was used as the counter electrode and an SCE electrode was used as the reference. The carbon dioxide was bubbled continuously during the reaction.
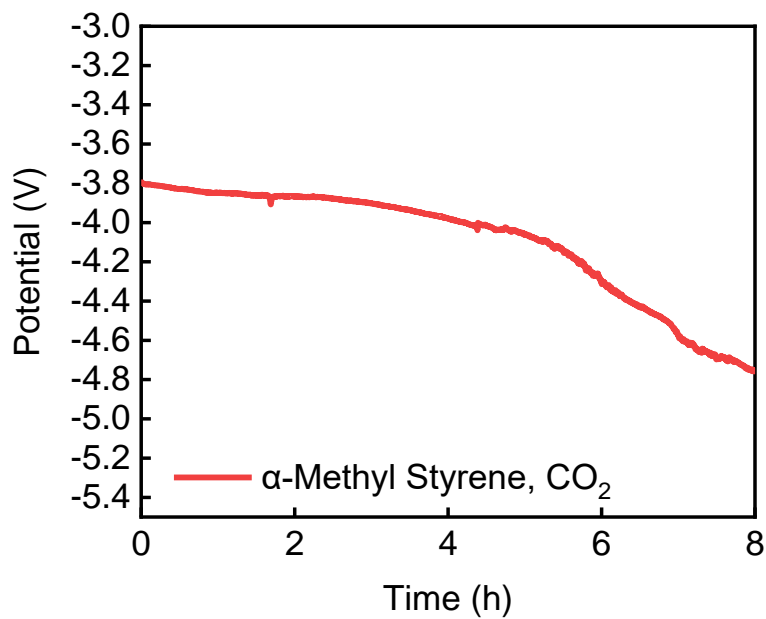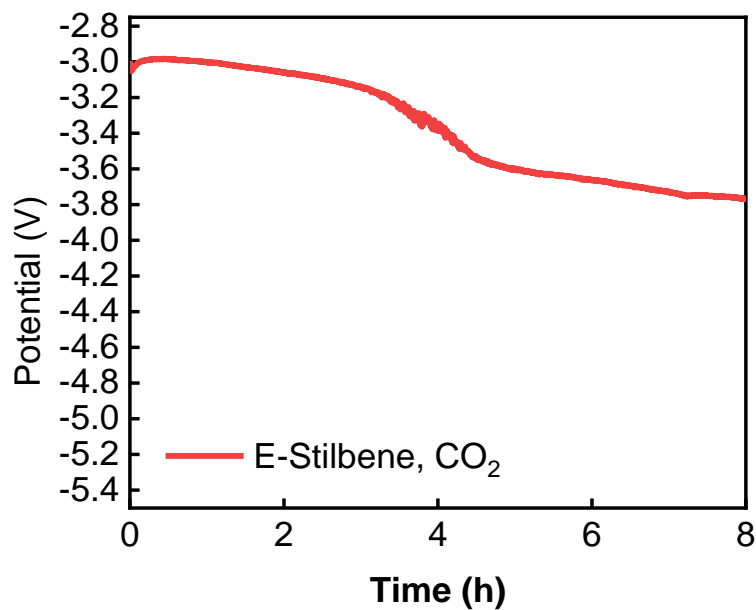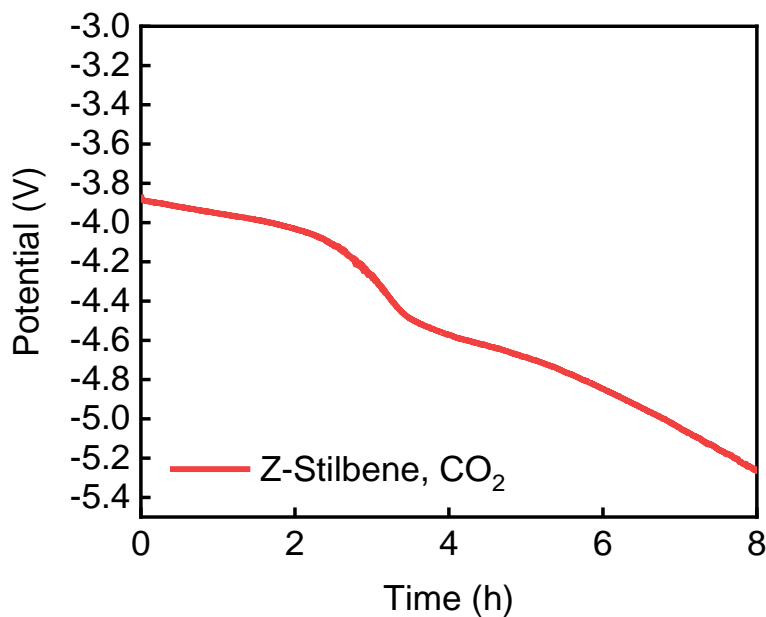
Figure 14: *Chronopotentiometry of a 3.5 mmol solution of α -Methyl Styrene in 20 mL DMF containing 0.1 M nBu₄NPF₆ supporting electrolyte at room temperature, with fixed current -35 mA/cm² for 8 hours. A Ni mesh (2×0.35 cm²) was used as the working electrode, a Mg rod was used as the counter electrode and an SCE electrode was used as the reference. The carbon dioxide was bubbled continuously during the reaction.*
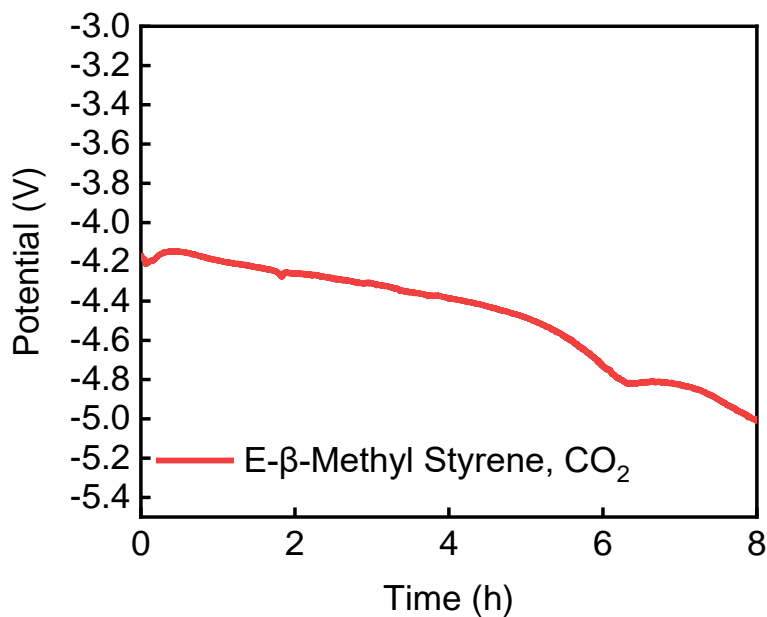
Figure 15: *Chronopotentiometry of a 3.5 mmol solution of E-β-Methyl Syrene in 20 mL DMF containing 0.1 M nBu₄NPF₆ supporting electrolyte at room temperature, with fixed current -35 mA/cm² for 8 hours. A Ni mesh (2×0.35 cm²) was used as the working electrode, a Mg rod was used as the counter electrode and an SCE electrode was used as the reference. The carbon dioxide bubbled continuously during the reaction.*
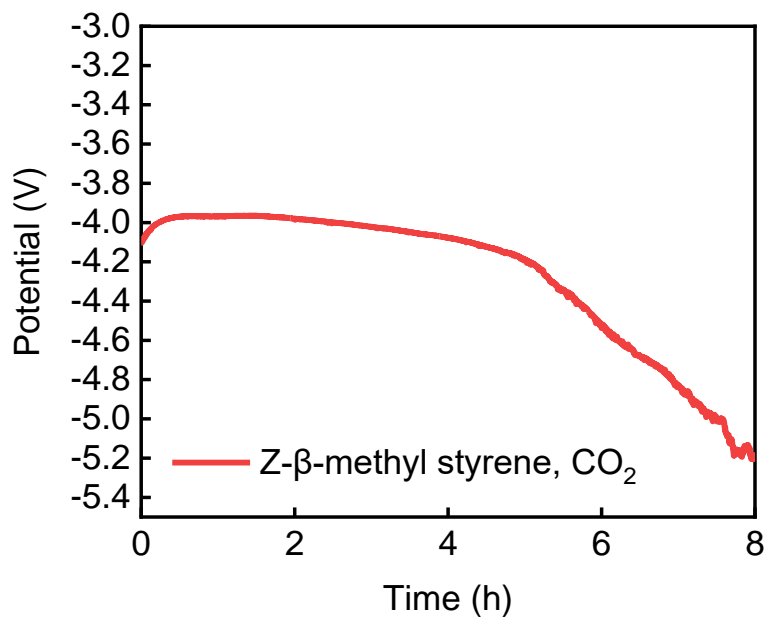
Figure 16: *Chronopotentiometry of a 3.5 mmol solution of Z-β-Methyl Syrene in 20 mL DMF containing 0.1 M nBu₄NPF₆ supporting electrolyte at room temperature, with fixed current -35 mA/cm² for 8 hours. A Ni mesh (2×0.35 cm²) was used as the working electrode, a Mg rod was used as the counter electrode and an SCE electrode was used as the reference. The carbon dioxide was bubbled continuously during the reaction.*
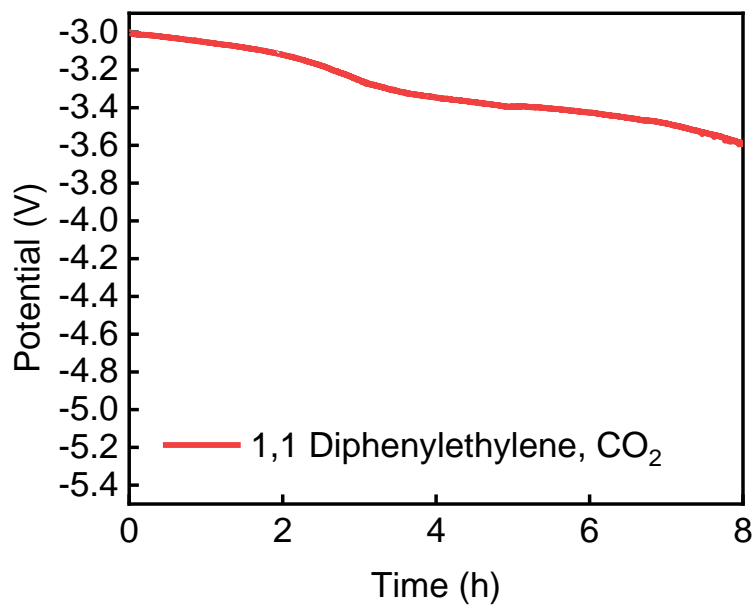
Figure 17: *Chronopotentiometry of a 3.5 mmol solution of 1,1 Diphenylethylene in 20 mL*

DMF containing 0.1 M nBu₄NPF₆ supporting electrolyte at room temperature, with fixed

current -35 mA/cm² for 8 hours. A Ni mesh (2×0.35 cm²) was used as the working electrode,

a Mg rod was used as the counter electrode and an SCE electrode was used as the

reference. The carbon dioxide was bubbled continuously during the reaction.

Figure 18: *Chronopotentiometry of a 3.5 mmol solution of E-Stilbene in 20 mL DMF containing 0.1 M nBu₄NPF₆ supporting electrolyte at room temperature, with fixed current -35 mA/cm² for 8 hours. A Ni mesh (2×0.35 cm²) was used as the working electrode, a Mg rod was used as the counter electrode and an SCE electrode was used as the reference. The carbon dioxide was bubbled continuously during the reaction.*

Figure 19: *Chronopotentiometry of a 3.5 mmol solution of Z-Stilbene in 20 mL DMF containing 0.1 M nBu₄NPF₆ supporting electrolyte at room temperature, with fixed current -35 mA/cm² for 8 hours. A Ni mesh (2×0.35 cm²) was used as the working electrode, a Mg rod was used as the counter electrode and an SCE electrode was used as the reference. The carbon dioxide was bubbled continuously during the reaction.*

In all the above presented chronopotentiometry graphe for varied alkenes, it is clearly seen that the voltage range between -3 to -5.5. However, most previous studies show the use of high applied voltage if chronoamperometry is the applied technique.

3.3.^{1}H NMR and ^{13}C NMR of All alkenes and products.

¹H NMR Styrene
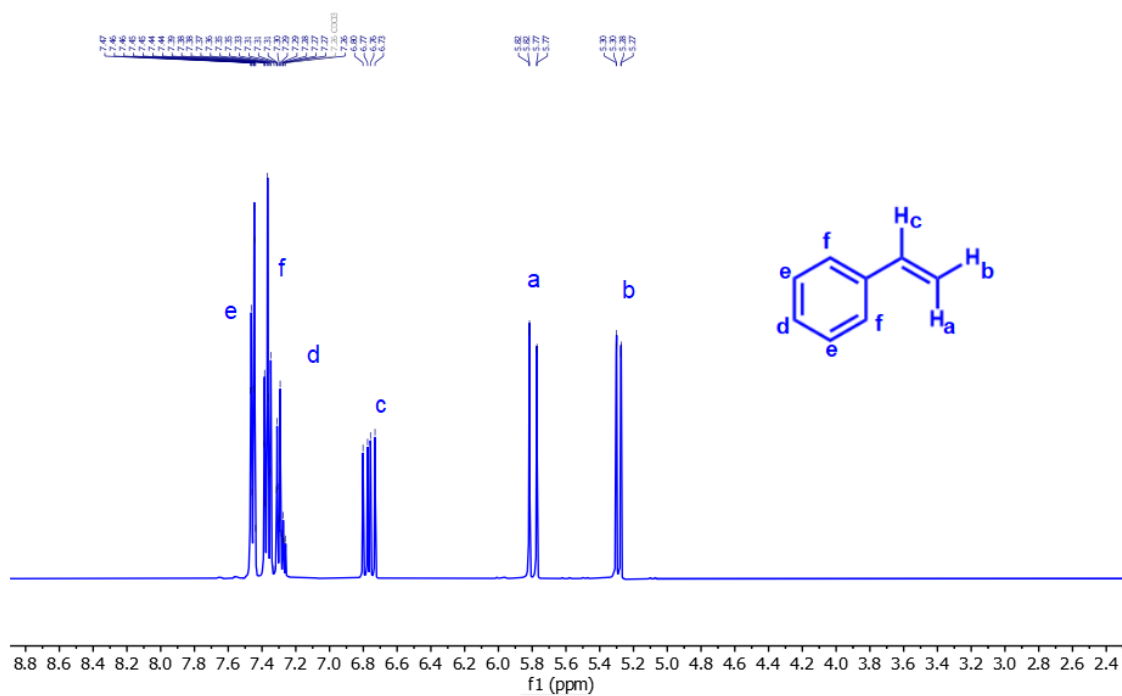
Figure 20. *¹H NMR of Styrene.*

¹H NMR (400 MHz, CDCl₃) δ 7.51 – 7.41 (m, 2H), 7.41 – 7.33 (m, 2H), 7.33 – 7.23 (m, 1H), 6.77 (dd, *J* = 17.6, 10.9 Hz, 1H), 5.80 (dd, *J* = 17.6, 0.9 Hz, 1H), 5.29 (dd, *J* = 10.9, 0.9 Hz, 1H).
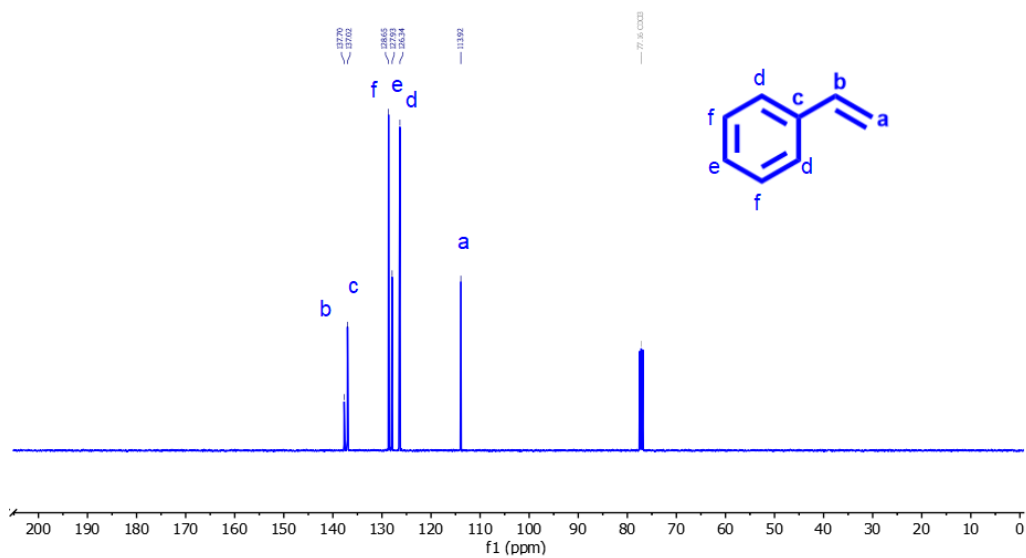
***Figure 21**. *^{13}C NMR of Styrene.*

<u>Styrene</u>: ^{13}C NMR (101 MHz, CDCl$_3$) δ 137.70, 137.02, 128.65, 127.93, 126.34, 113.92.
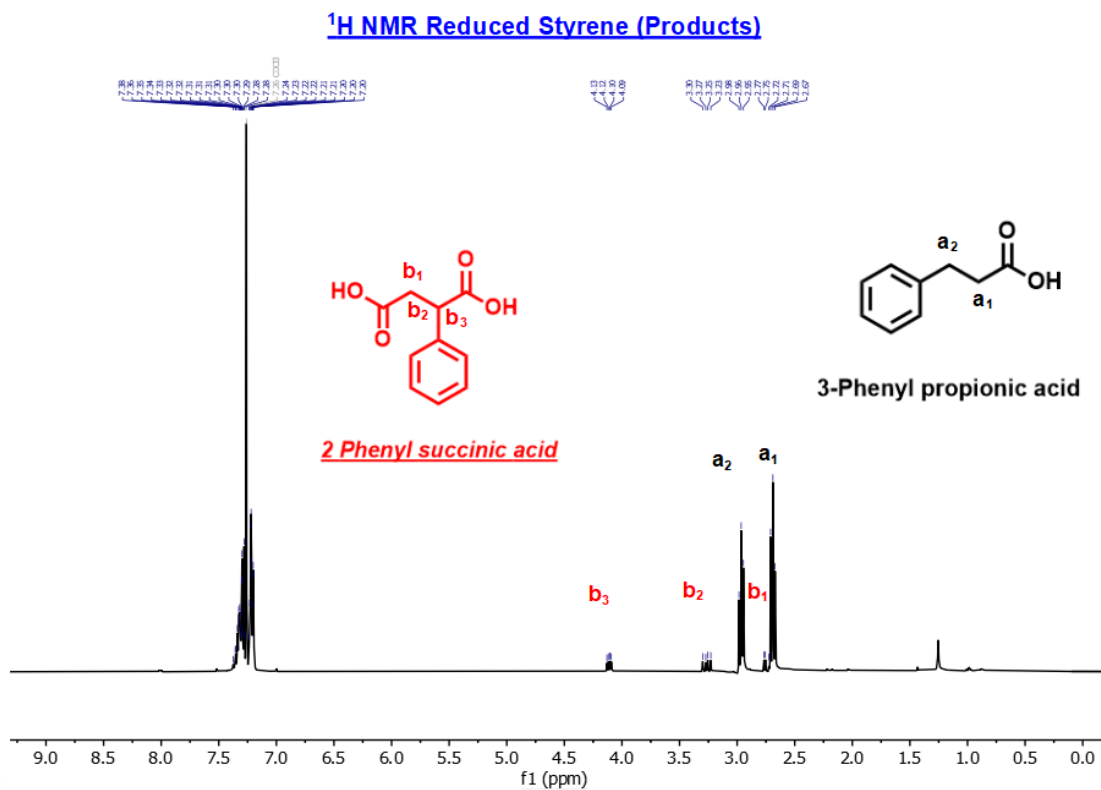
Figure 22. *^{1}H NMR of products of styrene reduction.*

3-Phenyl propionic acid: ^{1}H NMR (400 MHz, CDCl$_3$) δ 7.50 - 7.15 (m, 5H, Ph), 2.96 (t, J = 7.2 Hz, 2H, C*H$_2$*), 2.69 (t, J= 7.4 Hz, 2H, CH$_2$).

2-Phenyl succinic acid: ^{1}H NMR (400 MHz, CDCl$_3$): 7.33–7.38 (m, 4H, Ph), 7.25–7.28 (m, 1H, Ph), 4.11 (q, J = 5.1 Hz, 1H), 3.26 (dd, J=10.2 Hz, J=4.0 Hz, 1H), d 2.75 (dd, J=12.0 Hz, J=4.0 Hz, 1H).
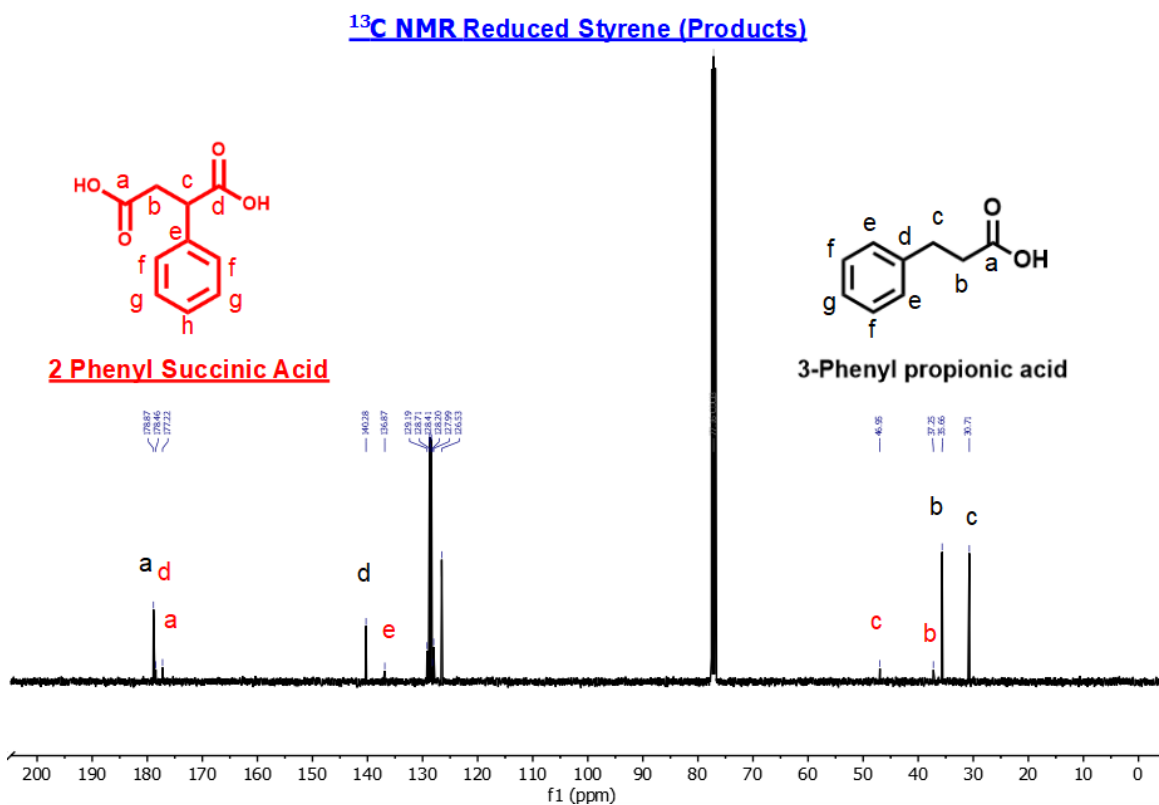
Figure 23. ^{13}C NMR of products of styrene reduction.

3-Phenyl propionic acid: ^{13}CNMR (101 MHz, CDCl$_3$) δ 178.87, 140.28, 128.71, 128.41, 126.53, 35.66, 30.71.

2-Phenyl succinic acid: ^{13}CNMR (101 MHz, CDCl$_3$) δ 178.46, 177.22, 136.87, 129.19, 127.99, 128.20, 46.95, 37.25.

Figure 24. *^{1}H NMR of α-Methyl Styrene.*

α-Methyl styrene: ^{1}H NMR (400 MHz, CDCl$_3$) δ 7.46 – 7.36 (m, 2H), 7.32 – 7.21 (m, 2H), 7.24 – 7.15 (m, 1H), 5.30 (s, 1H), 5.01 (s, 1H), 2.09 (t, *J* = 1.1 Hz, 3H).

¹³C NMR α-Methyl Styrene
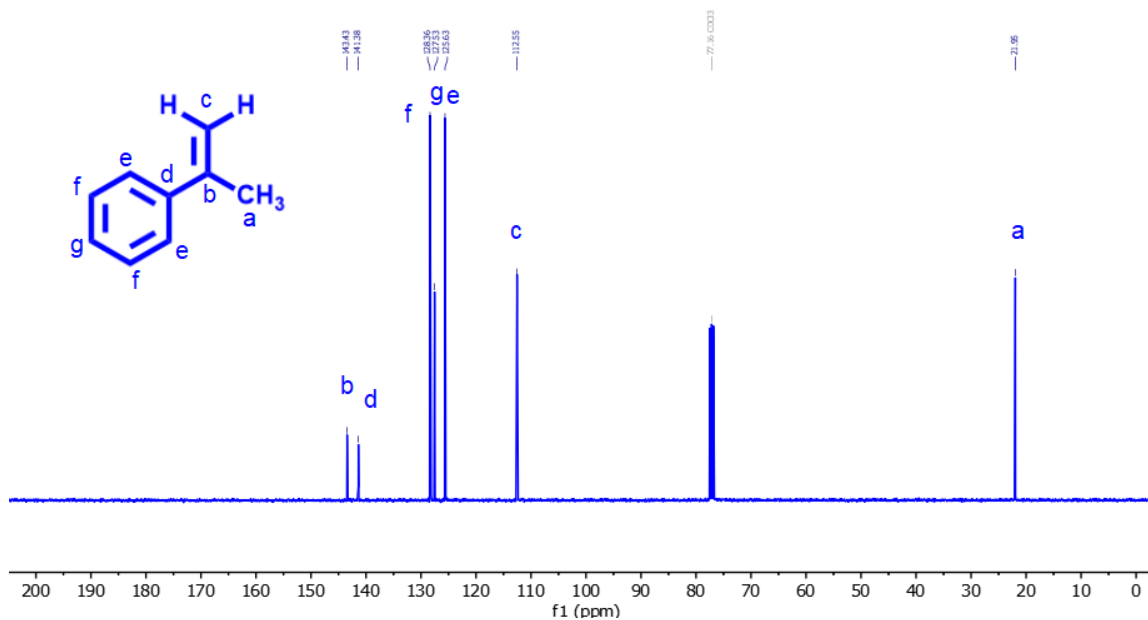
Figure 25. *¹³C NMR of α-Methyl Styrene.*

α-Methyl styrene :¹³C NMR (101 MHz, CDCl₃) δ 143.43, 141.38, 128.36, 127.53, 125.63, 112.55, 21.95.
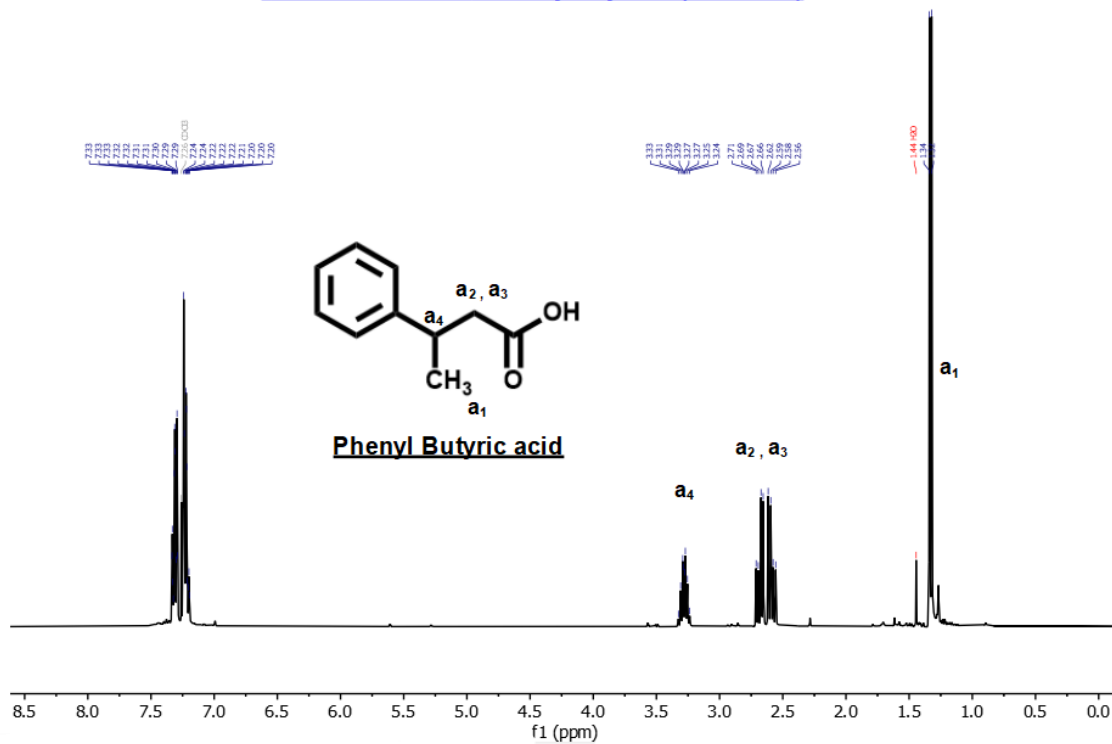
Figure 26. *¹H NMR of products of α-methylstyrene reduction.*

Phenyl butyric acid:¹H NMR (400 MHz, CDCl₃) δ 7.44 – 7.26 (m, 2H), 7.26 – 7.20 (m, 3H), 3.28 (dt, *J* = 8.3, 6.8 Hz, 1H), 2.62 – 2.56 (m, 2H), 1.33 (d, *J* = 7.0 Hz, 3H).
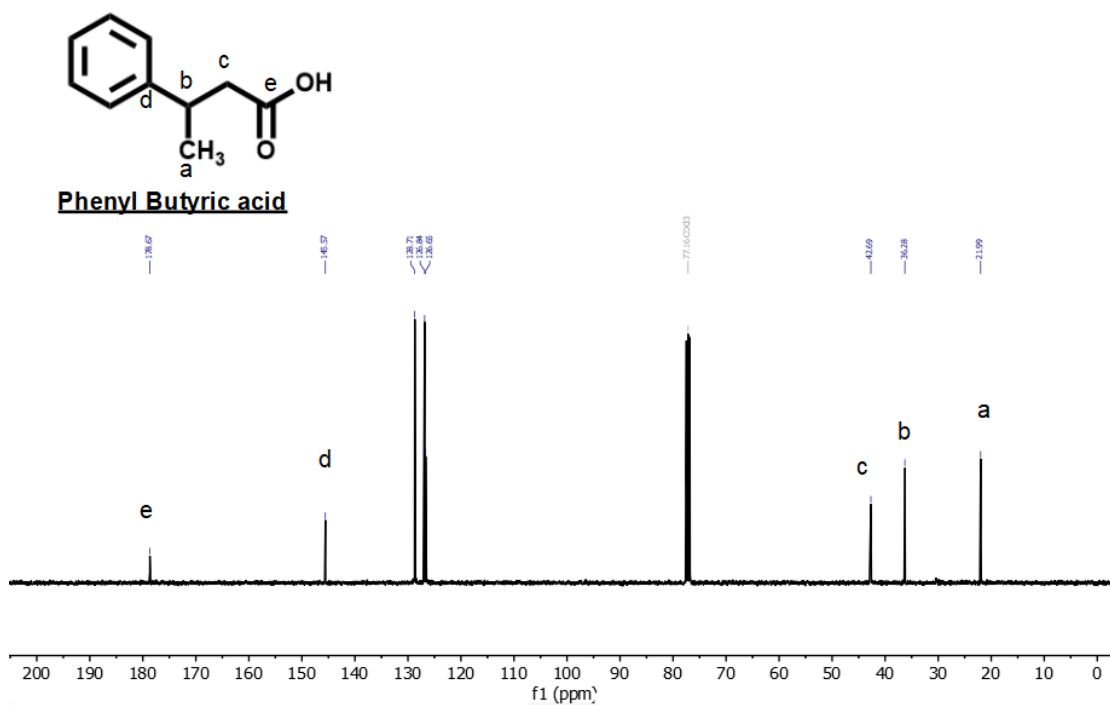
Figure 27. *^{13}C NMR of products of α-methylstyrene reduction.*

Phenyl butyric acid: ^{13}C NMR (101 MHz, CDCl$_3$) δ 178.67, 145.57, 128.71, 126.84, 126.65, 42.69, 36.28, 21.99.

¹H NMR E-β-Methyl styrene
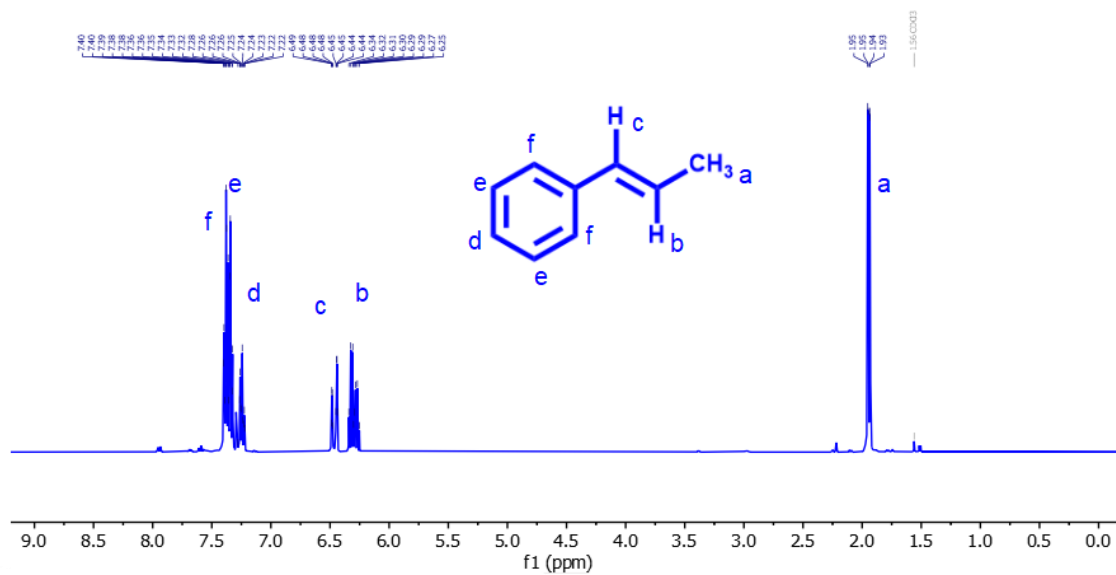
Figure 28*. ¹H NMR of E-β-Methyl Styrene.*

E-β-Methyl styrene: ¹H NMR (400 MHz, CDCl₃) δ 7.40 – 7.22 (m, 5H), 6.46 (dq, $J =$ 15.8, 1.7 Hz, 1H), 6.30 (dq, $J =$ 15.7, 6.5 Hz, 1H), 1.94 (dd, $J =$ 6.5, 1.6 Hz, 3H).
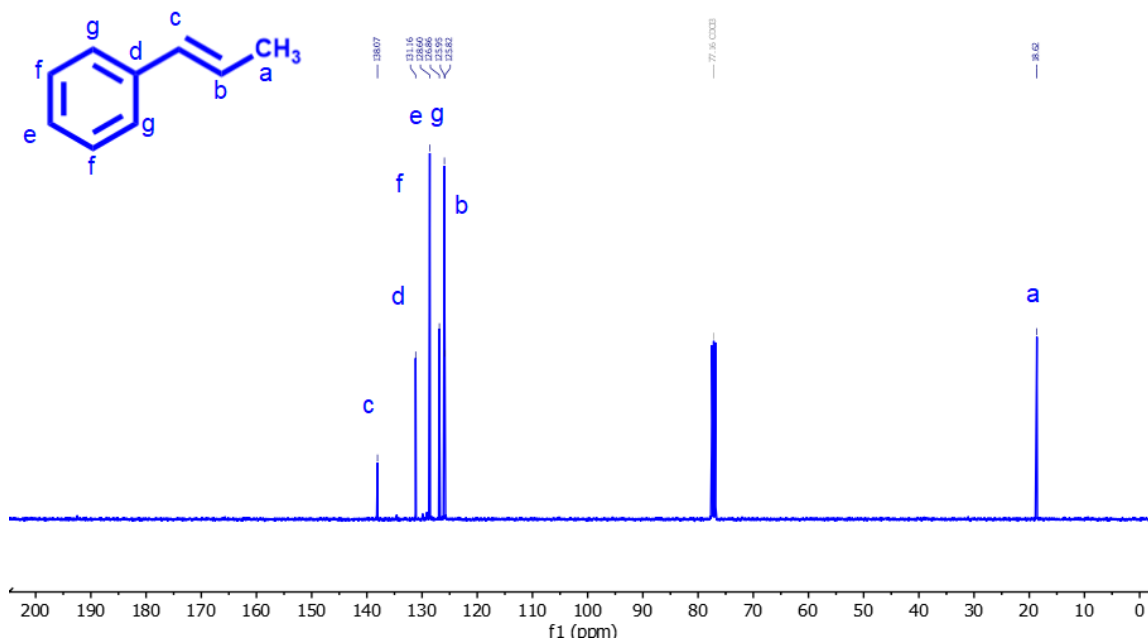
Figure 29. ^{13}*C NMR of E-β-Methyl Styrene.*

E-β-Methyl styrene: ^{13}C NMR (101 MHz, CDCl$_3$) δ 138.07, 131.16, 128.60, 126.86, 125.95, 125.82, 18.62.
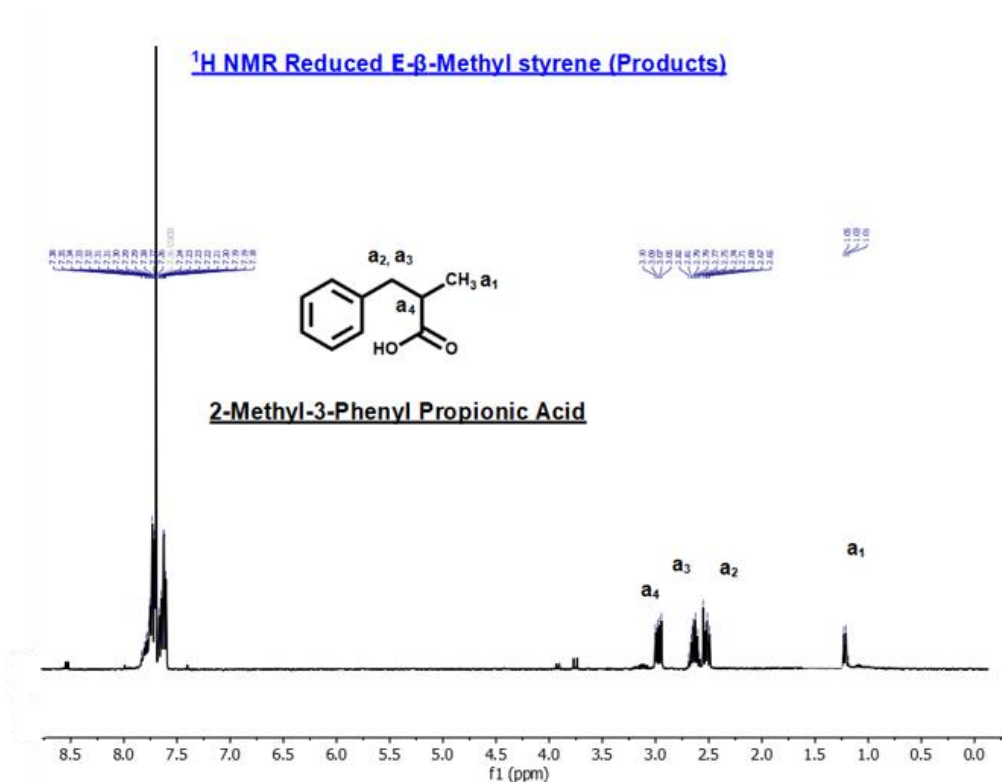
Figure 30. *^{1}H NMR of products of E-β-methylstyrene reduction.*

2-Methyl-3-phenylpropionic acid: ^{1}H NMR (400 MHz, CDCl$_3$) δ 7.35 – 7.28 (m, 5H), 3.08 (dd, J = 13.4, 6.4 Hz, 1H), 2.84 – 2.78 (m, 1H), 2.68 (dd, J = 13.4, 8.0 Hz, 1H), 1.04 (d, J = 7.3 Hz, 3H).
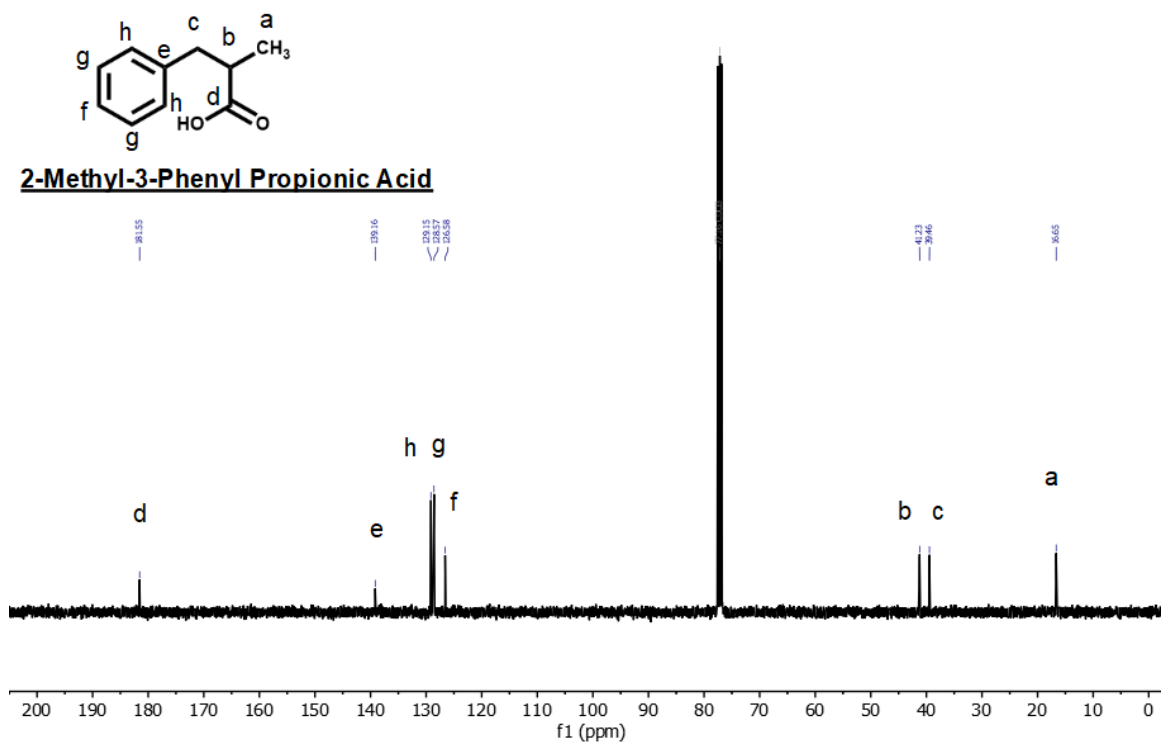
Figure 31. *^{13}C NMR of products of E-β-methylstyrene reduction.*

2-Methyl-3-phenylpropionic acid: ^{13}C NMR (101 MHz, CDCl$_3$) δ 181.55, 139.16, 129.15, 128.57, 126.58, 41.23, 39.46, 16.65.
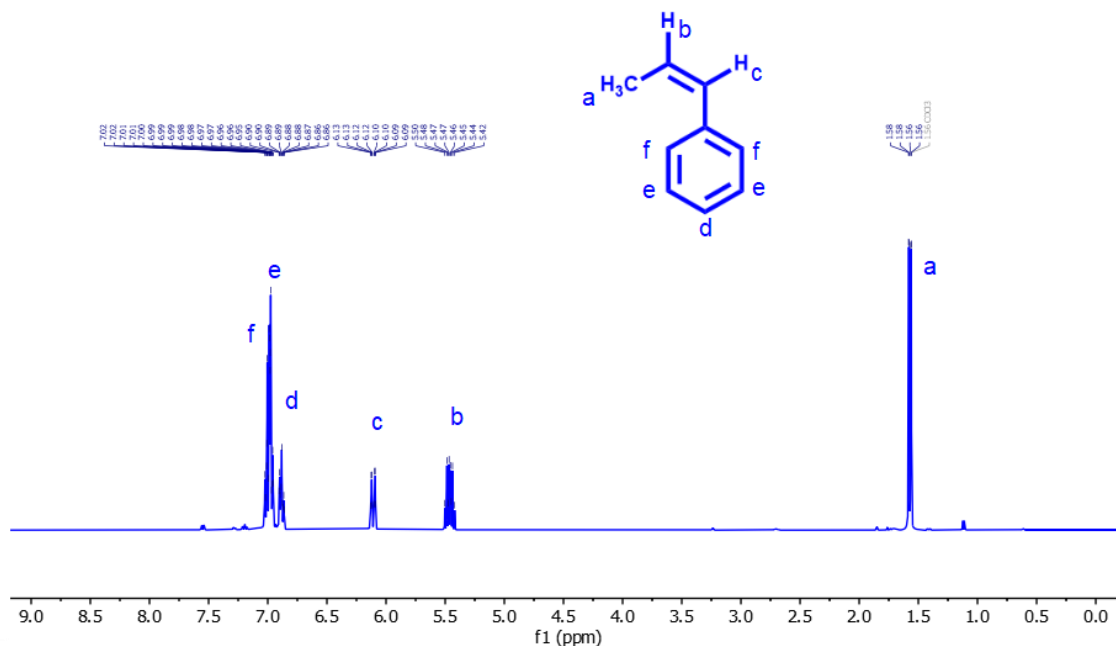
***Figure 32**. ¹H NMR of Z-β-Methyl Styrene.*

<u>Z-β-Methyl styrene</u>: ¹H NMR (400 MHz, CDCl₃) δ 7.02 – 6.91 (m, 4H), 6.94 – 6.84 (m, 1H), 6.11 (dq, *J* = 11.6, 1.9 Hz, 1H), 5.46 (dq, *J* = 11.6, 7.2 Hz, 1H), 1.56 (dd, *J* = 7.2, 1.9 Hz, 3H).
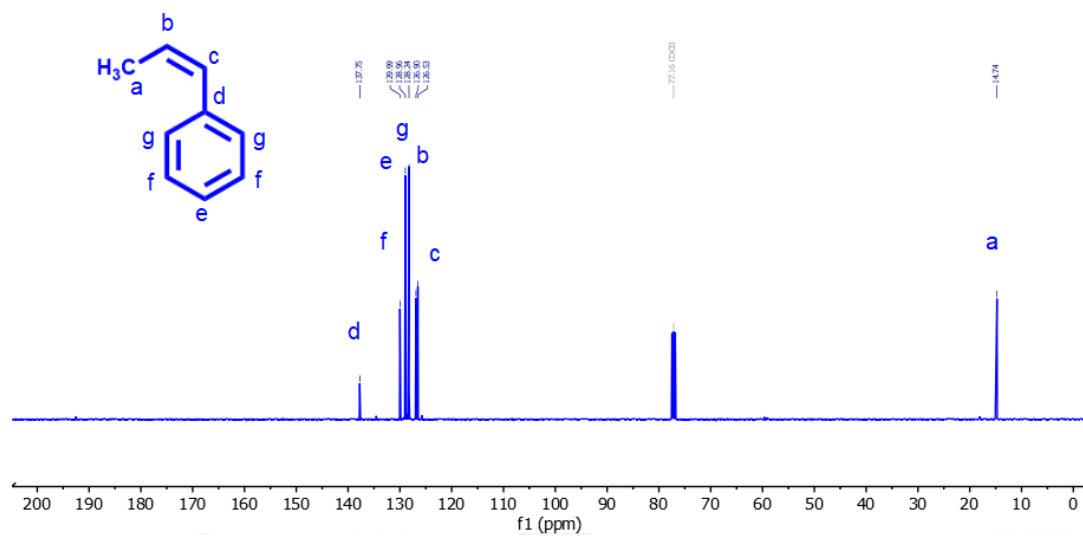
Figure 33. *^{13}C NMR of Z-β-Methyl Styrene.*

Z-β-Methyl styrene: ^{13}C NMR (101 MHz, CDCl$_3$) δ 137.75, 129.99, 128.96, 128.24, 126.90, 126.53, 14.74.
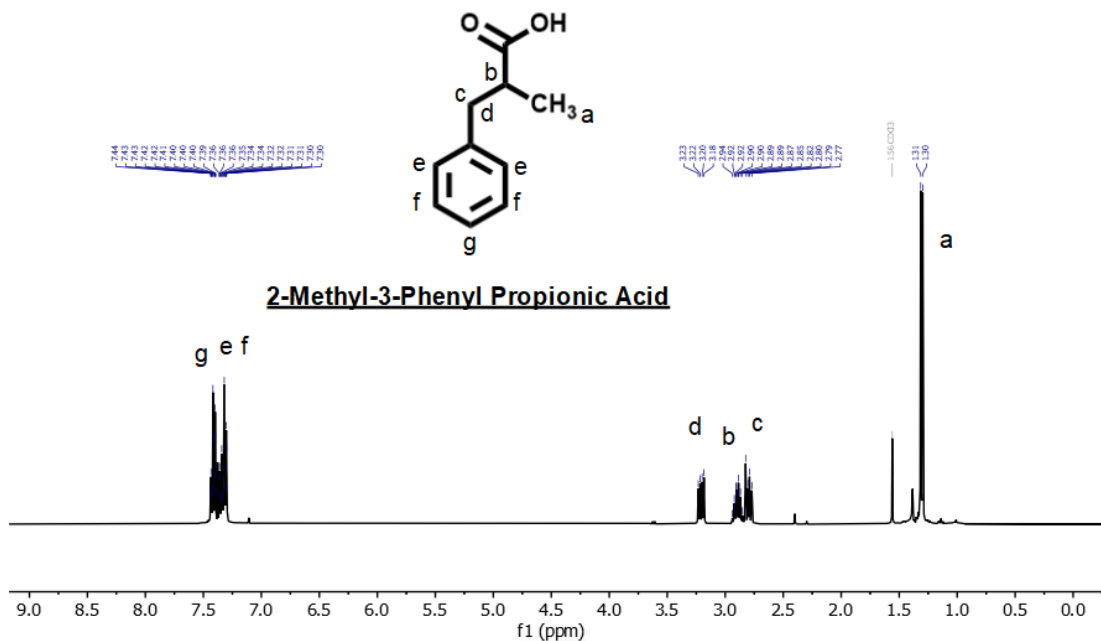
Figure 34. *¹H NMR of products of Z-β-methylstyrene reduction.*

2-Methyl-3-Phenyl propionic acid: ¹H NMR (400 MHz, CDCl₃) δ 7.42 (tt, J = 6.9, 1.1 Hz, 2H), 7.36 – 7.30 (m, 3H), 3.21 (dd, J = 13.3, 6.3 Hz, 1H), 2.89 (m, 1H), 2.80 (dd, J = 13.4, 8.0 Hz, 1H), 1.31 (d, J = 6.9 Hz, 3H).
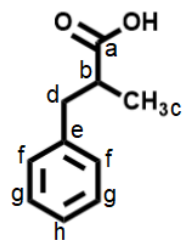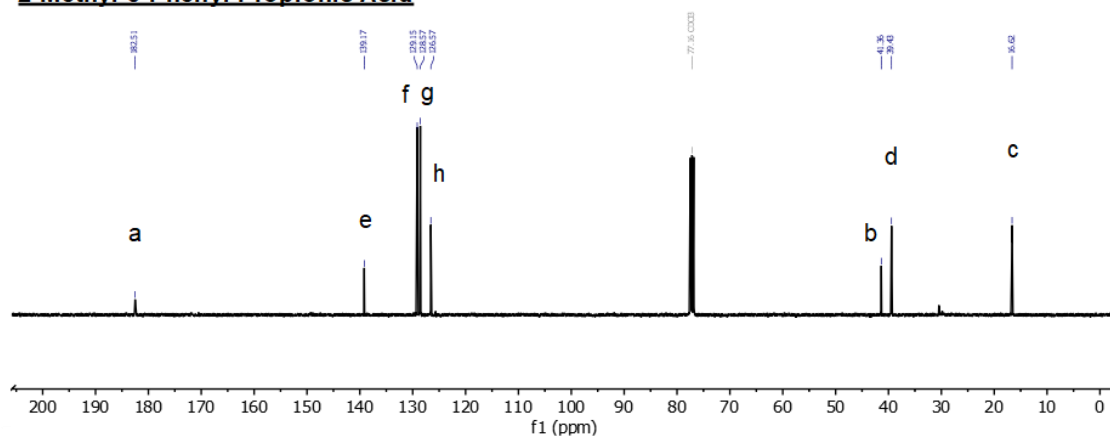
Figure 35. *^{13}C NMR of products of Z-β-methylstyrene reduction.*

2-Methyl-3-Phenyl propionic acid: ^{13}C NMR (101 MHz, CDCl$_3$) δ 182.51, 139.17, 129.15, 128.57, 126.57, 41.36, 39.43, 16.62.
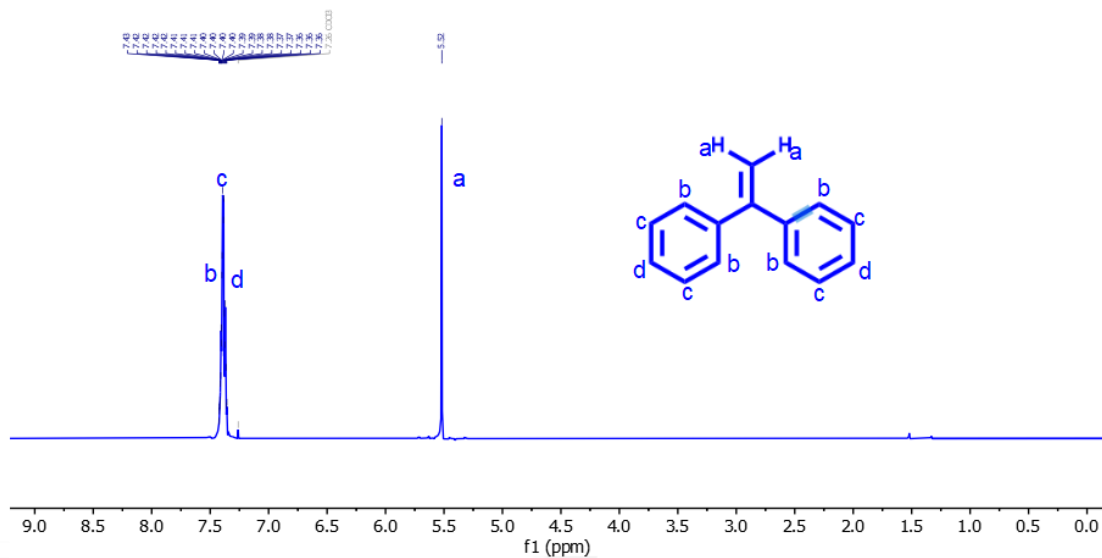
Figure 36. *¹H NMR of 1,1-Diphenylethylene.*

1,1-Diphenylethylene: ¹H NMR (400 MHz, CDCl₃) δ 7.47 – 7.31 (m, 10H), 5.52 (s, 2H).

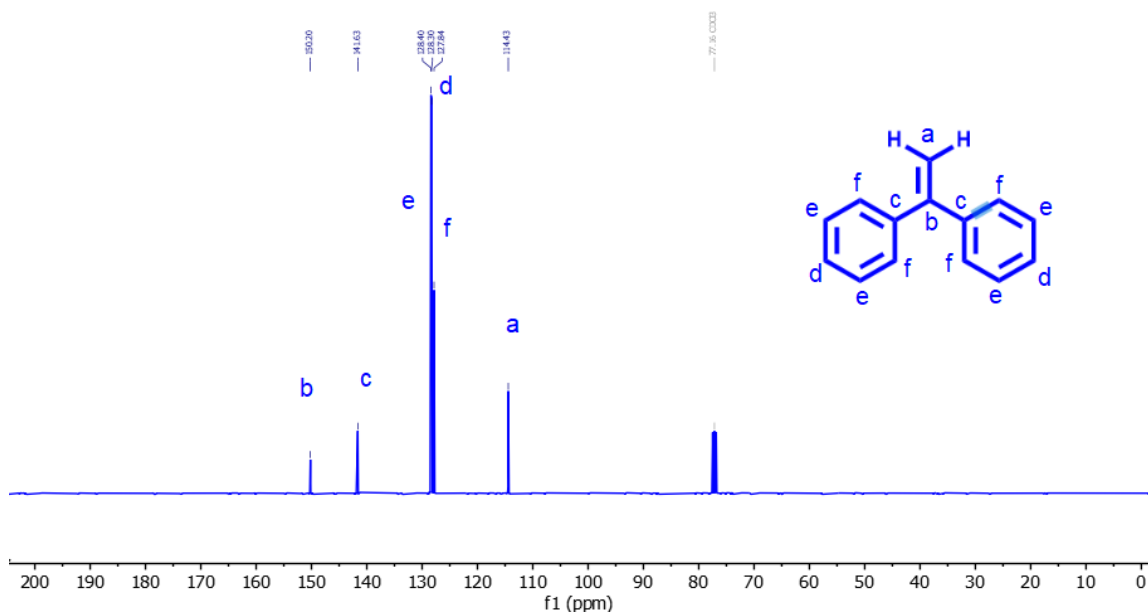**Figure 37**. *¹³C NMR of 1,1-Diphenylethylene.*

1,1-Diphenylethylene: ¹³C NMR (101 MHz, CDCl₃) δ 150.20, 141.63, 128.40, 128.30, 127.84, 114.43.
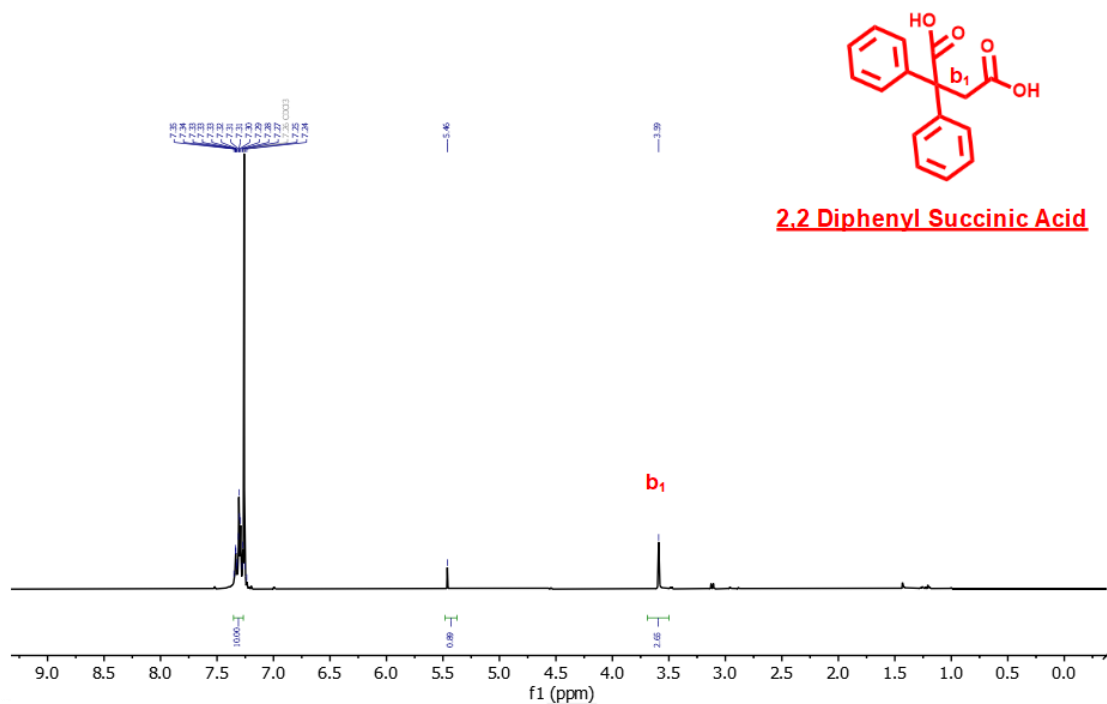
Figure 38. *¹H NMR of products of 1,1-Diphenylethylene reduction.*

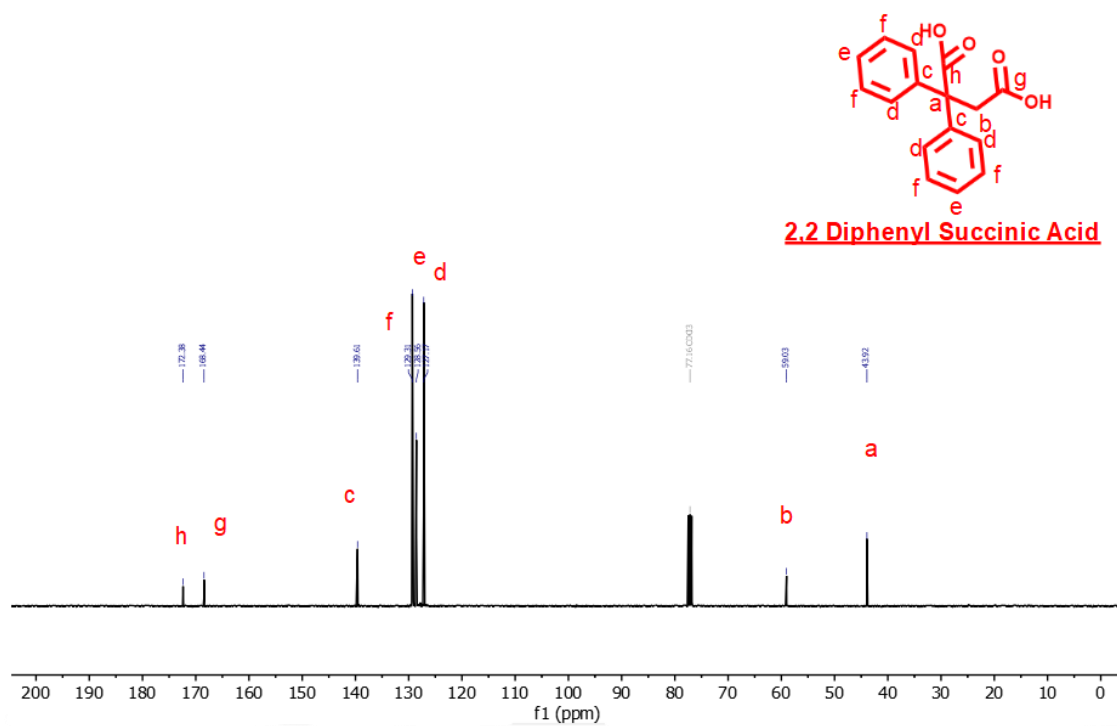**2,2 Diphenyl succinic Acid:** ¹H NMR (400 MHz, CDCl₃) δ 7.35 – 7.27 (m, 10H), 3.59 (s, 2H).

Figure 39. *^{13}C NMR of the products of 1,1-Diphenylethylene reduction.*

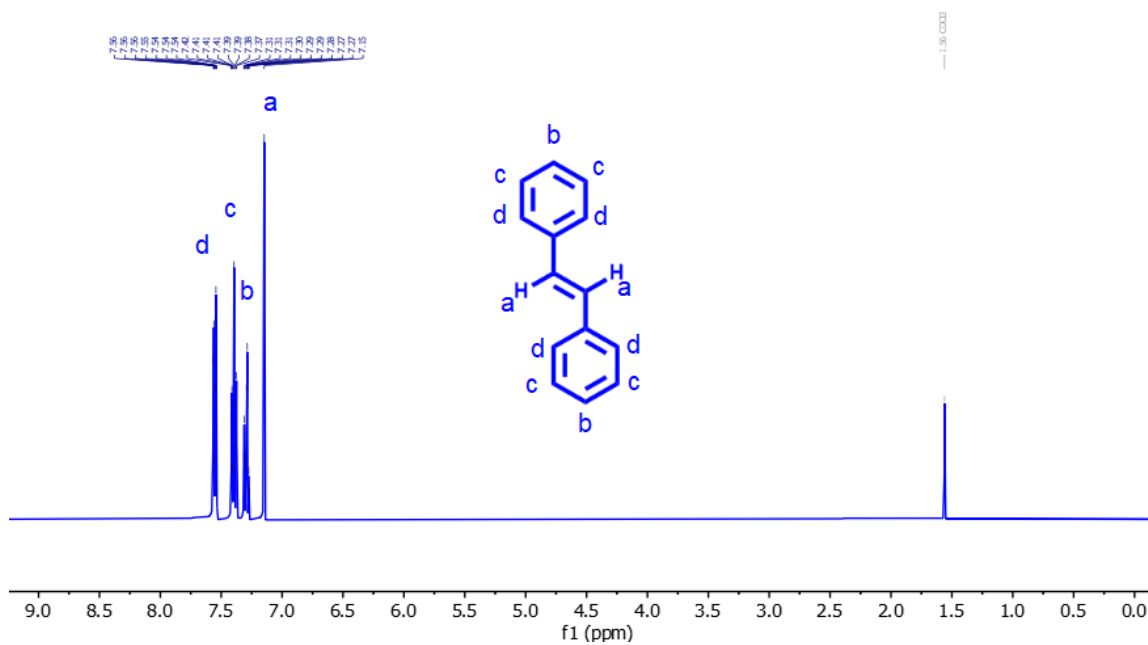**2,2 Diphenyl succinic Acid:** ^{13}C NMR (101 MHz, CDCl$_3$) δ 172.38, 168.44, 139.61, 129.31, 128.56, 127.17, 59.03, 43.92.

Figure 40*. ¹H NMR of E-Stilbene.*

E-Stilbene: ¹H NMR (400 MHz, CDCl₃) δ 7.56 – 7.45 (m, 4H), 7.45 – 7.33 (m, 4H),
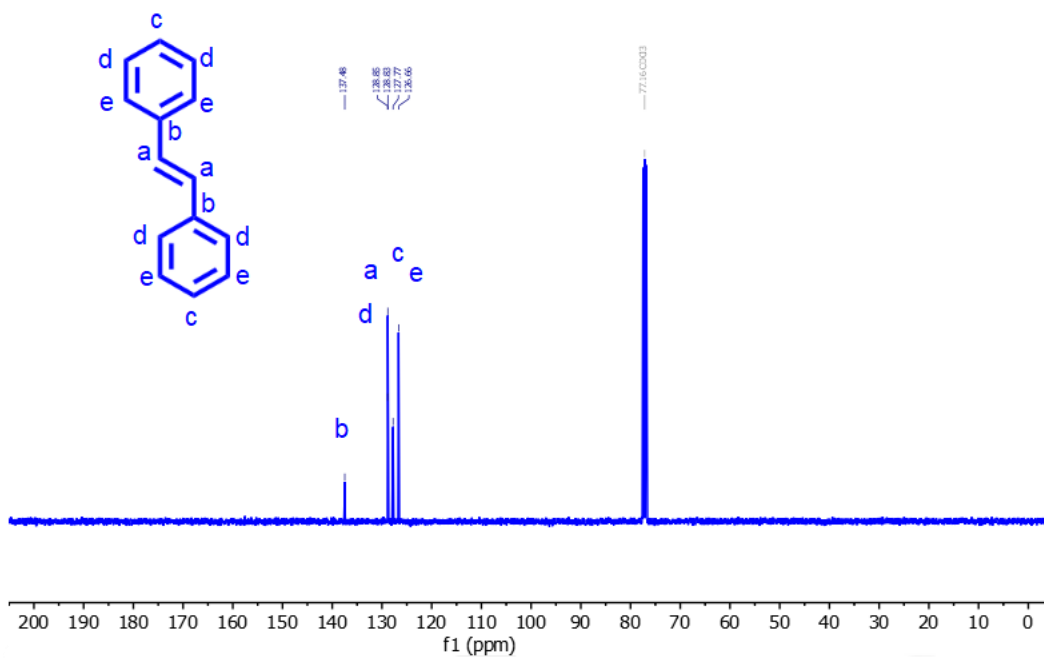
7.33 – 7.26 (m, 2H), 7.15 (s, 2H).

Figure 41. *¹³C NMR of E-Stilbene.*

E-Stilbene: ¹³C NMR (101 MHz, CDCl₃) δ 137.48, 128.85, 128.83, 127.77, 126.66.
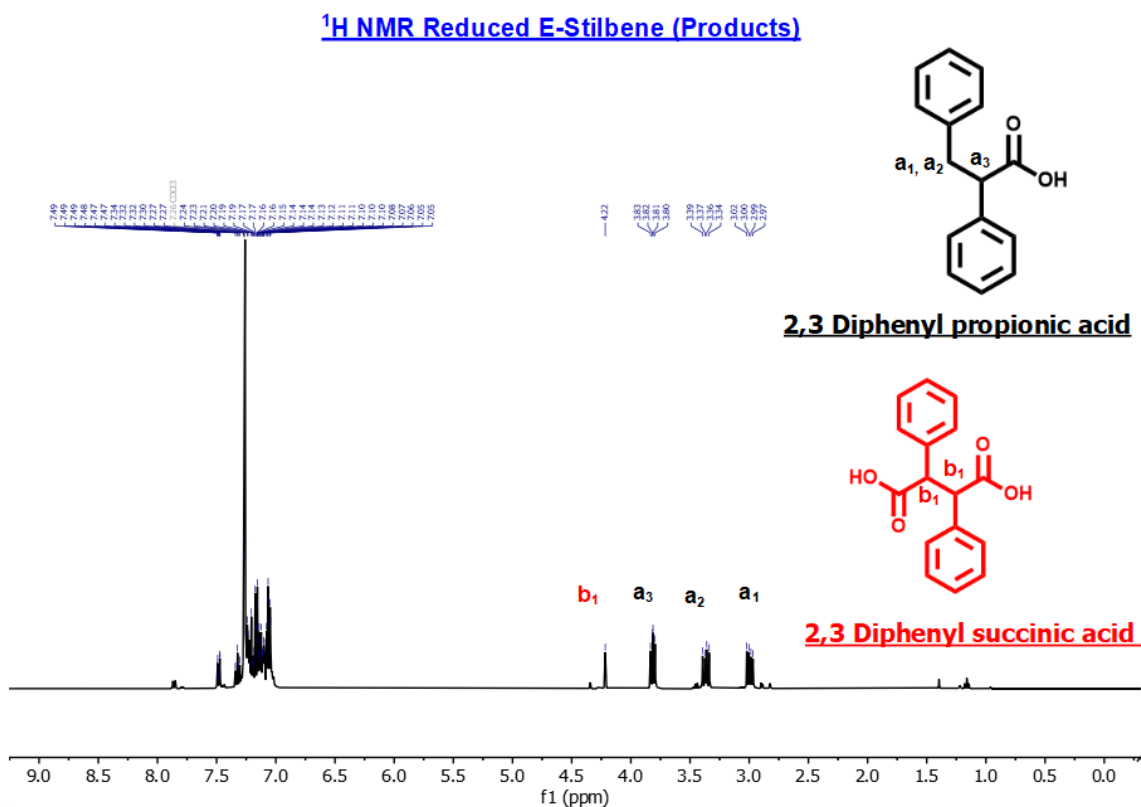
Figure 42. *^{1}H NMR of products of E-Stilbene reduction.*

2,3 Diphenyl propionic acid:^{1}H NMR (400 MHz, CDCl$_3$) δ 7.49-7.27 (m, 3H), 7.24 (dd, J = 9.1, 4.6Hz, 2H), 7.23-7.16 (m, 3H), 7.05 (d, J = 6.9 Hz, 2H), 3.83-3.80 (m, 1H), 3.39-3.34 (m, 1H), 3.02-2.97 (m, 1H).

2,3 Diphenyl succinic acid: ^{1}H NMR (400 MHz, CDCl$_3$) δ 7.15–7.13 (m, 6H), 7.10–7.05 (m, 4H), 4.22 (s, 2H).
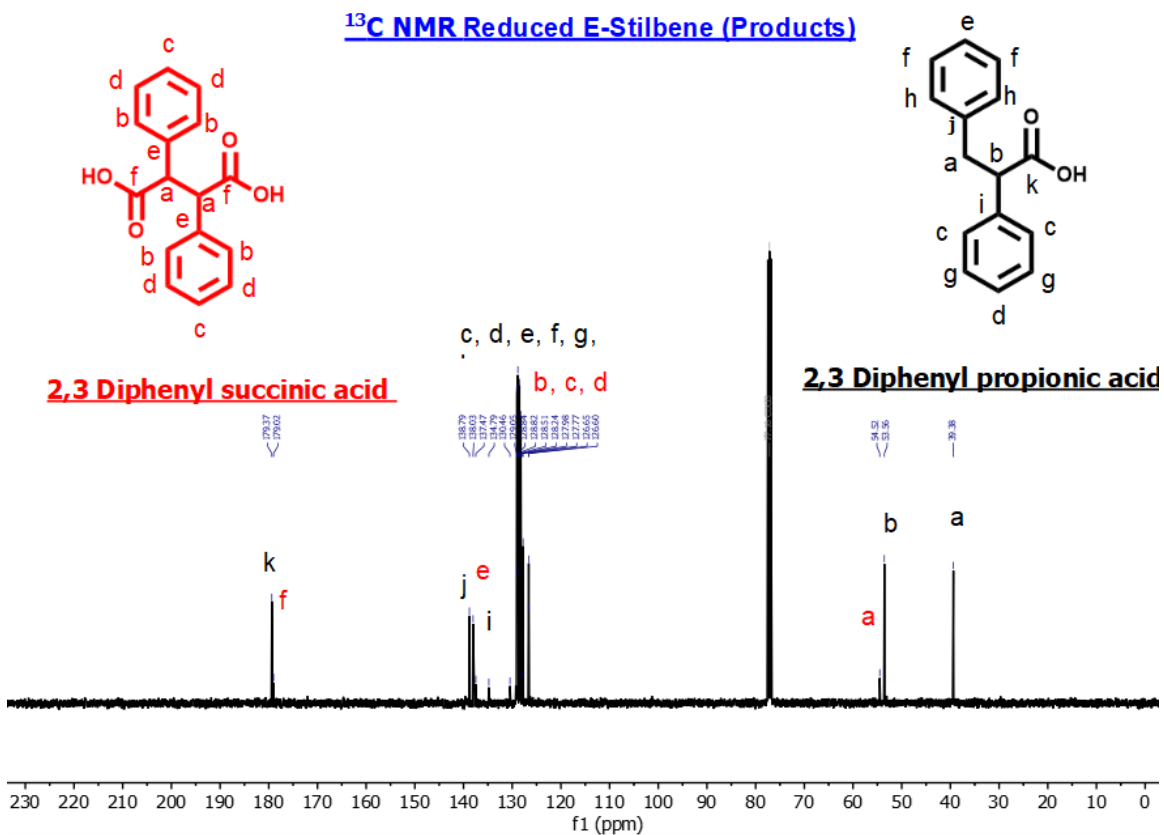
Figure 43. *¹³C NMR of products of E-Stilbene reduction.*

2,3 Diphenyl propionic acid: ¹³C NMR (101 MHz, CDCL₃) δ 179.37, 138.79, 138.03, 128.51, 128.24, 127.98, 127.77, 126.65, 126, 54.52, 39.38.

2,3 Diphenyl succinic acid: ¹³C NMR (101 MHz, CDCL₃) δ 179.02, 136.49, 129.05, 128.84, 127.77, 53.96.

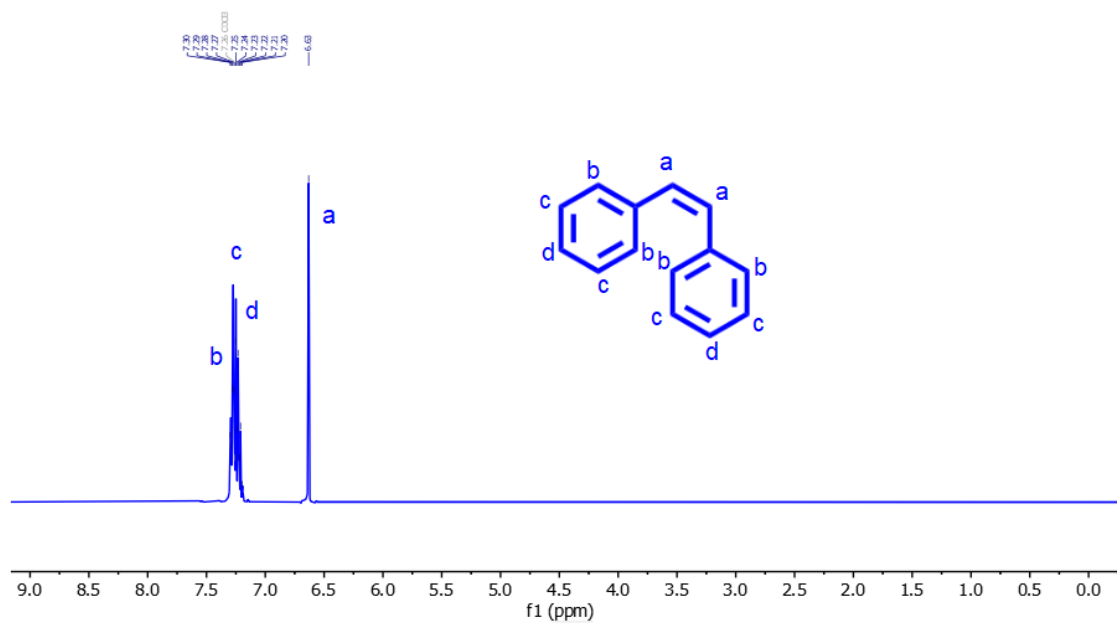***Figure 44***. *^{1}H NMR of Z-Stilbene.*

Z-Stilbene: ^{1}H NMR (400 MHz, CDCl$_3$) δ 7.30 – 7.20 (m, 10H), 6.63 (s, 2H).
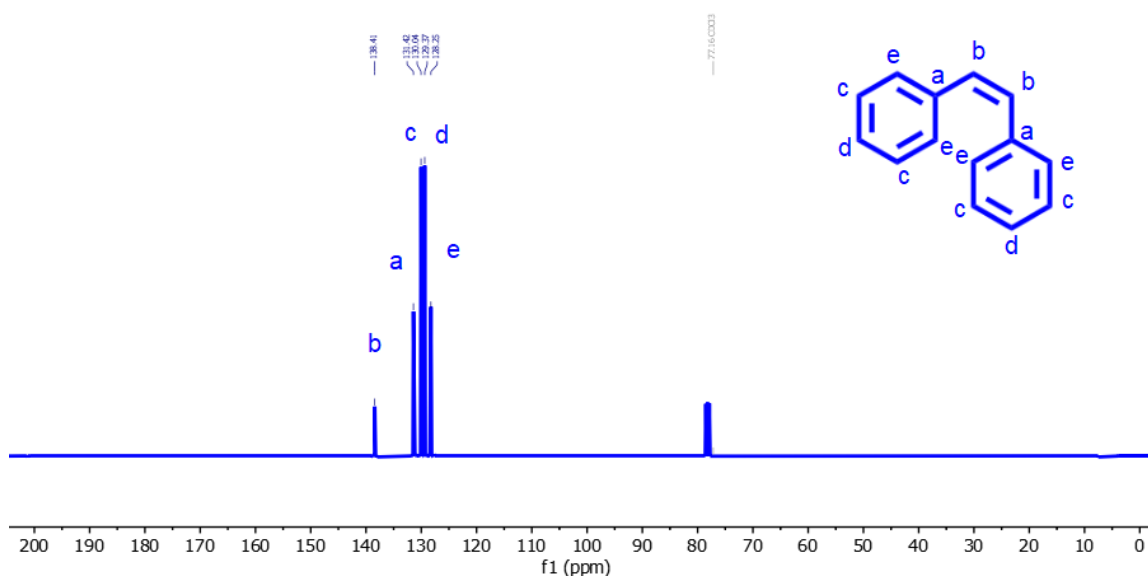
Figure 45. *¹³C NMR of Z-Stilbene.*

Z-Stilbene: ¹³C NMR (101 MHz, CDCl₃) δ 138.41, 131.42, 130.04, 129.37, 128.25.
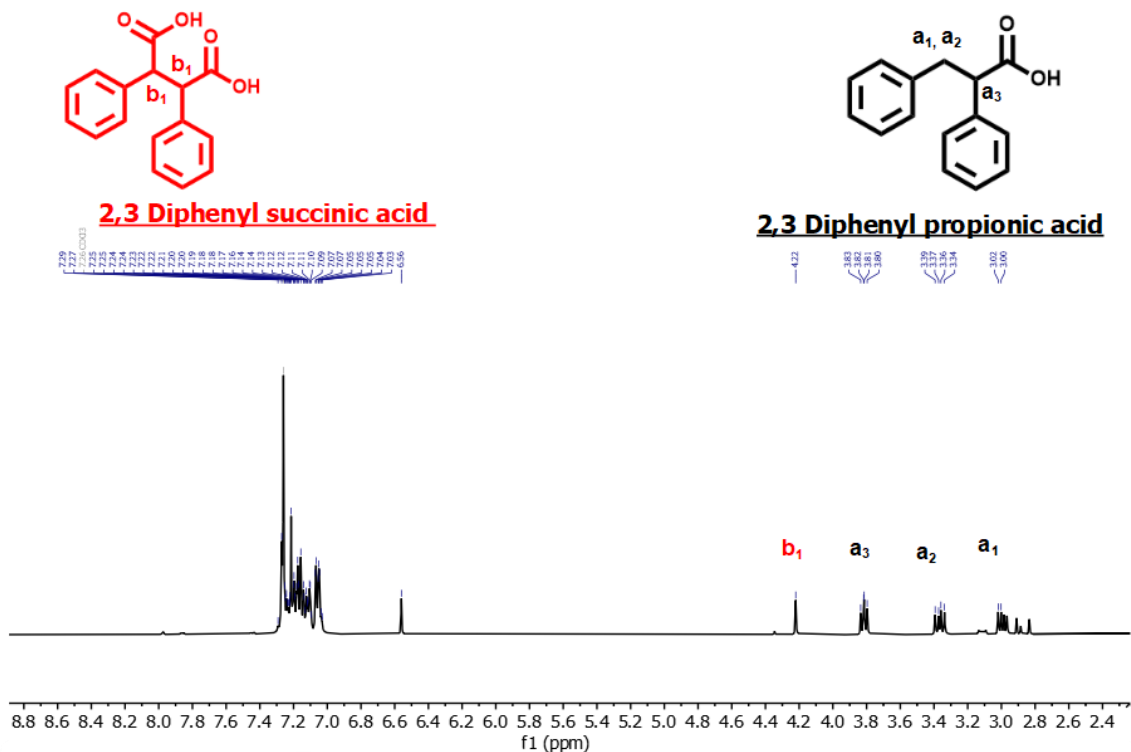
Figure 46. *¹H NMR of the products of Z-Stilbene reduction.*

2,3 Diphenyl propionic acid:¹H NMR (400 MHz, CDCl₃) δ 7.49-7.27 (m, 3H), 7.24 (dd, *J* = 9.1, 4.6Hz, 2H), 7.23-7.16 (m, 3H), 7.05 (d, *J* = 6.9 Hz, 2H), 3.83-3.80 (m, 1H), 3.39-3.34 (m, 1H), 3.02-2.97 (m, 1H).

2,3 Diphenyl succinic acid: ¹H NMR (400 MHz, CDCl₃) δ 7.15–7.13 (m, 6H), 7.10–7.05 (m, 4H), 4.22 (s, 2H).
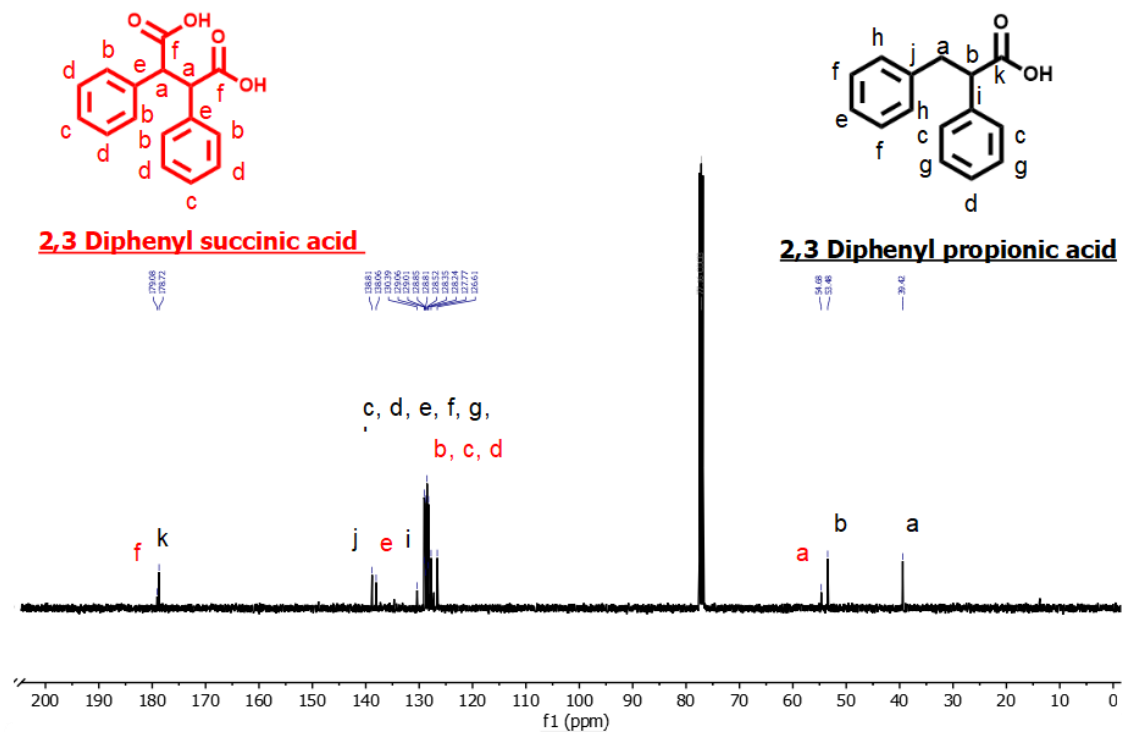
Figure 47. *¹³C NMR of the products of Z-Stilbene reduction.*

2,3 Diphenyl propionic acid: ¹³C NMR (101 MHz, CDCL₃) δ 178.72, 138.81, 130.39 128.81, 128.52, 128.35, 128.24, 127.77, 126.61, 53.48, 39.42.

2,3 Diphenyl succinic acid: ¹³C NMR (101 MHz, CDCL₃) δ 179.02, 136.49, 129.05, 128.84, 127.77, 53.96.

3.4. Mass Spectrometry (MS) and Infrared (IR).

Table 3. Molecular weight, MS, and IR for all alkenes and their products.

Entry	Alkene	Products	MS	IR (cm^{-1})	Melting point and appearance of products
1	Styrene	2-Phenyl Propionic Acid	(ESI): Mass calculated for $C_9H_{10}O_2$ ([M+H]$^-$): Mass cal. 149.0608; Mass found: 149.0610.	1684 (C=O) 3023 (O-H)	Beige solid M.p. 110 ºC
		2-Phenyl Succinic Acid	(ESI): Mass calculated for $C_{10}H_{10}O_4$ ([M+H]$^-$): Mass cal. 193.0506; Mass found: 193.0493.		
2	α-Methyl Styrene	Phenyl butyric Acid	(ESI): Mass calculated for $C_{10}H_{12}O_2$ ([M+H]$^-$): Mass cal. 163.0765; Mass found: 163.0765.	1698 (C=O) 2926 (O-H)	Yellow Liquid
3	E-β-Methyl Styrene	2-Methyl-3-Phenyl Propionic Acid	(ESI): Mass calculated for $C_{10}H_{12}O_2$ ([M+H]$^-$): Mass cal. 163.0765; Mass found: 163.0771.	1678 (C=O) 2863 (O-H)	Yellowish Liquid
4	Z-β-Methyl Styrene	2-Methyl-3-Phenyl Propionic Acid	(ESI): Mass calculated for $C_{10}H_{12}O_2$ ([M+HCOO]$^-$): Mass cal. 163.0765; Mass found: 163.0768.	1682 (C=O) 2891 (O-H)	Yellowish Liquid
5	1,1 Diphenylethylene	2,2 Diphenyl Succinic Acid	(ESI): Mass calculated for $C_{15}H_{14}O_2$ ([M+HCOO]$^-$): Mass cal. 225.0921; Mass found: 225.0925.	1701 (C=O) 3020 (O-H)	Beige solid M.p. 155 ºC
6	E-Stilbene	2,3 Diphenyl Propionic Acid	(ESI): Mass calculated for $C_{16}H_{14}O_2$ ([M+H]$^-$): Mass cal. 225.0921; Mass found: 225.0921.	1694 (C=O) 2899 (O-H)	White Solid M.p. 160 ºC
		2,3 Diphenyl Succinic Acid	(ESI): Mass calculated for $C_{16}H_{14}O_4$ ([M+H]$^-$): Mass cal. 269.0819; Mass found: 269.0821.		
7	Z-Stilbene	2,3 Diphenyl Propionic Acid	(ESI): Mass calculated for $C_{16}H_{14}O_2$ ([M+H]$^-$): Mass cal. 225.0921; Mass found: 225.0921.	1693 (C=O) 2847 (O-H)	White Solid+ Reactant Liquid Mixture
		2,3 Diphenyl Succinic Acid	(ESI): Mass calculated for $C_{16}H_{14}O_4$ ([M+H]$^-$): Mass cal. 269.0819; Mass found: 269.0821.		

3.5. Scanning electron microscope (SEM) and Energy Dispersion X-ray (EDX) analysis.

The morphology of the nickel mesh electrodes were analyzed using Zeiss Sigma variable-pressure field-emission scanning electron microscope (FESEM) in the Geoanalytical Electron Microscopy and Spectroscopy (GEMS) facility at the School of Geographical and Earth Sciences, University of Glasgow. The untreated and treated Ni samples were placed on samples holder and gold layer was applied for SEM imaging, while a carbon coating was utilized for EDX analysis to enhance electrical conductivity. The carbon coating will help to give clearer pictures for the sample as well as lowering the chance of backscattered electron emitted. In other words, many samples encounter issues related to poor conductivity, causing charging effects during SEM imaging. These charging phenomena can distort images and diminish the accuracy of analysis. The application of carbon coating addresses this challenge by creating a conductive layer. This coating aids in dissipating the charge, thereby improving image clarity and enhancing the precision of data analysis.

Figure 48. *Scanning electron microscopy-energy dispersive X-ray analysis (SEM-EDX)*

for (A, A'). Nickel mesh, before applying -35 mA for 8 hours at room temperature; (B, B')

Nickel mesh after applying -35 mA for 8 hours using the following parameters: 20 ml N,

N, Dimethylformamide (DMF), 3.5 mmol styrene, 0.1 M nBu_4NPF_6 under carbon

dioxide.

SEM images of nickel mesh (Figure 48) are presented alongside corresponding EDX images to provide complementary information about the surface morphology and elemental composition. SEM analysis reveals that the surface morphology of the Ni mesh electrodes significantly changes, and clustered particles are observed on the electrode surfaces due to the reduction of alkenes in the presence of CO_2. EDX analysis revealed

very low percentage of oxygen and magnesium after applying -35 mA for 8 hours. The presence of Magnesium and oxygen is due to the oxidation process occurs as the anode (Mg rod). This observation supports the idea that the formation of magnesium carboxylate compound occurs as an intermediate step before it undergoes protonation.
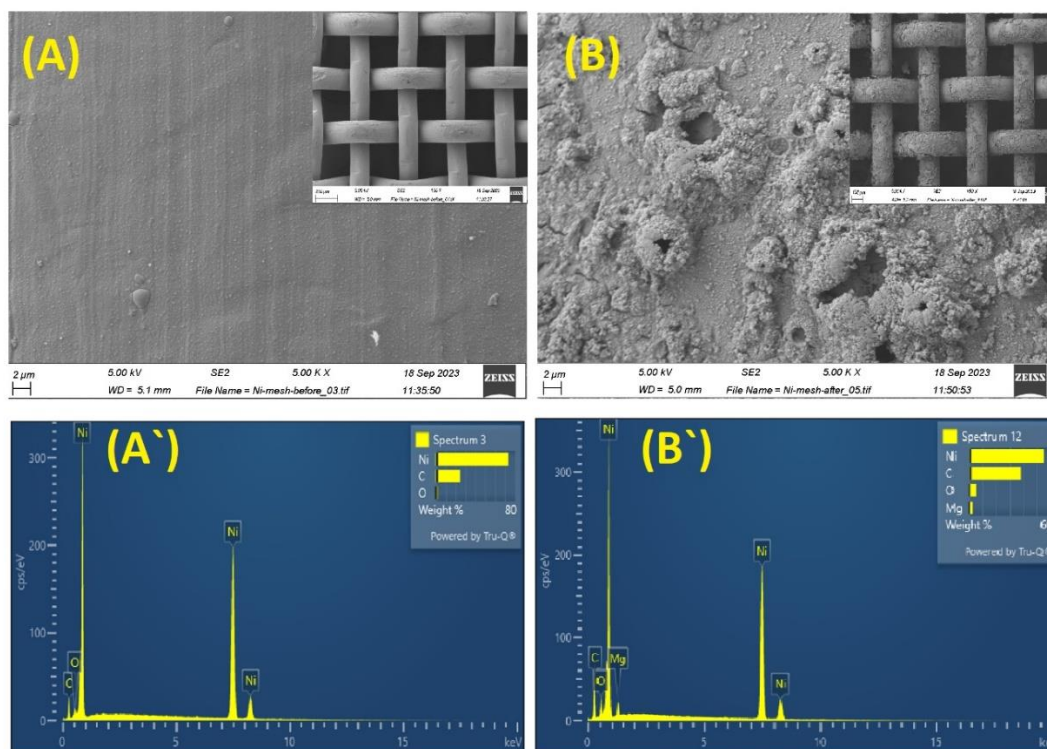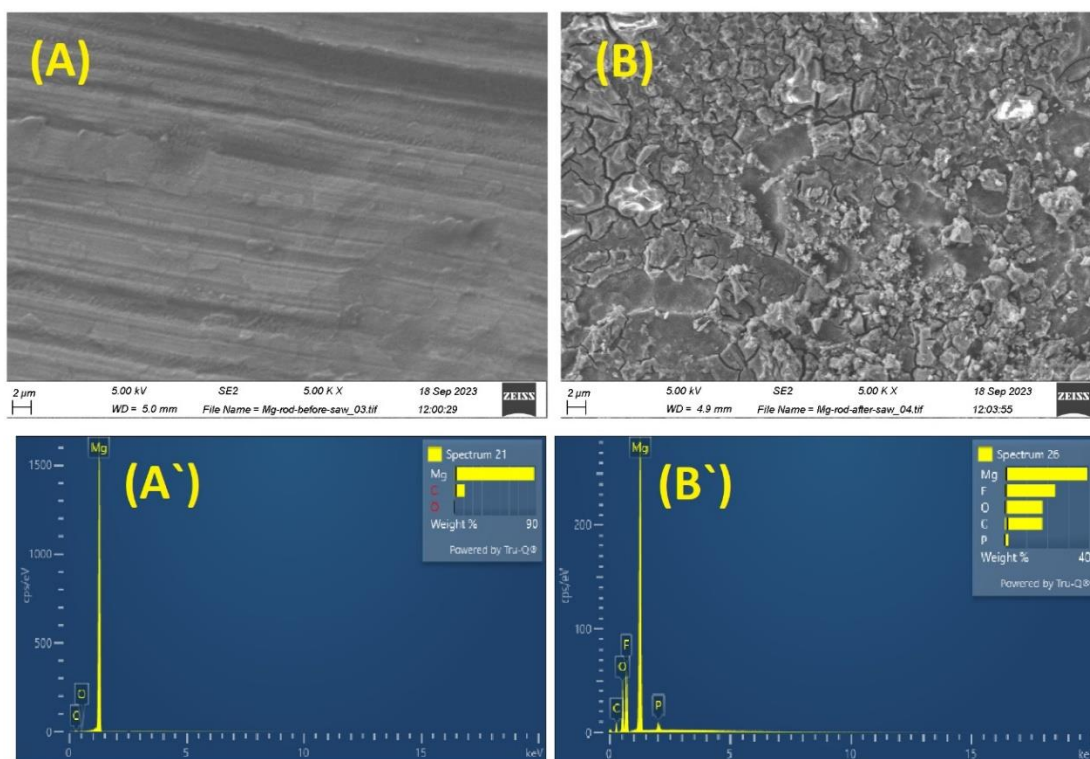

Figure 49. *Scanning electron microscopy-energy dispersive X-ray analysis (SEM-EDX) for (A, A'). Magnesium rod, before applying -35 mA for 8 hours at room temperature; (B, B') Magnesium rod after applying -35 mA for 8 hours using the following parameters: 20 ml N, N, Dimethylformamide (DMF), 3.5 mmol styrene, 0.1 M $nBu_4 NPF_6$ under carbon dioxide.*

Figure 49presents SEM-EDX analysis images of the Magnesium rod, both before and after eight hours of chronopotentiometry. In the initial state (A), the SEM image reveals the Magnesium rod's appearance prior to the chronopotentiometry process. Simultaneously, in (A'), the EDX analysis of the Magnesium rod showcases prominent peaks corresponding to Mg > C > O elements on its surface.

Subsequently, (B) displays the SEM image of the Magnesium rod after the completion of the chronopotentiometry, illustrating the effects of the electro-carboxylation process. Furthermore, (B') presents the EDX results, highlighting an increased abundance of Mg > O ≥ C elements, respectively. These images and analyses collectively demonstrate the alterations and elemental composition changes induced by the electro-carboxylation (oxidation) process on the Magnesium rod. However, some elements such as F, and P come from the nBu_4PF_6 electrolyte.

3.6.X-ray diffraction (XRD) analysis XRD.

X-ray diffraction (XRD) analysis were performed using Rigaku Mini Flex with CuKα radiation. The scanning diffraction angle 2θ range was from 5 to 80° at a speed of 5° minutes.
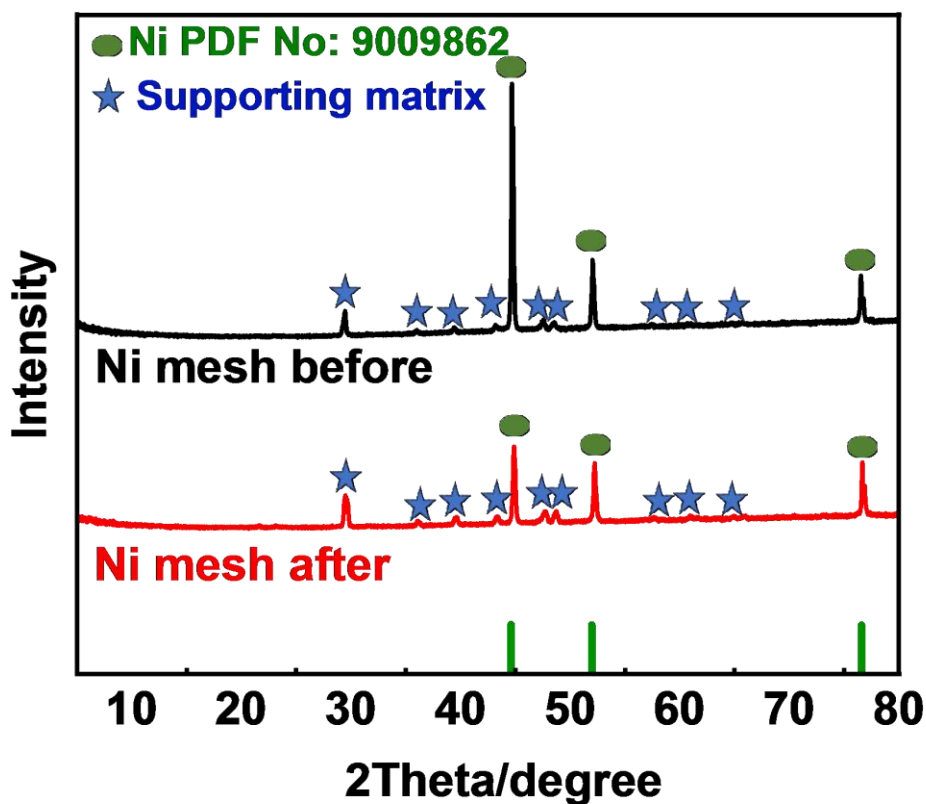
Figure 50. *X-ray diffraction (XRD) patterns for (A). Nickel mesh, before applying -35 mA*

for 8 hours at room temperature. color code: (black line); After applying -35 mA for 8

hours using the following parameters: 20 ml N, N, Dimethylformamide (DMF), 3.5 mmol

styrene, 0.1 M nBu₄NPF₆ under carbon dioxide (Red line), supporting matrix (blue tack).

The crystalline phases of untreated and treated Ni mesh electrodes have similar peaks that

appeared at about 45.18, 52.35 and 76.4 (Fig. 50), which can be indexed to the (111), (200)

and (220) planes of nickel (PDF Card No: 9009862). It is clearly seen that the crystal

structure of nickel mesh remains unchanged after treated 8 hours of chronopotentiometry

under CO_2.

4. Related Calculations.

a. Moles

$$\text{moles (n)} = \frac{mass\ of\ product\ (g)}{Molecular\ weight\ g/mole} \qquad \textbf{Equation 1}$$

In the case of obtaining one product after purification steps, the obtained product is weighted in grams, and then moles of product is calculated.

b. Mass in grams if a mixture of products is obtained.

$$= \frac{Integration\ of\ first\ product\ peak \times\ mass\ of\ product(s)in\ grams}{Integration\ of\ first\ product\ peak + Integration\ of\ second\ product\ peak} \qquad \textbf{Equation 2}$$

The obtained mixture is weighed after the purification process in grams. Then the mass in grams for each product is calculated from Equation 2. Note that the peaks of both products should have the same number of protons.

c. Charges are needed to convert moles of substrates.

$$Q = n \times e \times F \qquad \textbf{Equation 3}$$

Q   number of charges required to convert a number of moles of alkene (Coulomb)

n   number of moles of reactant (alkene).

e   number of electrons to reduce one molecule.

F   Faraday constant (A/mole).

d. Time is needed to convert mole of substrate.

$$t = \frac{Q}{I} \qquad \textbf{Equation 4}$$

t   Time required to pass the required charges (second).

Q   number of charges required to convert a number of moles of alkene (Coulomb).

I   Applied current in (Ampere).

e. Yield

$$\text{Yield \%} = \frac{moles\ of\ product}{mole\ of\ reactant} \times 100 \qquad \textbf{Equation 5}$$

f. Faradic Efficiency (FE).

For one product

$$\frac{moles\ of\ product \times number\ of\ electrones \times faradic\ constant}{number\ of\ charges\ passed} \times 100 \qquad \textbf{Equation 6}$$

For a mixture of products:

Calculate the faradic efficiency individually and then sum them up to get the total faradic efficiency.

g. Conversion.

$$= \frac{(Integration\ peak\ of\ first\ product + Integration\ peak\ of\ second\ product)}{(Integration\ peak\ of\ first\ product + Integration\ peak\ of\ second\ prouct)} \times 100 \qquad \textbf{Equation 7}$$

5. Conclusion.

Herein, we have studied the electro-carboxylation of a range of alkenes under 1 atm of CO_2 at 20 °C in DMF solution at a Ni working electrode. Our results present a departure from the prevailing literature in that most previous reports find that the di-carboxylic acids are by far the dominant reaction products, whereas our data show that the mono-carboxylates are formed preferentially in most cases. Through analysis of cyclic voltammograms of the substrates in the presence and absence of CO_2, we show that the addition of the first carbon dioxide molecule to the alkene occurs at the site β to the phenyl ring when this is available and that a mechanism where the alkene is first reduced at the electrode and then reacts with CO_2 is operating (although the simultaneous operation of a competing pathway whereby the CO_2 is reduced first and then this reacts with the neutral alkene cannot be excluded). Both mono- and di-carboxylic acids can then be produced, but with a preference for the mono-carboxylates in this work, a feature that comparison with the literature suggests is due to the choice of Ni as the working electrode, which is an effective material for electrochemical hydrogenations. Overall, these results offer the prospect that this system could be further developed to allow valuable mono-carboxylate products to be produced by the electro-carboxylation of the corresponding alkene precursors with high regio-selectivity.

6. References.

[1] Jitaru, M. Electrochemical Carbon Dioxide Reduction - Fundamental and Applied Topics (Review). *J. Chem. Technol. Metall.*, **42** (4), 333–344 (2007).

[2] Kibria, M. G., Edwards, J. P., Gabardo, C. M., Dinh, C. T., Seifitokaldani, A., Sinton, D., & Sargent, E. H. Electrochemical CO2 Reduction into Chemical Feedstocks: from Mechanistic Electrocatalysis Models to System Design. *Advanced Materials.*, **31** (31), 1807166 (2019).

[3] Song, Q. W., Zhou, Z. H. & He, L. N. Efficient, Selective and Sustainable Catalysis of Carbon Dioxide. *Green Chem.*, **19** (16), 3707–3728 (2017).

[4] Wang, J., Tan, H. Y., Zhu, Y., Chu, H., & Chen, H. M. Linking The Dynamic Chemical State of Catalysts with The Product Profile of Electrocatalytic CO2 Reduction. *Angew. Chem.*, **133** (32), 17394-17407 (2021).

[5] Yan, M., Kawamata, Y. & Baran, P. S. Synthetic Organic Electrochemical Methods Since 2000: On the Verge of a Renaissance. *Chem. Rev.*, **117** (21), 13230–13319 (2017).

[6] Wagner, A., Sahm, C. D., & Reisner, E. Towards Molecular Understanding of Local Chemical Environment Effects in Electro-and Photocatalytic CO2 Reduction. *Nat. Catal.*, **3** (10), 775-786 (2020).

[7] Badwal, S. P. S., Giddey, S. S., Munnings, C., Bhatt, A. I. & Hollenkamp, A. F. Emerging Electrochemical Energy Conversion and Storage Technologies. *Front. Chem*, **2** 1–28 (2014).

[8] Dickinson, H. L., & Symes, M. D. Recent progress in CO2 Reduction Using Bimetallic Electrodes Containing Copper. *Electrochem. Commun.,* **135**, 107212 (2022).

[9] a) Ran, C. K., Xiao, H. Z., Liao, L. L., Ju, T., Zhang, W., & Yu, D. G. Progress and Challenges in Dicarboxylation with CO2. *Natl. Sci. Open*, **2** (2), 20220024 (2023).

b) Liu, X.-F., Zhang, K., Tao, L., Lu, X.-B. & Zhang, W.-Z. Recent advances in electrochemical carboxylation reactions using carbon dioxide. *Green Chem. Eng.* **3**, 125-137 (2022).

c) Senboku, H. & Katayama, A. Electrochemical carboxylation with carbon dioxide. *Curr. Opin. Green Sus. Chem.* **3**, 50-54 (2017).

d)   Salehi, N. & Azizi, B. Electrochemical double carboxylation of unsaturated C-C bonds with carbon dioxide: An overview. *J. Chem. Lett.* **2**, 2-8 (2021).

[10] Filardo, G., Gambino, S., Silvestri, G., Gennaro, A., & Vianello, E. Electrocarboxylation of Styrene Through Homogeneous Redox Catalysis. *J. Electroanal. Chem. Interfacial Electrochem.*, **177** (1-2), 303-309 (1984).

[11] Gambino, S., Gennaro, A., Filardo, G., Silvestri, G. & Vianello, E. Electrochemical Carboxylation of Styrene. *J. Electrochem. Soc.*, **134** (9), 2172–2175 (1987).

[12] Dérien, S., Clinet, J. C., Duñach, E. & Périchon, J. Electrochemical Incorporation of Carbon Dioxide into Alkenes by Nickel Complexes. *Tetrahedron.*, **48** (25), 5235–5248 (1992).

[13] Senboku, H., Komatsu, H., Fujimura, Y., & Tokuda, M. Efficient Electrochemical Dicarboxylation of Phenyl-Substituted Alkenes: Synthesis of 1-Phenylalkane-1, 2-Dicarboxylic Acids. *Synlett.*, **2001** (03), 0418-0420 (2001).

[14] Yuan, G. Q., Jiang, H. F., Lin, C. & Liao, S. J. Efficient Electrochemical Synthesis of 2-Arylsuccinic Acids from CO2 and Aryl-Substituted Alkenes with Nickel as The Cathode. *Electrochim. Acta.*, **53** (5), 2170–2176 (2008).

[15] Alkayal, A., Tabas, V., Montanaro, S., Wright, I. A., Malkov, A. V., & Buckley, B. R. Harnessing Applied Potential: Selective β-Hydrocarboxylation of Substituted Olefins. *J. Am. Chem. Soc.*, **142** (4), 1780-1785 (2020).

Chapter 4: Electro carboxylation of styrene and stilbene using nickel mesh in the presence of a homogeneous electron transfer catalyst.

Synopsis

In Chapter 4, we will provide a concise overview of the preliminary investigation of improving the product (s) selectivity by adding benzonitrile as a homogeneous electron transfer catalyst in an alkene (styrene, or stilbene) reduction reaction along with carbon dioxide.

1. Introduction.

In order to improve the reduction reaction of carbon dioxide in the matter of product selectivity, benzonitrile has been used in many studies as an electron transfer catalyst in carbon dioxide reduction without involving chemical substrates [1]. A few studies investigated adding benzonitrile to reactions where styrene was reduced in the presence of carbon dioxide Table 1 [2, 3]. However, as far as we know, no study mentioned that benzonitrile has been added as a homogeneous catalyst in stilbene reduction in the presence of carbon dioxide. Hence, in this chapter, we investigated the results of adding benzonitrile in the electro-carboxylation of styrene and stilbene in the presence of carbon dioxide.

Filardo et al., 1984 investigated the electro-carboxylation of styrene through a homogenous catalyst such as benzonitrile using graphite as a cathode and aluminum as an anode. The reaction medium contained N,Nidimethylformamide (DMF), and tertbutyl ammonium bromide (Bu$_4$NBr), with styrene and 3.4×10^{-3} M benzonitrile. The reaction was a tank cell through which CO_2 was continuously bubbled while applying a controlled potential. The range was between -2.15 to -2.20 V vs Ag/Ag**I.** According to Filardo et al., 1984 [2], the obtained product mixture was 3-phenyl propionic acid (22%), and phenyl succinic acid (52%) with 85% conversion. However, another study [3] examined the electro-reduction of styrene in the presence of water as a protic agent at -1.9 V applied potential and 2.9×10^{-3} M benzonitrile. The obtained mixture was 3-phenyl propionic acid (30%), phenyl succinic acid (57%), and ethylbenzene (2%).

However, both studies   discuss the control of product selectivity with the addition of benzonitrile. These studies can be summaries as follows:

1. Lowering the percentage of other side products such as ethylbenzene even in the presence of water impurities.

2. Controlling the percentages of between mono and diacids by adding benzonitrile which focuses on passing the charges to carbon dioxide and alkene substrate. The reason for that is lowering the potential window during the reaction.

3. Adding right electron transfer homogenous catalyst will help to lower the chance of gelation which results from polymerization of the styrene due to the high reactivity of styrene towards polymerization.

Table 1. *A selection of conditions, conversions, and yields for the electro-reduction of styrene in the presence of CO_2 from the literature.*

Entry	Alkene	Reaction Conditions	Conversion	Products and Yield	Ref
1	Styrene	Working electrode: Graphite electrode Counter electrode: Aluminium electrode Medium: DMF, Bu$_4$NBr, and continuously bubbling CO_2, **3.4 ×10^{-3} M** benzonitrile. Technique: Control potential electrolysis (**−2.15 to −2.20 V** vs Ag/AgI). Cell type: diaphragmless tank cell Reaction temperature: Room temperature	85%	3-phenyl propionic acid (22%) Phenyl succinic acid (52%)	[2]
2	Styrene	Working electrode: Graphite electrode Counter electrode: Aluminum electrode Medium: DMF, Bu$_4$NBr, and continuously bubbling CO_2, **2.9 ×10^{-3} M** benzonitrile, **0.2 M H$_2$O protic agent.** Technique: Control potential electrolysis (**−1.9 V** vs. SCE). Cell type: diaphragmless tank cell Reaction temperature: Room temperature	50%	3-phenyl propionic acid (30%) Phenyl succinic acid (57%) Ethylbenzene (2%)	[3]
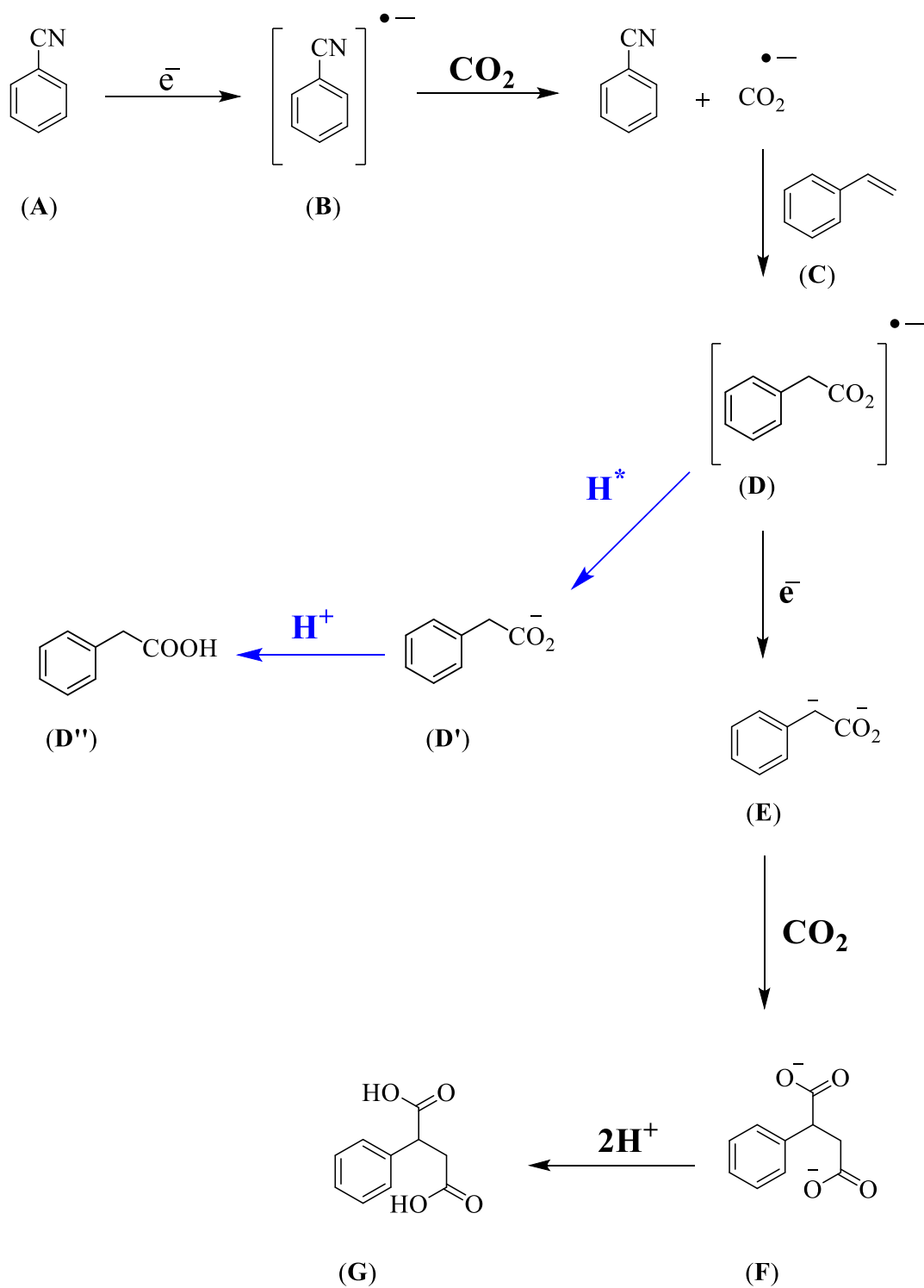
Scheme 1. *Explains the mechanism of the electro-carboxylation of carbon dioxide with alkene (styrene) with the addition of benzonitrile [4].*

The mechanism of the reaction is discussed in Aresta, M., & Forti, G., 2012 is summarized in Figure 1. By looking at the mechanism, it can be seen that the benzonitrile A will be reduced to its radical B and then this will transfer an electron to carbon dioxide to form a carbon dioxide radical. Following that, the carbon dioxide radical reacts with alkene C to produce D. By passing another electron, intermediate E is generated, which then reacts with carbon dioxide to give di-carboxylated acid F. Then F will become Diacid after protonation. The reaction can take another route to produce mono acids D" if there is a proton source during the reaction (Scheme 1).

2. Experimental steps.

Here all materials and experimental steps have been used/ applied as the same as it is mentioned in Chapter 3.

2.1. Materials:

Materials that are readily available for purchase (including supporting electrolytes, solvents, and alkenes) were used without undergoing any additional purification steps. Styrene (99% purity), trans-stilbene (98% purity) were purchased from commercial sources and used as received. All the alkenes used in this study were purchased from Alfa Aesar,. The solvent used in this study, N,N-dimethylformamide, anhydrous, 99.8% purity, was obtained from Alfa Aesar and packaged under Argon. The supporting electrolyte, tetrabutylammonium hexafluorophosphate (nBu$_4$NPF$_6$, 98% purity) at a concentration of

0.1 M, was purchased from ThermoFisher Scientific. Carbon dioxide, with a purity of 99%, was purchased from BOC Ltd.

2.2. Electrochemical procedures:

A BioLogic SP-150 potentiostat was employed for all cyclic voltammetry and chronopotentiometry experiments. The electrochemical carboxylation of the alkenes was conducted using a one-compartment electrochemical cell with five necks (see Figure 1, Chapter 1). The electrodes were situated in three of these necks, while the remaining two were designated for the gas inlet and outlet channels. The reference electrode utilized was a saturated calomel electrode (CHI150, supplied by IJ Cambria Scientific Ltd), and the counter electrode (anode) was a magnesium rod measuring 6.35 mm in diameter and 25.4 mm in length, at a purity of 99.95% (metal basis) from Alfa Aesar. A nickel disc (BASi, 3.0 mm diameter) or a nickel mesh (0.35×2 cm^2, woven wire, 60 mesh, made from 0.18 mm wire, supplied by Alfa Aesar) were used as the working electrodes for cyclic voltammetry and bulk electrolysis respectively. Before conducting bulk electrolysis, the Ni mesh underwent a 20-minute sonication in a bath containing 2 M HCl, followed by a rinse with DMF. Simultaneously, the magnesium rod received a 20-minute sonication in a DMF bath. Subsequently, both electrodes were allowed to air-dry. The bulk electrolysis process was initiated at room temperature (20 °C) with continuous stirring and a constant flow of CO_2.

3. Results and Discussion.

3.1. Cyclic voltammetry.

Cyclic voltammetry experiments were conducted under identical conditions and within the same cell as the bulk electrolysis, with the exception of using a Ni disc button working electrode (3mm diameter, BASi). Cyclic voltammograms were recorded under both argon (Ar) and carbon dioxide (CO_2) atmospheres for comparison, following 20 minutes of gas bubbling in each case. The working electrode was polished between experiments, and cyclic voltammetry was recorded at a scan rate of 10 mV/s over the voltage range of 0 V to -3 V vs. SCE, starting from 0 V.
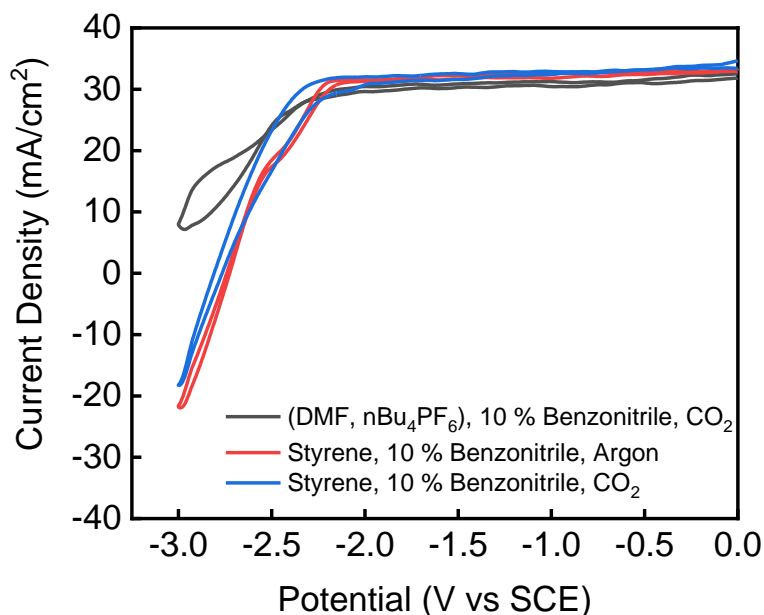

Figure 1: Cyclic Voltammetry of 3.5 mmol solution of Styrene in 20 mL DMF containing 0.1 M nBu₄PF₆ supporting electrolyte, 10 % Benzonitrile (BN), at room temperature, with scan rate of 10 mV/s. A Ni disc button (3 mm diameter) was used as the working electrode, a Mg rod was used as the counter electrode and an SCE electrode was used as the

reference. Color code: electrolyte saturated with 10 % Benzonitrile under CO_2 (Black line), electrolyte plus 3.5 mmol of styrene and 10 % Benzonitrile with Ar (Red line), electrolyte plus 3.5 mmol of styrene and 10 % Benzonitrile saturated with CO_2 (Blue line).

Interestingly, the reduction of styrene under argon in the presence of benzonitrile is a slightly different when it is under carbon dioxide Figure 1. That shows that the benzonitrile does act as a homogenous catalyst and the reaction would take the same route in the presence or absence of benzonitrile. Considering both cases, the cyclic voltammetry shows irreversibility. The increase in the yield might be due to the presence of benzonitrile would change the selectivity of the product or if we reach the extraction step and there still amount of benzonitrile (Boiling point of BN is 190℃) will change the polarity of aqueous phase and ether phase. Then it will save most of the product. Because benzonitrile is soluble in water.
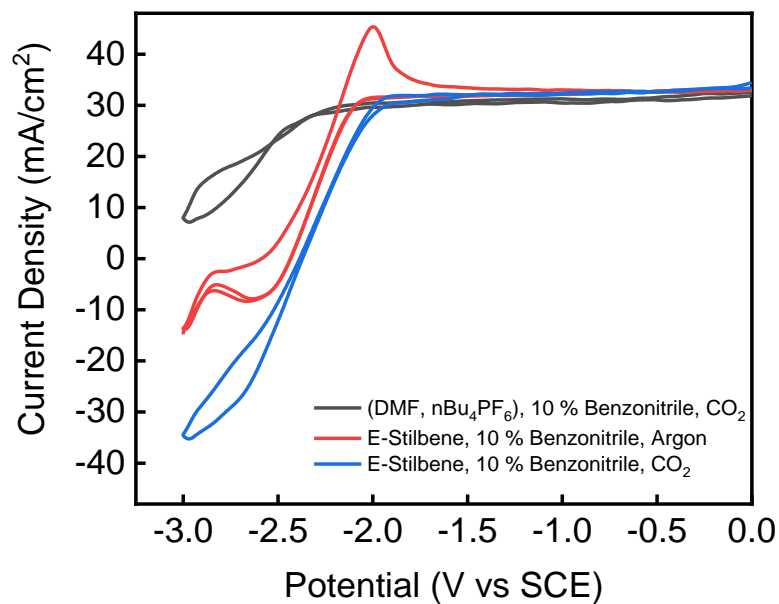
Figure 2: *Cyclic Voltammetry of 3.5 mmol solution of Trans-Stilbene in 20 mL DMF containing 0.1 M nBu₄PF₆ supporting electrolyte, 10 % Benzonitrile (BN), at room temperature, with scan rate of 10 mV/s. A Ni disc button (3 mm diameter) was used as the working electrode, a Mg rod was used as the counter electrode and an SCE electrode was used as the reference. Color code: electrolyte saturated with 10 % Benzonitrile under CO_2 (Black line), electrolyte plus 3.5 mmol of Trans-Stilbene and 10 % Benzonitrile with Ar (Red line), electrolyte plus 3.5 mmol of Trans-Stilbene and 10 % Benzonitrile saturated with CO_2 (Blue line).*

As an intensive study, Trans stilbene has been inspected under the same reaction conditions to show it is efficiency of being reduced and electrocarboxylated. As the aim of this extended project Chapter 3 to Chapter 4 results, is to investigate the effect of

adding benzonitrile as a homogenous catalyst regarding product selectivity under the same reaction parameters. Satisfaction achieved, styrene shows the change in the ratio between mono and di-carboxylated products. Styrene is fully reduced to phenyl propionic acid with no phenyl succinic acid shown in the NMR. However, Trans-stilbene electro-carboxylated in the presence of benzonitrile shows slight improvement in the matter of product selectivity with 8 % produce monoacid (NMR Figures 6, and 7, Chapter 4) .

3.2. Chronopotentiometry.

All phenyl substituted alkenes are subjected to applied current at -35 mA for 8 hours under the same reaction conditions in addition to 10 % of benzonitrile. Styrene, E-β-Methyl styrene, and E-stilbene give promising results regarding product selectivity. In addition, a massive amount of Z-Stilbene did not react in the presence of 10% benzonitrile, possibly as a result of polymerization leading to deposition and blocking of the mesh surface.
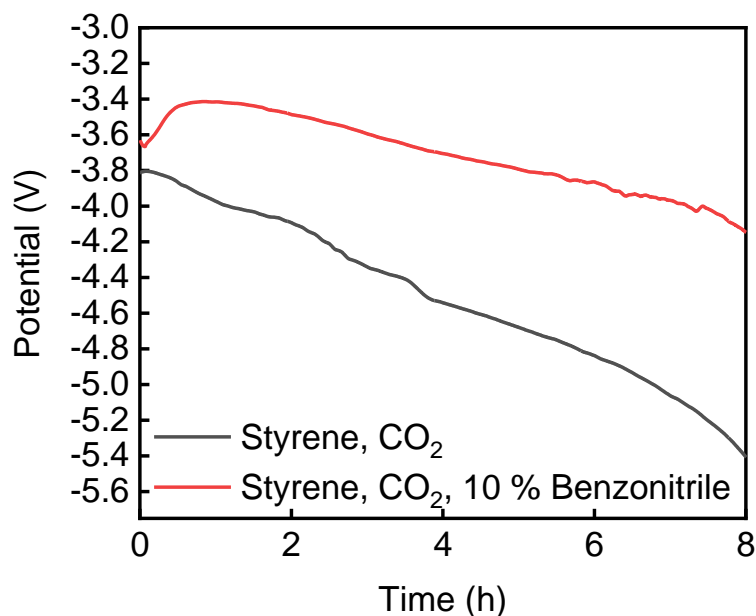
Figure 3: *Chronopotentiometry of a 3.5 mmol solution of Styrene in 20 mL DMF containing 0.1 M nBu₄NPF₆ supporting electrolyte, and 10 % Benzonitrile at room temperature, with fixed current -35 mA/cm² for 8 hours. A Ni mesh (2×0.35 cm²) was used as the working electrode, a Mg rod was used as the counter electrode and an SCE electrode was used as the reference. The carbon dioxide was bubbled continuously during the reaction.*

The graph (Figure 3) shows the voltage starts at -3.5 V increases slightly, and then becomes more negative during eight hours to end at around -4.1 V. If we compare the voltage range in the presence (Figure 3) / absence (Figure 13, Chapter 3), it is obviously can see the role of benzonitrile as an electron transfer homogeneous catalyst in the reaction mechanism which is consequently will change the product (s) selectivity. In the absence of benzonitrile,

the reaction starts at -3.8 V and ends around -5.3 V. However, that can be summarized as follows:

1- Absence of benzonitrile, styrene will be reduced before carbon dioxide.

2- The presence of benzonitrile, benzonitrile will be reduced first, then react will carbon dioxide to form carbon dioxide radical, which afterward will react with styrene.
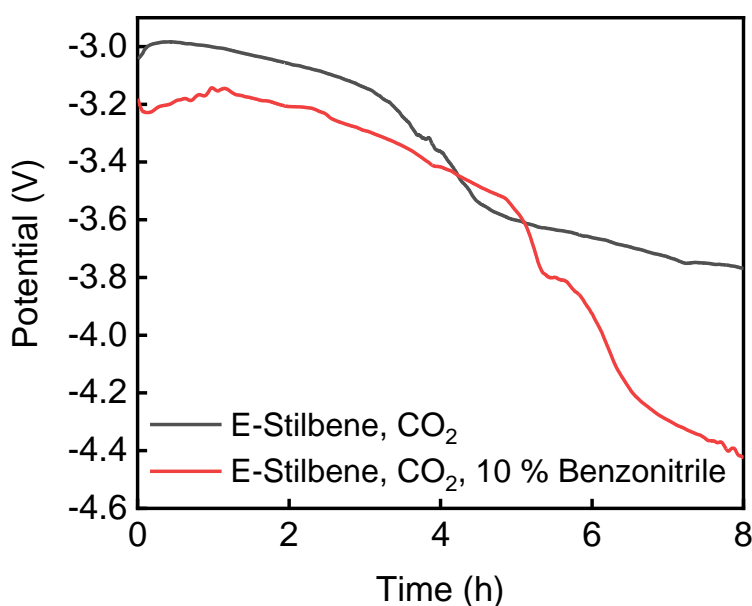

Figure 4: *Chronopotentiometry of a 3.5 mmol solution of E-Stilbene in 20 mL DMF containing 0.1 M nBu_4NPF_6 supporting electrolyte, and 10 % Benzonitrile at room temperature, with fixed current -35 mA/cm² for 8 hours. A Ni mesh (2×0.35 cm²) was used as the working electrode, a Mg rod was used as the counter electrode and an SCE electrode was used as the reference. The carbon dioxide was bubbled continuously during the reaction.*

The opposite occurs in the case of E-stilbene. The voltage during the chronopotentiometry of the E-stilebene one in the presence of benzonitrile did not exceed -4.7 V. Bear in mind that the voltage did not exceed -4 V in the absence of benzonitrile (Figure 18, Chapter 3). It is worth mentioning that no completion of the reaction in both methyl styrene and stilbene in the form Cis (Z). In addition, 1,1 diphenyl ethylene and α-methyl styrene have the same issue of reaction completion. That might be due to the symmetry of these alkenes and interaction with benzonitrile during the electro-carboxylation. Hereby, we will not show any of these results as they are incomparable with the results presented in chapters 3, and 4 regarding charge pass consistency.

4. Results and Discussion.

4.1. ^{1}H NMR and ^{13}C NMR of all alkenes and products.

^{1}H NMR Reduced Styrene (Product)
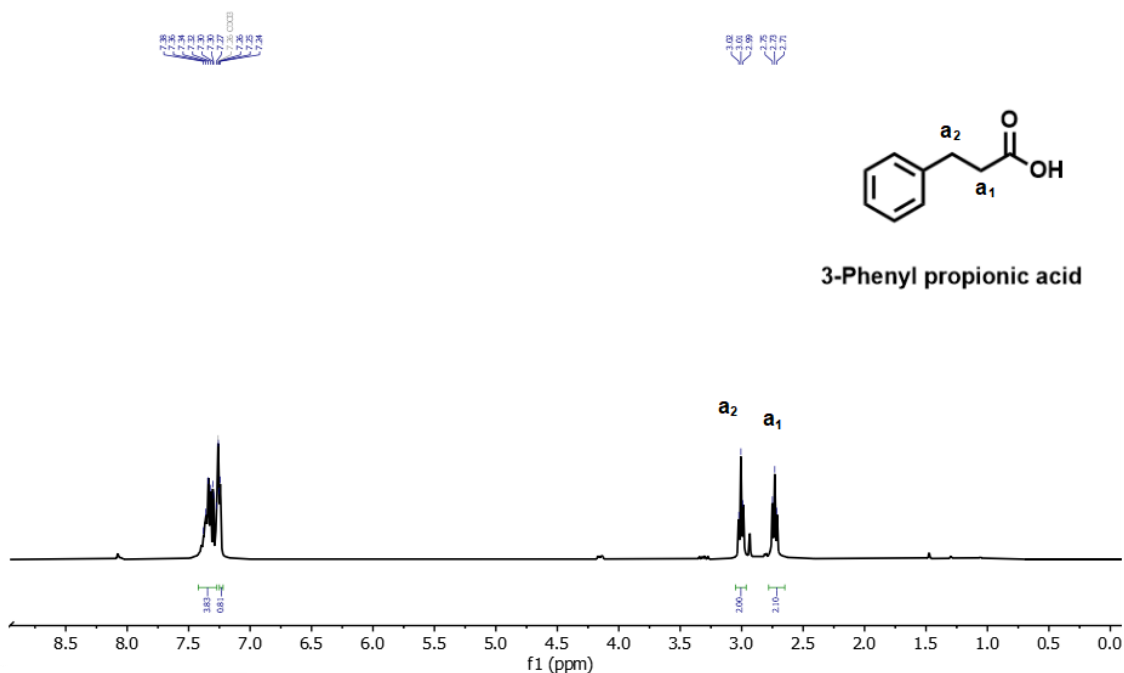**(Benzonitrile)**

3-Phenyl propionic acid

Figure 5. *^{1}H NMR of product of styrene reduction with benzonitrile catalyst.*

3-Phenylpropionic acid: ^{1}H NMR (400 MHz, CDCl$_3$) δ 7.38 - 7.24 (m, 5H, Ph), 2.99 (t,

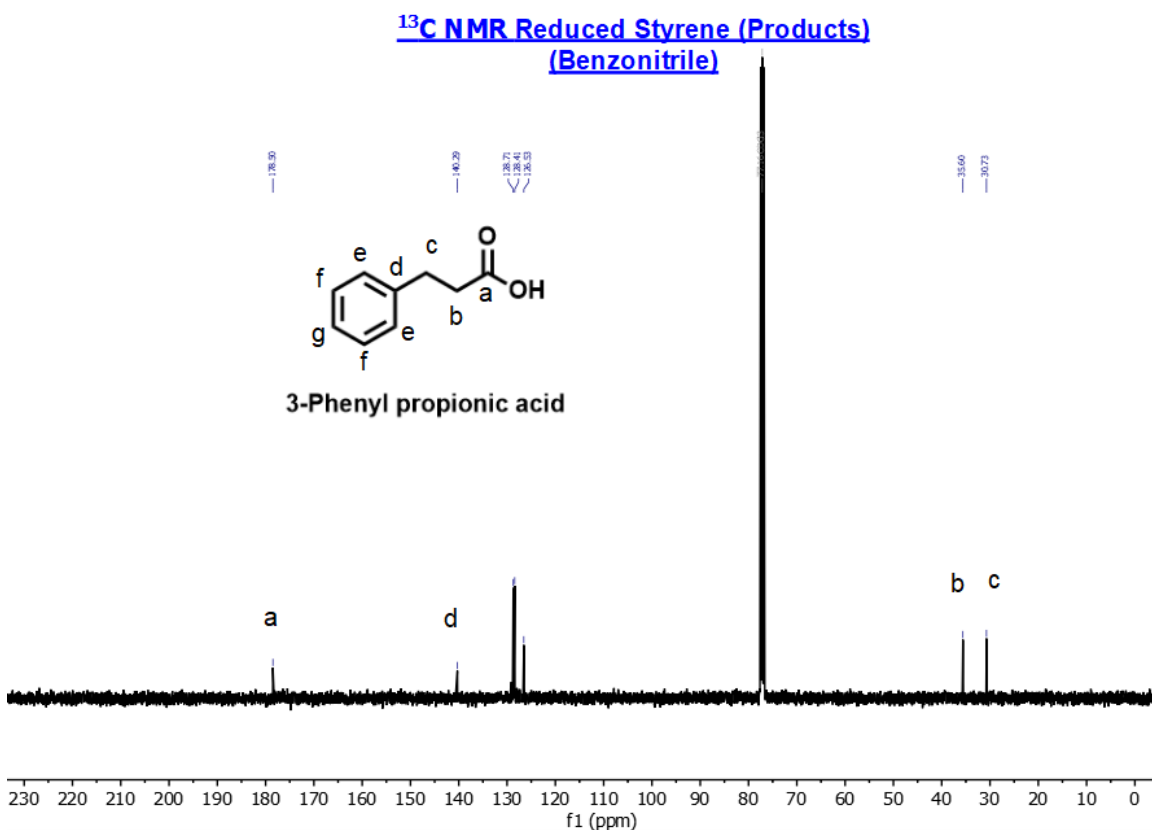*J* = 7.2 Hz, 2H, C*H*$_2$), 2.73 (t, *J*= 7.4 Hz, 2H, CH$_2$).

.

Figure 6. *^{13}C NMR of products of styrene reduction with benzonitrile catalyst.*

3-Phenyl propionic acid: ^{13}CNMR (101 MHz, CDCl$_3$) δ 178.90, 140.29, 128.71, 128.41,
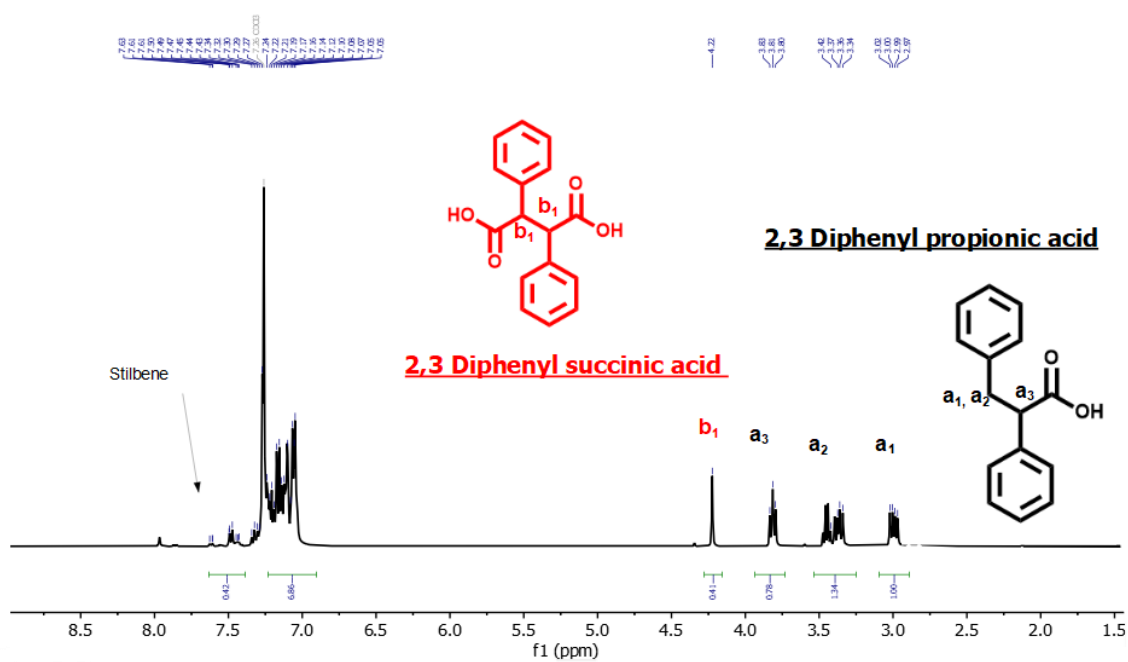
126.53, 35.60, 30.73.

Figure 7. *¹H NMR of products of E-stilbene reduction with benzonitrile catalyst.*

2,3-diphenyl propionic acid: ¹H NMR (400 MHz, CDCl₃) δ 7.49-7.27 (m, 3H), 7.24 (dd, *J* = 9.1, 4.6Hz, 2H), 7.23-7.16 (m, 3H), 7.05 (d, *J* = 6.9 Hz, 2H), 3.83-3.80 (m, 1H), 3.42-3.34 (m, 1H), 3.02-2.97 (m, 1H).

2,3-diphenyl succinic acid: ¹H NMR (400 MHz, CDCl₃) δ 7.15–7.13 (m, 6H), 7.10–7.05 (m, 4H), 4.22 (s, 2H).
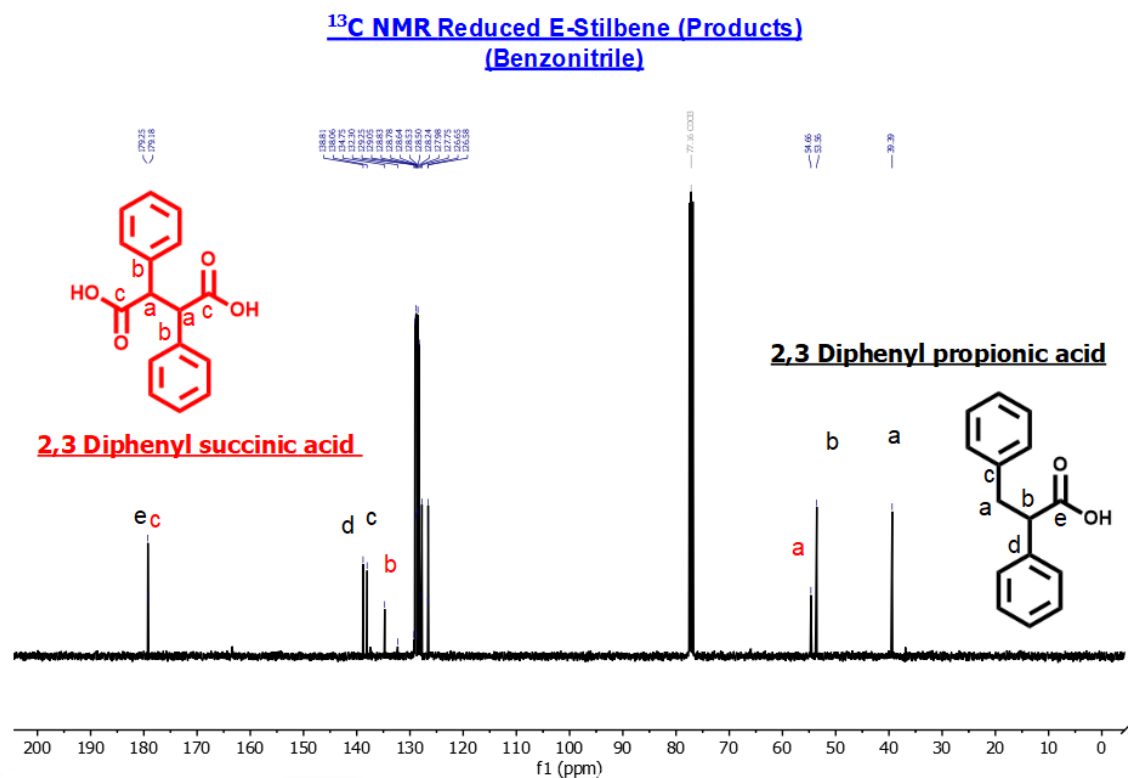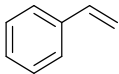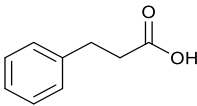
Figure 8. *13C NMR of products of E-stilbene reduction with benzonitrile catalyst.*

2,3-diphenyl propionic acid: ^{13}C NMR (101 MHz, CDCL₃) δ 179.25, 138.81, 138.06, 128.51, 128.24, 127.98, 127.77, 126.65, 126.00, 53.95, 39.39.

2,3-diphenyl succinic acid: ^{13}C NMR (101 MHz, CDCL₃) δ 179.18, 134.75, 129.05, 128.83, 127.75, 54.66.

Table 2: *conversions, isolated yields, and Faradaic efficiencies for the production of various carboxylic acids in the presence of benzonitrile (BN).*

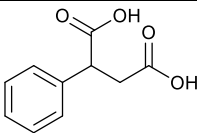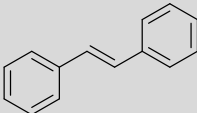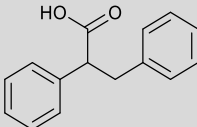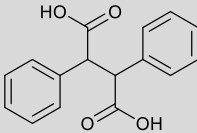| Entry	Substrate	With benzonitrile	Without benzonitrile	Product	With benzonitrile		Without benzonitrile	
		Substrate conversion (%)	Substrate conversion (%)		yield (%)	Faradic efficiency (%)	yield (%)	Faradic efficiency (%)
1	styrene	>99	>99	phenyl propionic acid	>99	67	53	36
				phenyl succinic acid	-	-	13	8
2	E-stilbene	85	>99	diphenyl propionic acid	70	8	62	41
				diphenyl succinic acid	12	47	15	10

The yield for each product is calculated by NMR integration and/or obtained grams summarized in Table 2. The reduction of styrene (Table 2, entry 1) tends to produce phenyl propionic acid, and no phenyl succinic acid is produced in the reaction where benzonitrile is added as a catalyst. On the other hand, the reaction with E-stilbene (Table 2, entry 2) showed that some reactants remained, giving a conversion of only 85%. The

187

selectivity of mono and diacids is almost the same as in the absence of benzonitrile with 8 % yield difference more selective to produce mono acid in the addition of benzonitrile.

5. **Related calculations.**

a. **Amount of homogeneous catalyst to the substrate.**

$$= \frac{Mass\ of\ reactant\ (g)}{Molecular\ weight\ of\ reactant\ g/mole} \times 0.01 \times Catalyst\ molecular\ weight\ g/mol$$

6. **Conclusion.**

The catalytic improvement of cyclic voltammetric peaks observed with the benzonitrile catalyst enables the assessment of the electron transfer rate constant from these aromatic anion radicals to CO_2. This determination is carried out as a function of the catalyst's standard potential. Consequently, it can be employed to modulate the potential, either lowering or increasing it, to influence product selectivity within the context of carbon dioxide electro-reduction and fixation processes.

From the array of NMR spectra provided above, it becomes apparent that two distinct situations unfold. The initial situation pertains to some compounds, which exhibit multiple additional peaks. This phenomenon can be ascribed to the polymerization of benzonitrile or alkene compounds that takes place during the reaction, leading to the depletion of materials in some instances. Consequently, this polymerization hinders the successful completion of alkene reduction by obstructing the porous mesh working electrode and preventing current flowing.

The second scenario arises with different phenyl-substituted alkenes such as styrene, demonstrating the influence of benzonitrile on altering the selectivity ratio between mono- and di-acids produced in the electro-carboxylation process. In addition, not much changes in the product selectivity of E-stilbene.

7. References.

[1]. Gennaro, A., Isse, A. A., Savéant, J. M., Severin, M. G., & Vianello, E. Homogeneous Electron Transfer Catalysis of The Electrochemical Reduction of Carbon Dioxide. Do Aromatic Anion Radicals React in an Outer-Sphere Manner? *J. Am. Chem. Soc.*, **118** (30), 7190-7196 (1996).

[2]. Filardo, G., Gambino, S., Silvestri, G., Gennaro, A., & Vianello, E. Electrocarboxylation of Styrene Through Homogeneous Redox Catalysis. *J. Electroanal. Chem. Interf. Electrochem.*, **177** (1-2), 303-309 (1984).

[3]. Gambino, S., Gennaro, A., Filardo, G., Silvestri, G., & Vianello, E. Electrochemical Carboxylation of Styrene. *J. Electrochem. Soc.*, **134** (9), 2172 (1987).

[4]. Aresta, M., & Forti, G. (Eds.). *Carbon Dioxide as a Source of Carbon: Biochemical and Chemical Uses* (Vol. 206). Springer Science & Business Media, (2012), p (348-350).

Chapter 5: Conclusion and Future Work.

Synopsis

In Chapter 5, we will summarize our work and highlight the most important results. Moreover, there will be some suggestions for those who are interested in electro-carboxylation reactions by giving some substrates, and electrodes that have not been investigated along with carbon dioxide and electro-carboxylation reactions.

1. Conclusion.

In the present era, annual anthropogenic CO_2 emissions are on the rise. When coupled with the existing surplus of approximately 1 trillion tons of CO_2 in the atmosphere, it signifies the presence of a vast reservoir of untapped CO_2 waiting to be harnessed. Exploiting this CO_2 as a fundamental building block (referred to as C1) for synthesizing complex chemicals with high molecular intricacy and, consequently, significant value, holds the potential to provide economic incentives for further investment.

Consequently, a substantial body of research is dedicated to efficiently producing such chemicals using CO_2 as either a starting material or an intermediate compound. This approach pertains to an intriguing category of complex chemicals, which is anticipated to experience a significant surge in production and demand. Hence, the production of these materials necessitates the initial step of regulating the variables that influence the resulting products. These factors can encompass chemical, physical, or mechanical challenges. As a result, scientists are actively seeking methods to manage these interactions, ultimately enhancing the selectivity of the outcomes. Therefore, the results of reaction control will greatly contribute to and shorten the subsequent steps. It is also possible to contribute to the creation of new vehicles that can contribute to the development of the modern era for a greener future in an accelerated manner.

In our study, we employed a mesh nickel electrode to enhance the selectivity of carboxylic acids generated from the reduction of alkene and carbon dioxide. The results exhibited a notable enhancement in the selectivity of monoacids over di acids, which

were produced in minor quantities from certain reduced alkenes. These results present an opportunity for future researchers to experiment with multiple mesh electrodes and investigate potential divergent outcomes compared to foil and plate electrodes. This is owing to the substantial surface area of mesh electrodes, which can lead to distinct molecular binding patterns on the surface. However, comparing the previous literature review and the used reaction conditions, it can be seen that there are many methods that the product selectivity would be changed, for instance, temperature, electrolyte, aqueous or organic solvents, carbon dioxide gas pressure, catalyst type, electrode geometry, and electrode elemental type. Moreover, the chosen electrochemical technique and cell design have a significant role in product selectivity. Most of the previous studies relied on the fixed current (chronopotentiometry) technique, while a few applied fixed potentials. Moreover, in this study, we have considered the adoption of extremely straightforward reaction conditions at ambient room temperature, all without the application of high pressure (on a laboratory scale). This approach serves as a preliminary study of a principle that holds potential for broader implementation within the manufacturing sector on a larger scale.

To epitomize our work, Chapter 1 introduces the importance of this work and discusses what is been done in the electro-carboxylation field by giving some examples of varied chemical substrates under various reaction conditions.

Then, Chapter 2, provides a simplified overview of the methodology used for analyzing the product samples. Additionally, give a peek at some theories behind the used instruments, for instance, nuclear magnetic resonance (NMR), Mass spectroscopy (MS),

Infrared analysis (IR), x-ray diffraction analysis (XRD), and scanning electron microscope (SEM) and energy dispersion x-ray (EDX).

Likewise, Chapter 3 presents our methodology during the electro-carboxylation reaction using Bio-Logic SP-150. The chapter then discussed how we dealt with the obtained crudes and purified the product(s). In addition, chapter 3 shows NMR and other analyses proven various carboxylic acid product(s) along with various analysis techniques. Then, the discussion then focuses on comparing the obtained cyclic voltammetry, and chronopotentiometry graphs between phenyl substituted alkene to another regarding chemical structure symmetry and substituted group effect versus the voltage range during the electro-carboxylation reaction. Furthermore, the surfaces of nickel and magnesium have been the image for intensive investigation to see what these electrodes were affected by this process and what material(s) are present on their surfaces after the reaction. This analysis also gives a comprehensive picture that covers an important aspect as part of this investigation.

To provide a thorough overview of this field, the experiment was replicated using identical reaction conditions, incorporating benzonitrile as a homogeneous catalyst. The inclusion of benzonitrile resulted in a modification of the products formed during the reduction of styrene, but it had a relatively minor impact on the products formed during the reduction of stilbene.

In summary, the electro-carboxylation approach is frequently regarded as an environmentally friendly and sustainable method for carboxylation reactions because it relies on electricity and eliminates the need for conventional stoichiometric reagents. As

in this project, proven the system works if the surface geometry is enhanced as well as the selectivity of the products can be more selective. Moreover, other factors such as the reaction temperature, carbon dioxide pressure which is examined in previous studies and it is compared to which results is obtained in this project. Creating a new methodology such as using electrode mesh to trap or capture carbon dioxide helps to reduce carbon dioxide and react it with the reduced alkenes before it flies out in such a system like the one is used in this project. In addition, applying the same reaction condition in as system such as flow cell will rise some mechanical issues such as overloading the system due to blocking of the membranes as used in the flow cell system by alkenes which are in their physical nature mostly are oily or have heavy molecular weight. Taking into consideration that solving this mechanical issue will open the door for industrial revolution.

2. Future work and suggestions.

As a future work and suggestion, it would be interesting to interpret various chemical substrates, which have not been reduced in any of the previous studies. Besides, manipulating the reaction conditions and comparing in between various results to achieve satisfactory findings and explore new materials. For instance, 4-[2-(4-aminophenyl) ethenyl] aniline A, and trans-4,4'-Dinitrostilbene B Figure 1, to name but a few. In addition, to the best of our knowledge, there are a few studies that have used titanium as a working electrode in the electro-carboxylation of alkenes.
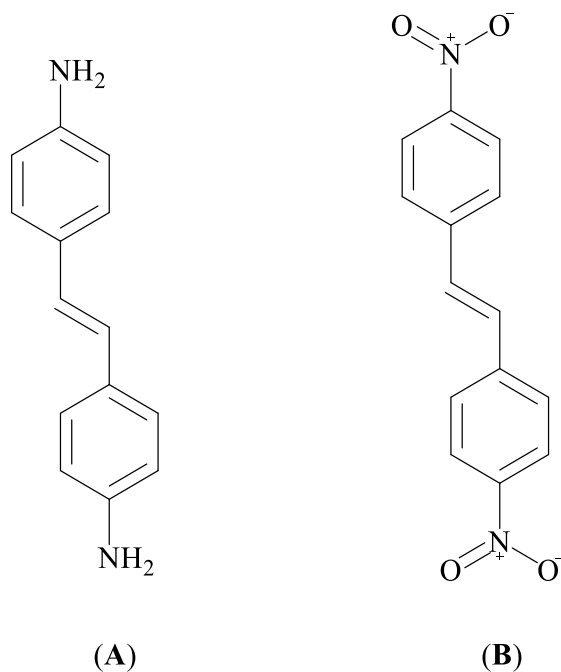
(A)   (B)

Figure 1. *Shows some suggested phenyl substituted alkene; (A) -[2-(4-aminophenyl) ethenyl] aniline, (B) trans-4,4'-Dinitrostilbene.*

Another suggestion, finding simpler and shorter purification plans as a part of synthesizing these electro-carboxylated products. Moreover, designing advanced cells can help to avoid many technical issues that could arise from the setup system resulting in inaccurate data.